

## ABSTRACT

Title of Document: BIOORGANIC CHEMISTRY OF  
SPHINGOLIPIDS: PORE FORMATION AND  
ANION TRANSPORT.

William Ayers Harrell, Jr.,  
Doctor of Philosophy, 2011

Directed By: Professor Jeffery T. Davis,  
Department of Chemistry and Biochemistry

Ceramide is an amphiphilic natural product that plays important roles in multiple cellular processes. Ceramide also is known to self-assemble into transmembrane pores under physiologically relevant concentrations. In order to study the role of ceramide's 1,3-diol functionality in the stabilization of transmembrane pores, ceramide analogs were prepared using protecting groups to block the 1,3-diol unit. Blocking the 1,3-diol with an acetal protecting group led to a drastic decrease in membrane-activity. Surprisingly, blocking the -OH groups of C2-ceramide **2** with simple esters yielded a C2-diacetate **16** analog with increased pore-forming activity.

Additionally, a new function of C2-ceramide **2** has been discovered that has important biological implications. Working below concentrations in which it self-assembles into transmembrane pores, C2-ceramide **2** facilitated the transmembrane transport of biologically relevant anions such as  $\text{Cl}^-$  and  $\text{HCO}_3^-$  via an anion exchange mechanism. The 1,3-diol functionality of the C2-ceramide **2** headgroup was found to

play an integral role in the binding and transport of anions, as the isopropylidene C2-ceramide **18** analog was unable to facilitate transmembrane anion transport.

*D-erythro*-Sphingosine **3**, produced naturally by the metabolism of ceramide, lacks the amide functionality in its hydrophilic head-group. Unlike C2-ceramide **2**, sphingosine **3** does not facilitate transmembrane Cl<sup>-</sup>/HCO<sub>3</sub><sup>-</sup> exchange. Possible reasons for this failure to facilitate the transmembrane transport of anions are discussed, namely that sphingosine **3** does not bind HCO<sub>3</sub><sup>-</sup> in a non-covalent manner. Instead, sphingosine **3** forms carbamates in the presence of HCO<sub>3</sub><sup>-</sup> and CO<sub>2</sub> in a solvent dependent manner.

BIOORGANIC CHEMISTRY OF SPHINGOLIPIDS: PORE FORMATION AND  
ANION TRANSPORT.

By

William Ayers Harrell, Jr.

Dissertation submitted to the Faculty of the Graduate School of the  
University of Maryland, College Park, in partial fulfillment  
of the requirements for the degree of  
Doctor of Philosophy  
2011

Advisory Committee:  
Professor Jeffery T. Davis, Chair  
Professor Marco Colombini  
Professor Philip DeShong  
Professor Daniel Falvey  
Professor Lyle Isaacs

© Copyright by  
William Ayers Harrell, Jr.  
2011

## Preface

I have worked on two main projects during my time in the Davis lab. For the purposes of this dissertation, I will focus on the new project I started involving the study of the amphiphilic natural product ceramide. For information on my previous project studying guanosine self-assembly, the reader is referred to the following research and review articles:

Ma, L.; Harrell, W. A., Jr.; Davis, J. T. Stabilizing Guanosine-Sterol Ion Channels with a Carbamate to Urea Modification in the Linker. *Org. Lett.* **2009**, *11*, 1599-1602.

Kaucher, M. S.; Harrell, W. A., Jr.; Davis, J. T. A Unimolecular G-Quadruplex that Functions as Synthetic Transmembrane Na<sup>+</sup> Transporter. *J. Am. Chem. Soc.* **2006**, *128*, 38-39.

Harrell, W. A., Jr.; Davis, J. T. Self-Assembly: Guanine Nucleobases. In *Encyclopedia of Supramolecular Chemistry*. [Online]; Atwood, J. L.; Steed, J. W., Eds.; Marcel Dekker: New York, 2006.

Kaucher, M. S.; Harrell, W. A., Jr.; Davis, J. T. The G-Quartet in Supramolecular Chemistry and Nanoscience. In *Quadruplex Nucleic Acids*, Neidle, S.; Balasubramanian, S., Eds.; Royal Society of Chemistry: Cambridge, U.K., 2006; pp 253-296.

## Acknowledgements

First I would like to thank Professor Jeffery T. Davis for being there whenever I needed advice, and having patience and confidence in me. You saw something in me that I didn't always see in myself, and I can't thank you enough for helping me get to this point. I would also like to thank my committee for their input and suggestions during my time here at the University of Maryland. I would like to thank Professor Lyle Isaacs and Professor Philip DeShong for helpful advice in both research and life in general. I would like to thank Professor Marco Colombini for getting me interested in studying ceramide, and Professor Daniel Falvey for agreeing to be on my committee last second and for helpful discussions.

I would also like to thank Dr. Bonnie Dixon for helping me realize that I have a passion for teaching. Your door was always open and you were always there when I needed someone to talk to. Thank you. I am also very grateful for the help of Dr. Yiu-Fai Lam for his help with NMR spectroscopy and running a top-notch facility.

I thank the UMD Department of Chemistry and Biochemistry and the US Department of Education for the GAANN fellowship that covered my tuition and stipend for one year. I would Dr. Philip Gale, Steve, Christine, Cally, and Jen for making me feel at home when I visited the University of Southampton.

A special thanks goes out to members of the Davis group, both past and present, especially Dr. Paul (is a jerk) Santacrose for his assistance when I first started in the group, and for teaching me the techniques I needed to be successful, Dr. (bad) Ling Ma for being crazy and at the same time keeping me sane, and Dr. Yom-Yom for being the voice of reason (twist your mouth). Thanks Mark, Jenny, Sofya,

Soumya, Monique, Monica, JJHP, Liesel, Soheila and Andrew for making it fun working in the lab.

I want to thank my fellow classmates Sara, Tony, Mike, old man Neil, Kelly, and Melissa for helping to make graduate school fun. I thank Matt for breaks at the Chem. Lounge, as well as on the course. A special thanks to Brian...without you, I would never have known the existence of the water dance. And then there's Becky, who has been a great number of things including honorary group member, a shrink, a jerk, a scapegoat...but most importantly, a friend.

Finally, I would like to thank my family. Mom and Dad thank you for always being supportive and for your advice over the years. You are the best parents in the world. Wade, I thank you for all of your insights and knowledge in the fields of G-quartets and hydrogen-“bonding”. And last, but certainly not least, I want to thank Katie putting up with me through all these years, I know I can be trying at times. Thank you for all of your support and love, you mean the world to me.

# Table of Contents

|  |           |
|--|-----------|
| Preface.....   | ii        |
| Acknowledgements.....  | iii       |
| Table of Contents.....   | v         |
| List of Tables.....  | ix        |
| List of Figures.....   | x         |
| List of Schemes.....   | xvi       |
| <b>Chapter 1: Bioorganic Chemistry of Sphingolipids.....</b>                             | <b>1</b>  |
| 1.1 Introduction.....  | 1         |
| 1.2 Thesis Organization.....   | 2         |
| 1.3 Biosynthesis of Sphingosine and Ceramide.....  | 3         |
| 1.4 Sphingolipids and Disease.....   | 5         |
| 1.5 Ceramide Induced Apoptosis via Membrane Permeation.....                              | 6         |
| 1.6 Membrane-Active Synthetic Ceramide Analogs.....                                      | 8         |
| 1.6.1 Gokel's Ceramide Mimics.....   | 8         |
| 1.6.2 Bieberich's Ceramide Mimic.....  | 10        |
| 1.6.3 Chanturiya's Sphingomyelin Mimic.....  | 12        |
| 1.6.4 Macchia and Danesi's Lipophilic Nucleobase Ceramide Mimics.....                    | 13        |
| 1.6.5 Smith's Synthetic Lipid that Transports Anions via a Relay Mechanism.....          | 14        |
| 1.7 Summary.....   | 17        |
| <b>Chapter 2: C2-Ceramide Diacetate Forms Large Pores in Phospholipid Membranes.....</b> | <b>18</b> |
| 2.1 Introduction.....  | 18        |
| 2.2 Ceramide Pores Allow the Release of Apoptosis-Inducing Cytochrome C.....             | 19        |
| 2.3 The Role of Ceramides 1,3-Diol Unit in Pore Formation.....                           | 21        |
| 2.4 Protected Ceramide Analogs as Potential Pro-Drugs.....                               | 22        |
| 2.5 Preparation of a <i>p</i> -Methoxybenzylidene C16-Ceramide Analog.....               | 24        |
| 2.6 Mitochondrial Permeabilization Assay.....  | 25        |



|   |    |
|---|----|
| 2.7 Preparation of C2-Ceramide <b>2</b> Analogs .....   | 27 |
| 2.8 Carboxyfluorescein (CF) Release Assay for Pore Formation.....   | 29 |
| 2.9 Pore Sizing using FITC-Dextrans.....  | 32 |
| 2.10 Mitochondrial Permeabilization Assay using C2-Diacetate <b>16</b> .....  | 35 |
| 2.11 Conclusions.....   | 36 |
| 2.12 Future Directions .....  | 38 |
| <b>Chapter 3: C2-Ceramide Facilitates Anion Exchange across<br/>Phospholipid Bilayers</b> .....                         | 39 |
| 3.1 Introduction.....   | 39 |
| 3.2 Small Molecule Natural Products that Transport Anions .....   | 40 |
| 3.2.1 Duramycin.....  | 41 |
| 3.2.2 Prodigiosin .....   | 42 |
| 3.2.3 Amphotericin B.....   | 44 |
| 3.2.4 Pamamycin-607 .....   | 45 |
| 3.3 Synthetic Anion Transporters that Utilize O-H···A <sup>-</sup> Interactions .....                                   | 47 |
| 3.3.1 Matile's Rigid-Rod Polyol <b>24</b> Forms Ion Channels .....  | 48 |
| 3.3.2 Catechols as Anion Transporters .....   | 49 |
| 3.4 Anion Binding Studies of C2-ceramide.....   | 51 |
| 3.4.1 The C2-Ceramide Tridentate Anion Binding Motif .....  | 51 |
| 3.4.2 Preparation and Characterization of Isopropylidene C2-Ceramide <b>18</b> .....                                    | 52 |
| 3.4.3 ESI-MS Evidence that C2-Ceramide <b>2</b> Binds Anions .....  | 54 |
| 3.4.4 <sup>1</sup> H NMR Evidence that C2-Ceramide <b>2</b> Binds Anions.....   | 55 |
| 3.5 Transmembrane Anion Transport by C2-Ceramide <b>2</b> .....   | 59 |
| 3.6 Anion Binding and Transport Studies of a C2-Ceramide Derivative with<br>Modifications to the Amide Side-Chain ..... | 63 |
| 3.6.1 Preparation of a Trifluoroacetyl C2-Ceramide Analog .....   | 64 |
| 3.6.2 <sup>1</sup> H NMR Evidence that Trifluoroacetyl C2-Ceramide <b>19</b> Binds Anions...                            | 65 |
| 3.6.3 Anion Transport Activity of Trifluoroacetyl C2-Ceramide <b>19</b> .....   | 66 |
| 3.7 Conclusions.....  | 70 |

|   |     |
|---|-----|
| <b>Chapter 4: Natural and Synthetic Small Molecules that Bind and Transport</b>                                 |     |
| Bicarbonate .....   | 71  |
| 4.1 Introduction.....   | 71  |
| 4.1.1 Chemistry and Biochemistry of Bicarbonate Anion and Carbon Dioxide  | 73  |
| 4.1.2 Why Study Bicarbonate Transport?.....   | 74  |
| 4.1.3 Chloride / Bicarbonate Exchange Proteins .....  | 75  |
| 4.1.5 Small Molecules that Facilitate the Transmembrane Transport of $\text{HCO}_3^-$                           | 76  |
| 4.2 C2-Ceramide <b>2</b> Binds and Transports $\text{HCO}_3^-$ .....  | 80  |
| 4.3 Tren-Based Small Molecules: A New Class of Bicarbonate Transporters.....                                    | 84  |
| 4.4 Thiourea Tren-Based Receptor Facilitates the Transport of $\text{HCO}_3^-$ .....                            | 85  |
| 4.5 Structurally Simple Thiourea-Based Bicarbonate Transporters .....   | 89  |
| 4.6 Biological and Environmental Impacts of Carbon Dioxide.....   | 93  |
| 4.7 Supramolecular Carbamate-Forming Systems .....  | 95  |
| 4.8 Anion Binding and Transport Properties of Sphingosine <b>3</b> .....  | 99  |
| 4.9 Sphingosine <b>3</b> forms Carbamates in the Presence of $\text{HCO}_3^-$ in $\text{CD}_2\text{Cl}_2$ ..... | 102 |
| 4.10 Sphingosine Carbamate <b>27</b> Formation via $\text{CO}_2$ Bubbling.....                                  | 106 |
| 4.11 Conclusions.....   | 111 |
| <b>Chapter 5: Conclusions and Future Directions</b> .....   | 113 |
| <b>Chapter 6: Experimental Procedures</b> .....   | 116 |
| 6.1 General Experimental .....  | 116 |
| 6.2 Synthetic Procedures.....   | 117 |
| 6.3 Carboxyfluorescein (CF) Liposome Assays .....   | 122 |
| 6.3.1 Liposome Preparation .....  | 122 |
| 6.3.2 CF Dye Release Assay <sup>47</sup> .....  | 122 |
| 6.4 FITC-Dextran Liposome Assays .....  | 123 |
| 6.4.1 Liposome Preparation .....  | 123 |
| 6.4.2 FITC-Dextran Release Assay .....  | 124 |
| 6.5 Lucigenin Liposome Assays .....   | 124 |

|   |     |
|---|-----|
| 6.5.1 Liposome Preparation .....  | 124 |
| 6.5.2 Anion Transport Assay .....   | 125 |
| 6.6 Direct Monitoring of Bicarbonate Transport via <sup>13</sup> C NMR..... | 126 |
| 6.6.1 Liposome Preparation .....  | 126 |
| 6.6.2 <sup>13</sup> C NMR Bicarbonate Transport Assays.....                 | 126 |
| 6.7 X-Ray Crystallographic Data.....  | 127 |
| 6.7.1 C2-pmb <b>15</b> .....  | 127 |
| 6.7.2 Isopropylidene C2-Ceramide <b>18</b> .....                            | 130 |
| Bibliography .....  | 133 |

## List of Tables

|   |     |
|---|-----|
| <b>Table 1.1.</b> Diseases caused by misregulation of sphingolipids .....   | 6   |
| <b>Table 3.1.</b> Binding constants ( $K_a$ ) of C2-ceramide <b>2</b> and trifluoroacetyl<br>C2-ceramide <b>19</b> with TBACl in $CD_2Cl_2$ ..... | 66  |
| <b>Table 4.1.</b> Bicarbonate plays a key role in multiple biological functions .....   | 74  |
| <b>Table 4.2.</b> Henry's Constants ( $k_H$ ) for $CO_2$ in Select Solvents .....   | 94  |
| <b>Table 6.1.</b> Crystal data and structure refinement for UM#1807. ....   | 129 |
| <b>Table 6.2.</b> Crystal data and structure refinement for UM # 1793 .....   | 132 |

## List of Figures

|  |    |
|--|----|
| <b>Figure 1.1.</b> Structure of C16-ceramide <b>1</b> , C2-ceramide <b>2</b> and sphingosine <b>3</b> . .....  | 1  |
| <b>Figure 1.2.</b> Biosynthesis of C16-ceramide <b>1</b> and sphingosine <b>3</b> . .....  | 4  |
| <b>Figure 1.3.</b> C16-ceramide <b>1</b> forms pores in planar phospholipid membranes. ....  | 7  |
| <b>Figure 1.4</b> C16-ceramide mimics <b>4-7</b> . .....   | 9  |
| <b>Figure 1.5.</b> Structural similarities between C16-ceramide <b>1</b> and C16-serinol <b>8</b> . ....   | 11 |
| <b>Figure 1.6.</b> Sphingomyelin <b>9</b> and a synthetic sphingomyelin mimic <b>10</b> . .....  | 12 |
| <b>Figure 1.7.</b> C2-ceramide <b>2</b> analogs utilizing the nucleobases uracil <b>11</b> and thiouracil <b>12</b> as the polar headgroup region. ....  | 13 |
| <b>Figure 1.8.</b> Smith's synthetic phospholipid anion transporter <b>13</b> . .....  | 14 |
| <b>Figure 1.9.</b> Proposed anion transport relay mechanism for compound <b>13</b> . .....   | 16 |
| <b>Figure 2.1.</b> Molecular dynamics simulation of a C16-ceramide <b>1</b> nanopore. ....   | 21 |
| <b>Figure 2.2.</b> a) Hydrogen bonding of the 1,3-diol unit of C16-ceramide <b>1</b> helps form the inner wall of the pore. b) Vertical columns of ceramides held together by amide hydrogen bonding. .... | 22 |
| <b>Figure 2.3.</b> <sup>1</sup> H NMR spectrum of C16-pmb <b>14</b> in CDCl <sub>3</sub> . .....   | 25 |
| <b>Figure 2.4.</b> Mitochondrial permeability assay comparing C16-ceramide <b>1</b> and C16-pmb <b>14</b> . .....  | 26 |
| <b>Figure 2.5.</b> Crystal structure of C2-pmb <b>15</b> . .....   | 28 |
| <b>Figure 2.6.</b> CF release assay comparing C2-ceramide <b>2</b> and C2-pmb <b>15</b> . .....  | 31 |
| <b>Figure 2.7.</b> CF release assay comparing C2-ceramide <b>2</b> and C2-diacetate <b>16</b> . .....  | 32 |
| <b>Figure 2.8.</b> a) General structure of a FITC-dextran. b) Size-exclusion chromatography showing the sizes of FD4 and FD10 relative to cytochrome c. ....   | 33 |
| <b>Figure 2.9.</b> FITC-dextran release assay results comparing C2-ceramide <b>2</b> , C2-pmb <b>15</b> , and C2-diacetate <b>16</b> . .....   | 35 |

|   |    |
|---|----|
| <b>Figure 2.10.</b> Mitochondrial permeabilization assay comparing C2-ceramide <b>2</b> to C2-diacetate <b>16</b> . .....   | 36 |
| <b>Figure 2.11.</b> Schematic representation of a possible water stabilized C2-diacetate <b>16</b> pore. ....   | 37 |
| <b>Figure 2.12.</b> Cyclic ortho ester protected C2-ceramide analog.....  | 38 |
| <b>Figure 3.1.</b> Structure of duramycin <b>20</b> , a natural product anion transporter.....  | 41 |
| <b>Figure 3.2.</b> The structure of prodigiosin <b>21</b> and the complex <b>21</b> ·HCl. ....  | 42 |
| <b>Figure 3.3.</b> a) The structure of AmB <b>22</b> . b) Results from reverse potential planar membrane studies of AmB <b>22</b> at pH = 2 showing a negative potential, corresponding anion selective channel formation.....  | 44 |
| <b>Figure 3.4.</b> Molecular dynamics simulation of self-assembled AmB <b>22</b> channel. ...   | 45 |
| <b>Figure 3.5.</b> Structure of pamamycin-607 <b>23</b> and an example of a pamamycin-607 <b>23</b> lipophilic anion pair with KMnO <sub>4</sub> . ....   | 46 |
| <b>Figure 3.6.</b> Schematic representation of the narrowest pore region of the ClC chloride channel. <sup>135</sup> .....  | 48 |
| <b>Figure 3.7.</b> Matile's rigid polyol <b>24</b> , an AmB <b>22</b> mimic. ....   | 49 |
| <b>Figure 3.8.</b> Bis-catechol <b>25</b> facilitates the transmembrane transport of anions, while the protected derivative <b>26</b> does not. ....  | 50 |
| <b>Figure 3.9.</b> Model showing the binding of Cl <sup>-</sup> by C2-ceramide <b>2</b> . ....  | 51 |
| <b>Figure 3.10.</b> <sup>1</sup> H NMR spectrum (in CDCl <sub>3</sub> ) of isopropylidene C2-ceramide <b>18</b> distinguished by the loss of the broad -OH signals at 2.5 ppm and the appearance of protons 9 and 10 of the isopropylidene functionality. Additionally, a 1 ppm upfield shift of the -NH proton is observed when compared to C2-ceramide <b>2</b> . ....  | 53 |
| <b>Figure 3.11.</b> Depiction of the crystal structure of isopropylidene C2-ceramide <b>18</b> . The ends of the lipophilic tails have been removed for clarity.....  | 54 |
| <b>Figure 3.12.</b> ESI-MS (negative mode) of C2-ceramide <b>2</b> ·Cl <sup>-</sup> adduct. A solution of C2-ceramide <b>2</b> (2 mM) and TBACl (6 mM) in CD <sub>2</sub> Cl <sub>2</sub> was injected using MeOH as the eluant. ESI-MS [M+Cl] <sup>-</sup> calculated for C <sub>20</sub> H <sub>39</sub> ClNO <sub>3</sub> <sup>-</sup> 376.26, found 376.21. Experimental variables are listed above the spectrum..... | 55 |

|   |    |
|---|----|
| <b>Figure 3.13.</b> $^1\text{H}$ NMR of C2-ceramide <b>2</b> in dry and wet $\text{CD}_2\text{Cl}_2$ showing resolution of the hydroxyl protons in the water saturated $\text{CD}_2\text{Cl}_2$ solution.....   | 56 |
| <b>Figure 3.14.</b> Stack plot from $^1\text{H}$ NMR titrations of C2-ceramide <b>2</b> (2 mM) with increasing concentrations of tetrabutylammonium chloride (TBACl) in $\text{CD}_2\text{Cl}_2$ . .....  | 57 |
| <b>Figure 3.15.</b> Job plot of C2-ceramide <b>2</b> with TBACl showing 1:1 binding.....  | 57 |
| <b>Figure 3.16.</b> Stack plot from $^1\text{H}$ NMR titrations of isopropylidene C2-ceramide <b>18</b> (2 mM) with TBACl in $\text{CD}_2\text{Cl}_2$ . .....   | 58 |
| <b>Figure 3.17.</b> C2-ceramide <b>2</b> and isopropylidene C2-ceramide <b>18</b> were added at a 1 mol% compound to lipid ratio to a buffered solution of liposomes containing CF and DPX. At these concentrations, no large pores are formed by either compound. ....   | 60 |
| <b>Figure 3.18.</b> C2-ceramide <b>2</b> was added at a 15 mol% compound to lipid ratio to a buffered solution of liposomes containing CF and DPX. At this concentration, C2-ceramide forms pores in the phospholipid membrane large enough for to allow the escape of CF and/or DPX. ....  | 60 |
| <b>Figure 3.19.</b> Chloride transport assay using EYPC liposomes (100 nm, 200 $\mu\text{M}$ ) with external nitrate (100 mM $\text{NaNO}_3$ ) in 20 mM HEPES buffer (pH = 7.4). Upon addition of C2-ceramide <b>2</b> (2 $\mu\text{M}$ , 1 mol%), the increase in lucigenin fluorescence indicates $\text{Cl}^-$ efflux. Only C2-ceramide <b>2</b> promoted the anion exchange of $\text{Cl}^-/\text{NO}_2^-$ . .... | 61 |
| <b>Figure 3.20.</b> Chloride transport assay using EYPC liposomes (100 nm, 200 $\mu\text{M}$ ) with external sulfate (75 mM $\text{Na}_2\text{SO}_4$ ) in 20 mM HEPES buffer (pH = 7.4). Very little activity is observed for either compound. ....   | 63 |
| <b>Figure 3.21.</b> Stack plot from $^1\text{H}$ NMR titrations of trifluoroacetyl C2-ceramide <b>19</b> (2 mM) with increasing concentrations of TBACl in $\text{CD}_2\text{Cl}_2$ . ....  | 65 |
| <b>Figure 3.22.</b> Chloride transport assay using EYPC liposomes (100 nm, 50 $\mu\text{M}$ ) with external nitrate (100 mM $\text{NaNO}_3$ ) in 20 mM HEPES buffer (pH = 7.4). The compounds were added at a concentration of 2 $\mu\text{M}$ (4 mol%). An increase in lucigenin fluorescence indicates $\text{Cl}^-$ efflux.....  | 67 |
| <b>Figure 3.23.</b> Chloride transport assay using EYPC liposomes (100 nm, 50 $\mu\text{M}$ ) with external bicarbonate (100 mM $\text{NaHCO}_3$ ) in 20 mM HEPES buffer (pH = 7.4). The compounds were added at a concentration of 2 $\mu\text{M}$ (4 mol%). An increase in lucigenin fluorescence indicates $\text{Cl}^-$ efflux.....   | 68 |

|   |    |
|---|----|
| <b>Figure 3.24.</b> Chloride transport assay using EYPC liposomes (100 nm, 50 $\mu$ M) with external sulfate (75 mM Na <sub>2</sub> SO <sub>4</sub> ) in 20 mM HEPES buffer (pH = 7.4). The compounds were added at a concentration of 2 $\mu$ M (4 mol%). Little activity was observed for any of compounds tested.....  | 68 |
| <b>Figure 3.25.</b> CF dye release assays. C2-ceramide <b>2</b> and trifluoroacetyl C2-ceramide <b>19</b> were added EYPC liposomes containing 20 mM CF in a 10 mM HEPES buffer at pH =7. Compounds were added at a) 4 mol% and b) 50 mol%.....   | 69 |
| <b>Figure 4.1.</b> Structure of prodigiosin <b>21</b> , a proposed structure of a prodigiosin <b>21</b> ·HCO <sub>3</sub> <sup>-</sup> complex, and the structure of isophthalamide <b>38</b> .....   | 77 |
| <b>Figure 4.2.</b> <sup>13</sup> C-NMR experiments showing that prodigiosin <b>21</b> is able to facilitate Cl <sup>-</sup> /HCO <sub>3</sub> <sup>-</sup> exchange. The titration sequence for monitoring the transmembrane transport of bicarbonate ions is as follows: <sup>13</sup> C NMR spectra (i) before and (ii) after the addition of the chloride pulse to EYPC vesicles containing H <sup>13</sup> CO <sub>3</sub> <sup>-</sup> ; (iii) after the addition of prodigiosin <b>21</b> , isophthalamide <b>38</b> or DMSO blank; (iv) after the addition of Mn <sup>2+</sup> . Figure used with permission from reference <sup>206</sup> ..... | 78 |
| <b>Figure 4.3.</b> Octafluorocalix[4]pyrrole <b>39</b> facilitates Cl <sup>-</sup> /HCO <sub>3</sub> <sup>-</sup> exchange.....   | 79 |
| <b>Figure 4.4.</b> Urea- and thiourea-based compounds for the study of HCO <sub>3</sub> <sup>-</sup> transport.....   | 80 |
| <b>Figure 4.5.</b> Stack plot from <sup>1</sup> H NMR titrations of 2 mM solutions of C2-ceramide <b>2</b> with TEAHCO <sub>3</sub> in CD <sub>2</sub> Cl <sub>2</sub> . The line shows the change in the chemical shift of the C2-ceramide <b>2</b> amide –NH signal with increasing concentration of TEAHCO <sub>3</sub> .....  | 81 |
| <b>Figure 4.6.</b> Chloride transport assay using EYPC liposomes (100 nm, 200 $\mu$ m) containing Cl <sup>-</sup> and lucigenin, with external bicarbonate (100 mM) in a 20 mM HEPES buffer (pH = 7.4). C2-ceramide <b>2</b> and isopropylidene C2-ceramide <b>18</b> were added at concentrations of 1 mol % (relative to phospholipid concentration).....   | 82 |
| <b>Figure 4.7.</b> For comparison purposes, fluorescence data from the chloride transport assays using C2-ceramide <b>2</b> is plotted as a function of initial fluorescence (F <sub>0</sub> ).....   | 83 |
| <b>Figure 4.8.</b> Examples of membrane active tren-based amides.....   | 84 |
| <b>Figure 4.9.</b> a) Tren-based anion receptors <b>28-31</b> synthesized by the Gale group. b) Crystal structure of two tren <b>31</b> molecules with a single bound carbonate anion.....  | 86 |



|   |     |
|---|-----|
| <b>Figure 4.10.</b> Chloride sensitive electrode studies with tren receptors <b>28-31</b> . .....   | 87  |
| <b>Figure 4.11.</b> $^{13}\text{C}$ NMR liposome assay directly monitoring the release of $\text{H}^{13}\text{CO}_3^-$ . 88   |     |
| <b>Figure 4.12.</b> $^{13}\text{C}$ NMR evidence of $\text{H}^{13}\text{CO}_3^-/\text{Cl}^-$ exchange promoted by 4 mol% of receptors <b>28-31</b> a) before and b) after addition of a 50 mM NaCl pulse to EYPC vesicles containing 100 mM $\text{NaH}^{13}\text{CO}_3$ buffered to pH 7.4 with 20 mM HEPES, dispersed in 75 mM $\text{Na}_2\text{SO}_4$ buffered to pH 7.4 with 20 mM HEPES; c) following addition of <b>28-31</b> or DMSO; d) following addition of 0.5 mM $\text{MnCl}_2$ , a paramagnetic line broadening agent that only affects external bicarbonate. .... | 89  |
| <b>Figure 4.13.</b> a) Structurally simple urea- and thiourea-based receptors. b) Model illustrating possible complex between thiourea <b>37</b> and bicarbonate. ....  | 90  |
| <b>Figure 4.14.</b> Chloride sensitive electrode studies using compounds <b>32-37</b> . ....  | 91  |
| <b>Figure 4.15.</b> $^{13}\text{C}$ NMR evidence of $\text{H}^{13}\text{CO}_3^-/\text{Cl}^-$ exchange promoted by 4 mol% of receptors <b>32-37</b> a) before and b) after addition of a 50 mM NaCl pulse to EYPC vesicles containing 100 mM $\text{NaH}^{13}\text{CO}_3$ buffered to pH 7.4 with 20 mM HEPES, dispersed in 75 mM $\text{Na}_2\text{SO}_4$ buffered to pH 7.4 with 20 mM HEPES; c) following addition of <b>32-37</b> or DMSO; d) following addition of 0.5 mM $\text{MnCl}_2$ , a paramagnetic line broadening agent that only affects external bicarbonate. .... | 92  |
| <b>Figure 4.16.</b> Linear supramolecular polymer that traps $\text{CO}_2$ via carbamate formation. ....  | 96  |
| <b>Figure 4.17.</b> Mono-lysine <b>40</b> forms an ammonium carbamate salt <b>41</b> upon bubbling with $\text{CO}_2$ in $\text{CDCl}_3$ . ....   | 97  |
| <b>Figure 4.18.</b> Ito's 3-(1-naphthyl)propylamine <b>42</b> forms carbamic acid <b>43</b> or ammonium carbamate <b>44</b> in a solvent dependent manner. ....   | 98  |
| <b>Figure 4.19.</b> C2-ceramide <b>2</b> and sphingosine <b>3</b> . ....  | 99  |
| <b>Figure 4.20.</b> Titrations of sphingosine <b>3</b> with TBACl in $\text{CD}_2\text{Cl}_2$ give rise to small shifts in the head group protons. ....   | 100 |
| <b>Figure 4.21.</b> Initial $^{13}\text{C}$ NMR experiments to determine if sphingosine <b>3</b> promotes $\text{H}^{13}\text{CO}_3^-/\text{Cl}^-$ exchange. Sphingosine <b>3</b> does not facilitate the exchange bicarbonate with chloride under these conditions. ....   | 101 |
| <b>Figure 4.22.</b> Titration of sphingosine <b>3</b> with $\text{TEAHCO}_3$ in $\text{CD}_2\text{Cl}_2$ shows the formation of sphingosine carbamate <b>27</b> . ....  | 103 |

|   |     |
|---|-----|
| <b>Figure 4.23.</b> $^1\text{H}$ NMR spectrum following the addition of 3 eq. of TEAHCO <sub>3</sub> to a 2 mM solution of sphingosine <b>3</b> in CD <sub>2</sub> Cl <sub>2</sub> . This gives approximately a 1:1 mixture of sphingosine <b>3</b> and sphingosine carbamate <b>27</b> . ..... | 104 |
| <b>Figure 4.24.</b> $^1\text{H}$ NMR of a) sphingosine <b>3</b> , b) sphingosine carbamate <b>27</b> , and c) TEAHCO <sub>3</sub> blank in CD <sub>2</sub> Cl <sub>2</sub> . .....  | 105 |
| <b>Figure 4.25.</b> $^{13}\text{C}$ NMR of a) sphingosine <b>3</b> , b) sphingosine carbamate <b>27</b> , and c) TEAHCO <sub>3</sub> blank in CD <sub>2</sub> Cl <sub>2</sub> . .....   | 105 |
| <b>Figure 4.26.</b> CO <sub>2</sub> bubbling apparatus. ....  | 106 |
| <b>Figure 4.27.</b> $^1\text{H}$ NMR of a) CO <sub>2</sub> blank, b) sphingosine <b>3</b> , and c) sphingosine carbamate <b>27</b> following CO <sub>2</sub> bubbling in d <sub>6</sub> -DMSO. ....   | 108 |
| <b>Figure 4.28.</b> $^{13}\text{C}$ NMR of a) CO <sub>2</sub> blank, b) sphingosine <b>3</b> , and c) sphingosine carbamate <b>27</b> following CO <sub>2</sub> bubbling in d <sub>6</sub> -DMSO. ....  | 108 |
| <b>Figure 4.29.</b> Sphingosine ammonium carbamate <b>45</b> formed upon bubbling CO <sub>2</sub> through a solution of sphingosine <b>3</b> in d <sub>6</sub> -DMSO. ....  | 109 |
| <b>Figure 4.30.</b> 1 vs. 4 hours bubbling CO <sub>2</sub> through a 15 mM solution of sphingosine <b>3</b> in d <sub>6</sub> -DMSO. ....   | 110 |
| <b>Figure 4.31.</b> Model of a possible conformation of the sphingosine ammonium carbamate <b>45</b> , showing both intra- and intermolecular hydrogen bond stabilization of the carbamate. ....  | 111 |
| <b>Figure 6.1.</b> A view of UM#1807 showing the anisotropic atomic displacement ellipsoids for the non-hydrogen atoms are shown at the 25% probability level. Hydrogen atoms are displayed with an arbitrarily small radius. ....  | 128 |
| <b>Figure 6.2.</b> A view of 4 symmetrically independent molecules in the unit cell of UM#1793. Anisotropic atomic displacement ellipsoids for the non-hydrogen atoms are shown at the 30% probability level. Hydrogen atoms are displayed with an arbitrarily small radius. ....               | 131 |

## List of Schemes

|   |    |
|---|----|
| <b>Scheme 2.1.</b> General strategy for the development of ceramide pro-drugs. ....   | 23 |
| <b>Scheme 2.2.</b> Preparation of C16-pmb <b>14</b> .....   | 24 |
| <b>Scheme 2.3.</b> Preparation of C2-diacetate <b>16</b> . ....   | 29 |
| <b>Scheme 2.4.</b> CF release assay.....  | 30 |
| <b>Scheme 2.5.</b> FITC-dextran (FD10) release assay.....   | 34 |
| <b>Scheme 3.1.</b> Preparation of isopropylidene C2-ceramide <b>18</b> . ....   | 52 |
| <b>Scheme 3.2.</b> Preparation of trifluoroacetyl C2-ceramide <b>19</b> . ....  | 64 |
| <b>Scheme 4.1.</b> Equilibrium reaction starting with CO <sub>2</sub> , moving through HCO <sub>3</sub> <sup>-</sup> and ending with carbonate. The pKa values are located below the equilibrium arrows. Carbonic anhydrases (CA) enhance the rate of the CO <sub>2</sub> hydration and HCO <sub>3</sub> <sup>-</sup> dehydration reactions. .... | 73 |
| <b>Scheme 4.2.</b> Reversible carbamate formation between two primary amines and one molecule of CO <sub>2</sub> .....  | 95 |

# Chapter 1 : Bioorganic Chemistry of Sphingolipids

## 1.1 Introduction

The compounds C16-ceramide **1** and C2-ceramide **2** are sphingolipids that consist of a sphingosine **3** base connected via an amide linkage to an aliphatic fatty acid chain. Ceramides are involved in the regulation of a range of important cellular processes including cell differentiation, autophagy, cell senescence, skin water barrier homeostasis, and apoptosis.<sup>1-5</sup> Due to the fact that ceramides are so important for cell metabolism, there is a need to better understand the molecular mechanism that they use to impart function.

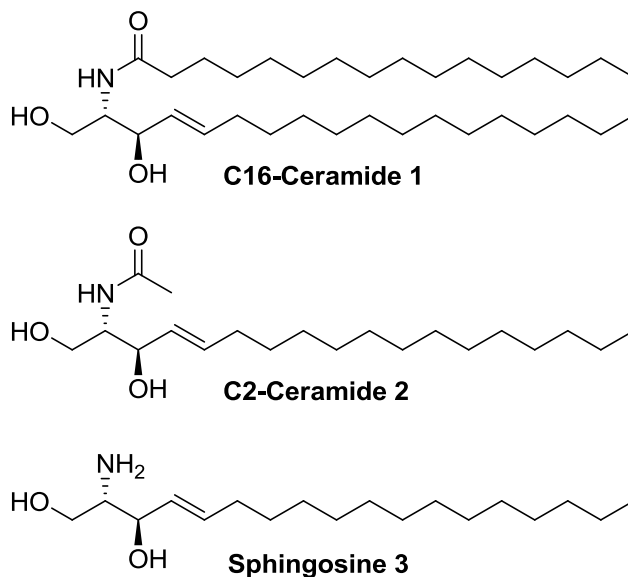


**Figure 1.1.** Structure of C16-ceramide **1**, C2-ceramide **2** and sphingosine **3**.

The role of ceramide in apoptosis sparked our interest in the amphiphilic natural product. One key finding is that the apoptotic activity of ceramide may be due to its ability to permeabilize lipid membranes.<sup>6</sup> It is proposed that ceramides may induce apoptosis via self-assembly into large pores that span phospholipid membranes.<sup>7</sup> This thesis, “Bioorganic Chemistry of Sphingolipids: Pore Formation and Anion Transport” describes the discovery of a new ceramide analog that forms large pores in phospholipid membranes, as well as discovery that the natural product ceramide can facilitate the transmembrane transport of anions below pore forming concentrations.

## 1.2 Thesis Organization

This thesis is organized into six chapters. One initial goal of this work was to develop ceramide analogs that possess potential anti-tumor properties. This work led to the discovery of a ceramide analog that is more active in forming pores in phospholipid membranes than natural ceramide. Additionally, we have discovered that ceramide facilitates the transmembrane transport of anions under physiologically relevant conditions.

The discussion in **Chapter 1** focuses on the bioorganic chemistry of various sphingolipids along the ceramide metabolic pathway. Implications of ceramide in genetic diseases and apoptosis will be briefly discussed, as well as examples of synthetic ceramide mimics with interesting membrane properties. The general introduction in **Chapter 1** will be brief, as more tailored introductory portions precede each chapter. **Chapter 2** focuses on the discovery of a ceramide analog with

increased membrane activity in terms of transmembrane pore formation. Insights into the role of ceramides 1,3-diol in the self-assembly into channels will be discussed. In **Chapter 3**, I discuss studies uncovering a new function for ceramide, at concentrations where transmembrane pores are not formed. We have discovered that ceramide belongs to a very small group of natural products that facilitate the transmembrane transport of anions. **Chapter 4** focuses on the development of various compounds that function as transmembrane bicarbonate transporters. **Chapter 5** describes future directions. Finally, **Chapter 6** contains the experimental protocols used for the research described in **Chapters 2-4**.

### 1.3 Biosynthesis of Sphingosine and Ceramide

The formation of ceramide is catalyzed by membrane-bound enzymes in the endoplasmic reticulum.<sup>8</sup> The first step in the biosynthesis of sphingolipids is the serine palmitoyltransferase catalyzed condensation of L-serine and palmitoyl-CoA (**Figure 1.2**).<sup>9-11</sup> The resulting 3-ketosphinganine is stereoselectively reduced by 3-ketosphinganine reductase to generate sphinganine, which is then acylated with a fatty acid chain by sphinganine N-acyl transferase to give dihydroceramide. A *trans* double bond is then regioselectively introduced by dihydroceramide desaturase. The resulting ceramides can be a mixture of analogs with varying chain lengths at the amide linkage. While ceramides have been found in nature with N-acyl fatty acids ranging from 2 to 28 carbons in length, C16-ceramide **1** is the major species present in humans.<sup>10,12</sup> Interestingly, sphingosine **3** is not directly produced from sphinganine, and is only generated from the degradation of ceramide **1** by ceramidase.

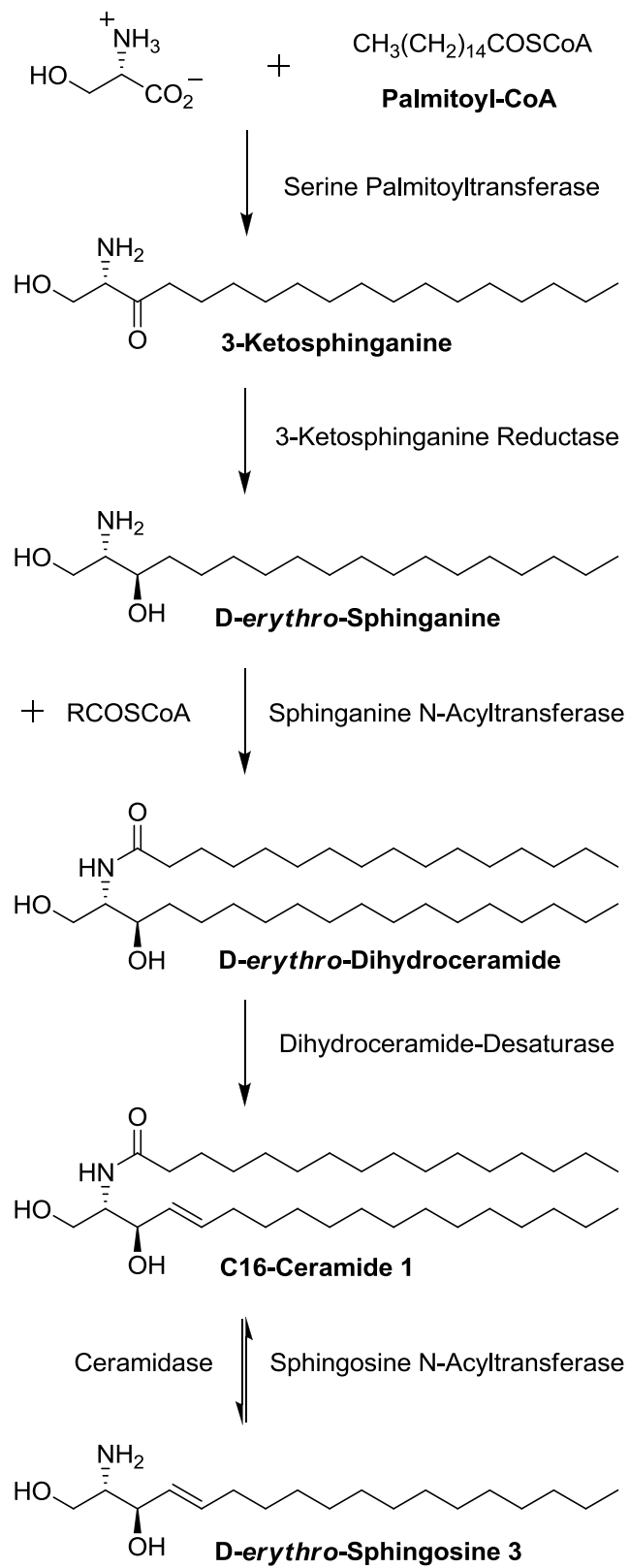


**Figure 1.2.** Biosynthesis of C16-ceramide 1 and sphingosine 3.

## 1.4 Sphingolipids and Disease

The sphingolipidoses are a group of inherited diseases that are included in the larger group of lysosomal storage diseases.<sup>13,14</sup> Sphingolipidoses are caused by defects in genes that encode for proteins involved in the lysosomal degradation of sphingolipids.<sup>15-17</sup> There are about 40 genetically different forms of lysosomal storage diseases known, of which at least 9 are due to the defective sphingolipid degradation (**Table 1.1**).<sup>14,17</sup> Sphingolipidoses are characterized by the build-up of unmetabolized sphingolipids within cells. For instance, Farber lipogranulomatosis (Farber disease) is caused by a deficiency of lysosomal ceramidase, and subsequent storage of unmetabolized C16-ceramide **1** in the lysosome.<sup>18</sup> This causes C16-ceramide **1** to build-up in the lungs, liver, skeletal muscle joints, and bones.<sup>4</sup> The most common symptoms include progressive and painful joint deformations, problems breathing, and subcutaneous nodules called lipogranulomas.<sup>19</sup> Interestingly, the build-up of ceramide caused by Farber disease does not cause apoptosis or other cell-signaling responses associated with C16-ceramide **1**.<sup>20</sup>



**Table 1.1.** Diseases caused by misregulation of sphingolipids

| <b>Disease</b>                      | <b>Misregulated Sphingolipid</b> | <b>Defective Protein</b>                   | <b>Ref.</b> |
|-------------------------------------|----------------------------------|--|-------------|
| Farber                              | C16-ceramide <b>1</b>            | Ceramidase                                 | 18-20       |
| Moriquio B                          | GM1-ganglioside                  | GM1- $\beta$ -galactosidase                | 21,22       |
| Tay-Sachs<br>Sandhoff<br>AB Variant | GM2-ganglioside                  | $\beta$ -Hexosaminidase                    | 23-28       |
| Neimann-Pick                        | Sphingomyelin                    | Sphingomyelinase                           | 29-32       |
| Gaucher                             | Glucosylceramide                 | Glucosylceramide- $\beta$ -glucosidase     | 33-37       |
| Fabry                               | Globotriaosylceramide            | $\alpha$ -Galactosidase A                  | 38-40       |
| Krabbe                              | Galactoceramide                  | Galactosylceramide- $\beta$ -galactosidase | 41-43       |

### **1.5 Ceramide Induced Apoptosis via Membrane Permeation**

While ceramide and similar sphingolipids have implications in a variety of disease states, our interest in these sphingolipids stems from the ability of C16-ceramide **1** and C2-ceramide **2** to induce apoptosis. Studies have shown that endogenous ceramide levels increase in cells just before undergoing apoptosis.<sup>44-46</sup> Additionally, C16-ceramide **1** has been shown to cause membrane destabilization through leakage and fusion of vesicles.<sup>6</sup> Aggregation and fusion of ceramide rich liposomes were detected as an increase in light scattering of the liposomal mixture. The cause of membrane destabilization remained unknown until Colombini and Siskind discovered that both C16-ceramide **1** and C2-ceramide **2** form large, stable channels in planar phospholipid membranes.<sup>7</sup> **Figure 1.3** shows a representative

trace from electrophysiological planar membrane studies on C16-ceramide **1**. Colombini observed specific opening and closing events in these studies that are characteristic of channel formation and subsequent collapse. Interestingly, C16-dihydroceramide, which lacks the *trans* double bond of C16-ceramide **1**, shows no activity in this assay under the same conditions. In fact, Colombini has also shown that C16-dihydroceramide actually interferes with the ability of C16-ceramide **1** to self-assemble into an active pore.<sup>47</sup> This information suggests that the *trans* double bond of C16-ceramide **1** is structurally important for the formation of transmembrane channels, perhaps by providing some degree of conformational rigidity.

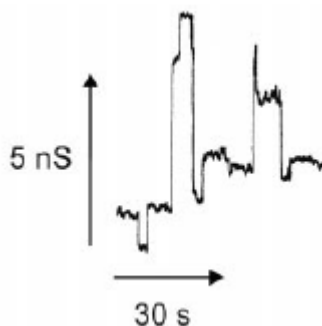


**Figure 1.3.** C16-ceramide **1** forms pores in planar phospholipid membranes. Figure used with permission from reference 7.

Additionally, Colombini discovered that when C16-ceramide **1** and C2-ceramide **2** were added to mitochondrial suspensions, they could induce the release of the apoptosis-inducing cytochrome *c*.<sup>48</sup> These ceramide pores not only allowed the release of the 12 kDa cytochrome *c*, but also increased the permeability of the mitochondrial outer membrane to other small proteins with a molecular weight of less than 60 kDa.<sup>49</sup> These studies suggest that ceramide self-assembly into pores in the mitochondrial outer membrane, and the subsequent release of cytochrome *c*, may be

the reason that C16-ceramide **1** induces apoptosis in natural systems. A more detailed description of the putative transmembrane channels formed by C16-ceramide **1** can be found in **Section 2.2** and **2.3** of this dissertation.

## **1.6 Membrane-Active Synthetic Ceramide Analogs**

There has been a large amount of work published on synthetic ceramide analogs that have been used to specifically investigate sphingolipid metabolism and function. Recent reviews by Delgado,<sup>11,50</sup> Kolter,<sup>9</sup> Bittman,<sup>51</sup> and Hermetter<sup>52</sup> provide excellent discussions on this subject. For the purposes of this introductory chapter, I will focus on ceramide mimics and synthetic lipids that either form pores or facilitate the transport of ions across phospholipid membranes, or that are specifically shown to induce apoptosis, as this research is most pertinent to the research described in this dissertation.

### **1.6.1 Gokel's Ceramide Mimics**

Research in the lab of George Gokel has produced a series of C16-ceramide mimics **4-7** that contain two lipophilic tails connected to a –OH containing headgroup via an amide linkage.<sup>53</sup> Results from liposome assays suggest that compounds **5** and **7** form pores in phospholipid membranes.

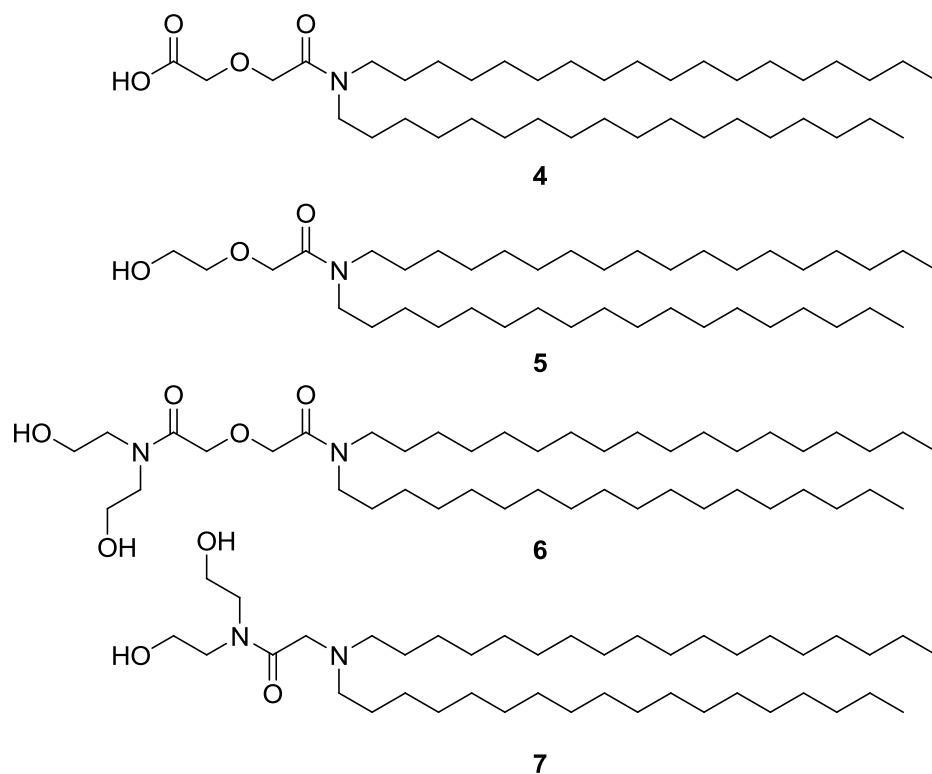


**Figure 1.4** C16-ceramide mimics **4-7**.

C16-ceramide mimics **4-7** were tested in chloride release assays using the chloride sensitive fluorescent dye lucigenin. Liposomes were prepared containing lucigenin and KCl. In the presence of  $\text{Cl}^-$ , the fluorescence of lucigenin is quenched. Upon the transport of intravesicular  $\text{Cl}^-$  out of the liposome, an increase in lucigenin fluorescence is observed. C16-ceramide mimics **4** and **6** were not active in this assay as they showed little activity above the baseline fluorescence. Upon the addition of compounds **5**, **7**, or C16-ceramide **1**, an increase in fluorescence was observed. Compound **5** was approximately as effective as C16-ceramide **1** at releasing chloride from the liposomes, while compound **7** was more active than C16-ceramide **1** in this assay.

Additionally, Gokel tested compounds **5-7** in a carboxyfluorescein release liposomal assay. Carboxyfluorescein is a small organic dye with an approximate diameter of 10 Å that self-quenches at high concentrations.<sup>54</sup> Liposomes were prepared containing carboxyfluorescein at self-quenching concentrations. Upon the addition of compounds **5-7**, an increase in fluorescence was observed corresponding to the carboxyfluorescein release, and subsequent dilution into the extravesicular buffer. C16-ceramide mimic **7** was significantly more active in this assay than were compounds **5** and **6**.

While it is clear from these experiments that Gokel's C16-ceramide mimics **5** and **7** do form pores in phospholipid membranes, there are some flaws in his interpretation of the results from the chloride transport assays. He suggests that C16-ceramide **1** and compounds **5** and **7** act as chloride transporters. However, the concentration of compounds he used in these assays (15 mol%) was well above known ceramide pore forming concentrations (10 mol%).<sup>3,55</sup> In this case, he is presumably observing chloride release due to large transmembrane pore formation, and not by anion specific transport.

### 1.6.2 Bieberich's Ceramide Mimic

Work in the Bieberich lab has shown that C16-serinol **7**, a C16-ceramide **1** mimic, induces apoptosis when added to cancerous neuroblastoma cells.<sup>56</sup> Structurally, C16-serinol **8** is similar to C16-ceramide **1** in that it contains a lipophilic tail attached to a polar headgroup via an amide linkage (**Figure 1.5**). Additionally, the polar head group of C16-serinol **8** is similar to that of C16-ceramide in that it

contains two –OH groups. The only major structural difference is the lack of a second hydrophobic tail that contains the *trans* double bond associated with the sphingolipid base.

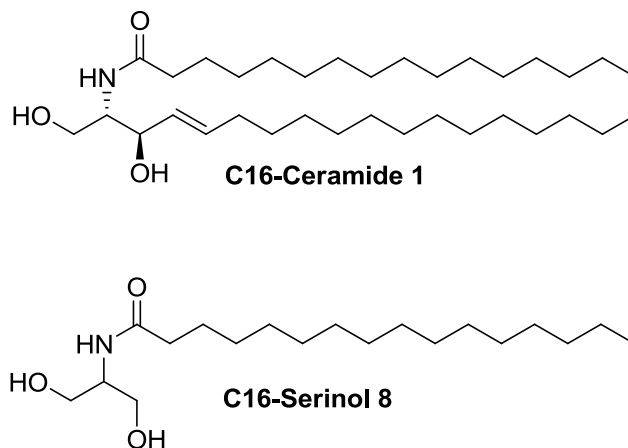


**Figure 1.5.** Structural similarities between C16-ceramide **1** and C16-serinol **8**.

While the Bieberich lab tested a variety of chain lengths ranging from C8- to C18-serinol, they found that C16-serinol **8**, containing the same length tail as C16-ceramide **1**, was the most effective at inducing apoptosis in neuroblastoma cells. They found that addition of C16-serinol **8** to these cancerous cells caused an increase in endogenous C16-ceramide **1** levels. Based on this information, they speculated that C16-serinol **8** induced apoptosis stems from the competitive inhibition of acid ceramidase, the enzyme that breaks down C16-ceramide **1** into sphingosine **3** (**Figure 1.2**). The build-up of endogenous C16-ceramide **1**, either through signaling pathways or through mitochondrial pore formation, induced apoptosis in the neuroblastoma cells.

### 1.6.3 Chanturiya's Sphingomyelin Mimic

Sphingomyelin **9** is the phospholipid version of C16-ceramide **1**. It is produced endogenously from C16-ceramide **1** and sphingomyelin synthase. Misregulation of sphingomyelin has implications in the onset of Niemann-Pick disease (Table 1.1), as well as ulcerative colitis and atherosclerosis.<sup>10,57</sup> Research from the lab of Chanturiya describes the development of a cationic sphingomyelin mimic **10** that form pores in phospholipid bilayers.<sup>58</sup>

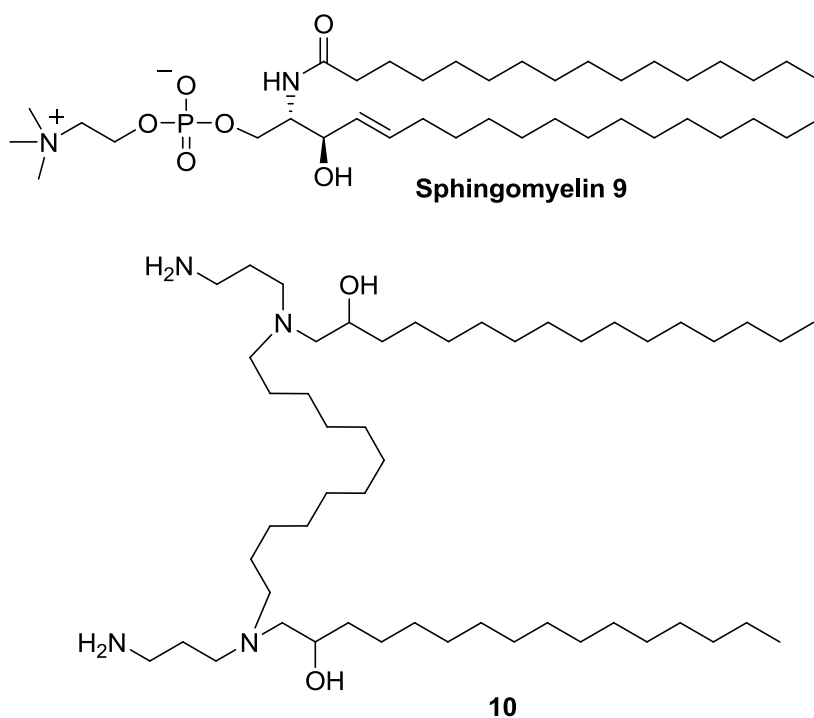


**Figure 1.6.** Sphingomyelin **9** and a synthetic sphingomyelin mimic **10**.

The membrane-active sphingomyelin mimic **10** reported by Chanturiya is a dimer of two sphingomyelin mimic units connected via a dodecyl acyl chain. Each monomer possesses two –OH units, as well as two primary amines and two tertiary amines comprising the amphiphilic headgroup. Under physiological conditions, the

amines are presumably protonated yielding a cationic lipid. When compound **10** was added to planar phospholipid membranes, discrete opening and closing events were observed. Additionally, reverse potential experiments using sphingomyelin mimic **10** suggested that the channels formed by this compound were selective for anions.

#### 1.6.4 Macchia and Danesi's Lipophilic Nucleobase Ceramide Mimics

In an attempt to develop new and better apoptosis-inducing drugs, Macchia and Danesi developed an interesting example of a conformationally restrained C2-ceramide **2** analog.<sup>59</sup> In their studies, Macchia and Danesi replaced the polar headgroup region of ceramide with a uracil **11** or thiouracil **12** nucleobase.

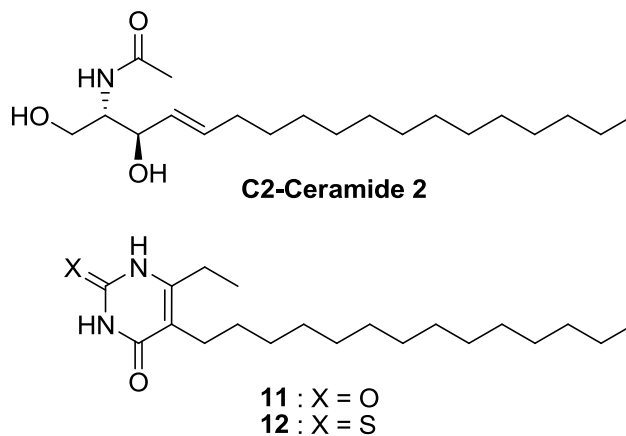


**Figure 1.7.** C2-ceramide **2** analogs utilizing the nucleobases uracil **11** and thiouracil **12** as the polar headgroup region.

These constrained analogs and C2-ceramide **2** were tested in their ability to inhibit cell growth in leukemia cells. Compounds **11** and **12** proved to be significantly more active than C2-ceramide **2** in regards to inhibition of cell proliferation in the leukemia cell line tested. The thiouracil analog **12** was the most active ( $IC_{50} = 1.7 \mu\text{M}$ ), followed by the uracil analog **11** ( $IC_{50} = 7.9 \mu\text{M}$ ). C2-



ceramide **2** was the least active of the three, with an  $IC_{50} = 31.6 \mu\text{M}$ . Additionally, all three compounds were added to leukemia cells at concentrations ( $50 \mu\text{M}$ ) well above the  $IC_{50}$  values to test for the release of cytochrome c. All three compounds induced cytochrome c release before the onset of apoptosis, with the thiouracil analog **12** being the most active, and C2-ceramide **2** being the least active. This is the first study to use lipophilic nucleobases as ceramide mimics. While the polar headgroup is altered significantly in these analogs when compared to that of C2-ceramide **2**, one could envision that the hydrogen-bonding motifs inherent in the uracil nucleobase may also assist in the self-assembly into transmembrane pores in a similar manner to that of ceramide.

### 1.6.5 Smith's Synthetic Lipid that Transports Anions via a Relay Mechanism

While not directly a ceramide mimic, Brad Smith and coworkers have developed a synthetic phospholipid with interesting membrane properties.<sup>60</sup> They designed an anion transporter with an anion recognition unit (urea) attached at the end of one of the phospholipid acyl chains to give compound **13**.

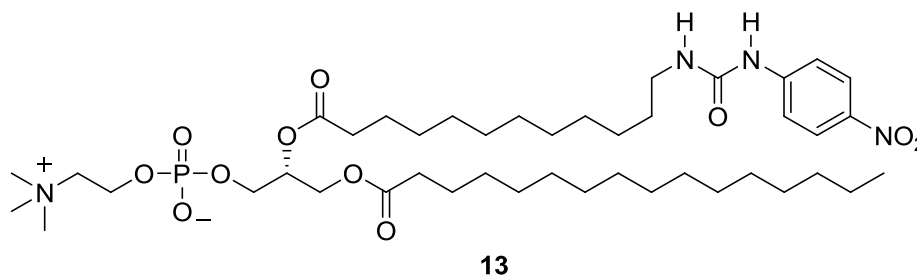


**Figure 1.8.** Smith's synthetic phospholipid anion transporter **13**.

Smith and coworkers initially studied the ability of compound **13** to facilitate anion transport across phospholipid membranes. Liposomes were prepared containing  $\text{NO}_3^-$  and lucigenin, a  $\text{Cl}^-$  sensitive fluorescent dye. Compound **13** was pre-incorporated into the phospholipid bilayer during liposome preparation. Upon the addition of extravesicular  $\text{Cl}^-$ , a decrease in fluorescence was observed corresponding to  $\text{Cl}^-$  influx into the liposomes. However, when  $\text{SO}_4^{2-}$  was used as the intravesicular anion, the rate of  $\text{Cl}^-$  influx was greatly reduced. This is consistent with an anion exchange mechanism in that  $\text{Cl}^-$  influx only occurs with the concurrent efflux of another monovalent anion. Sulfate anion is more hydrophilic and therefore not as easily transported as the singly charged chloride or nitrate anions.

Additionally, Smith proposed a relay mechanism as the method in which phospholipid **13** functions as an anion transport agent (**Figure 1.9**). He gives two main arguments to support his proposed mechanism. First, when compound **13** is not pre-incorporated into the liposomal membrane, no  $\text{Cl}^-$  transport was observed. For anion transport to occur via the proposed relay mechanism, compound **13** is not of sufficient length to span the entire membrane, and must reside in both the inner and outer leaflets of the phospholipid bilayer in order for transport to occur. Thus, without pre-incorporation, compound **13** could not equilibrate into both layers of the liposomal bilayer membrane within the experimental timeframe. Smith suggests that this provides initial evidence for a relay mechanism such as depicted in **Figure 1.9**, as this mechanism requires compound **13** to reside in both the inner and outer leaflets of the phospholipid bilayer. However, this result is not a particularly convincing argument in support of this proposed relay mechanism. For instance, another possible

explanation would be that when compound **13** was added to the external buffer containing the liposomes, it simply precipitated out of solution and therefore was never incorporated into the liposomes at all. Another possible explanation is that compound **13** may aggregate with itself into some sort of micelle type structure when added to the extravesicular buffer. In this case, insertion into the liposomal membrane could be slowed to the point that no activity was observed within the experimental timeframe.

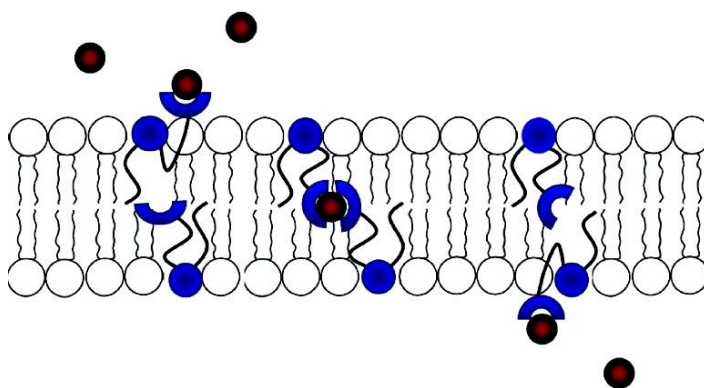


**Figure 1.9.** Proposed anion transport relay mechanism for compound **13**. Figure used with permission from reference 60.

However, Smith offered a second, more convincing argument for his proposed relay mechanism. For these experiments, liposomes were prepared using phospholipids of varying lengths. Chloride transport by compound **13** decreased as bilayer thickness increased. When the acyl carbon chain of the bilayer phospholipids was increased from 14 to 18, a sharp decrease in anion transport was observed. No transport was observed when the bilayer phospholipid chain length was above 18. Since compound **13** has an acyl chain length of 15, Smith concluded that it was not long enough to span each leaflet of the bilayer according to the proposed relay mechanism. The increased bilayer thickness created a gap between the urea

recognition units within each bilayer leaflet, thus shutting down the relay of Cl<sup>-</sup> from **13** in one leaflet to another molecule of **13** on the other leaflet.

## **1.7 Summary**

Ceramide is an amphiphilic natural product with implications in multiple disease states and cellular processes, including apoptosis. Ceramide's role in apoptosis may arise from its ability to permeabilize membranes. One possible way in which ceramide induces apoptosis is through self-assembly into large pores in the mitochondrial outer membrane. Pores formed by ceramide are large enough to release the apoptosis-inducing cytochrome c. A number of ceramide mimics have been developed in order to take advantage of the membrane properties of this unique amphiphile. In this thesis, I will discuss a new ceramide analog that is more active than naturally occurring ceramide in terms of forming large pores in phospholipid membranes. Additionally, I will describe a newly discovered function of ceramide that has implications in the regulation of the transmembrane transport of anions in natural systems.

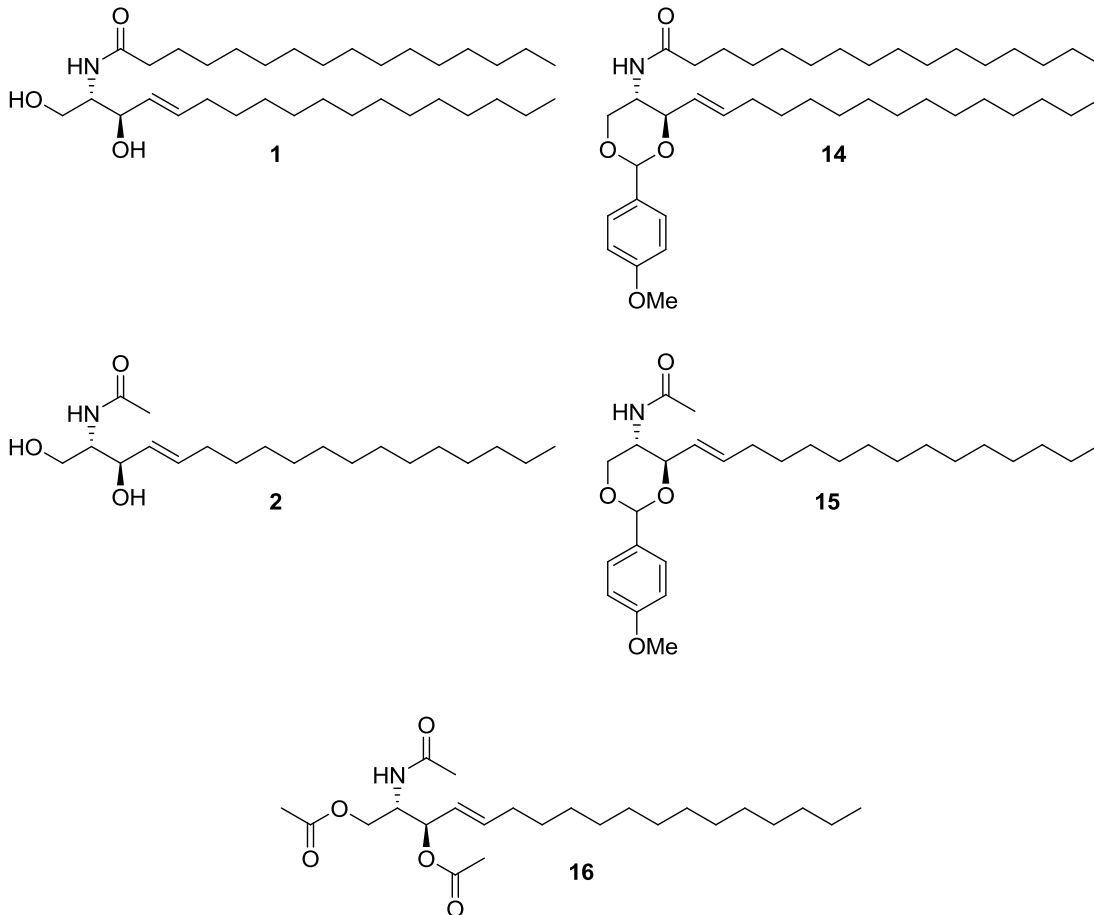
## **Chapter 2 : C2-Ceramide Diacetate Forms Large Pores in Phospholipid Membranes**

*Some of the experimental work described in this chapter was performed in collaboration with Dr. Marco Colombini in the Department of Biology at the University of Maryland. Dr. Peter Y. Zavalij determined the crystal structure of C2-pmb 15 that is described in this chapter.*

### **2.1 Introduction**

One original goal of the research described in this dissertation was the preparation and development of ceramide analogs that possess potential anti-tumor properties. Ceramide **1** is known to play important roles in the regulation of multiple cellular processes, including cytosolic protein phosphatase activation, cell differentiation and apoptosis.<sup>1-3,61,62</sup> Using pH sensitive modifications to the ceramide head group, we hoped to render ceramide “inactive” until it reached the target cell or organelle. This work also explores the role of the 1,3-diol unit in the self-assembly of ceramide into membrane-active structures using protected ceramide analogs **14-16 (Chart 2.1)**.

**Chart 2.1**



## 2.2 Ceramide Pores Allow the Release of Apoptosis-Inducing Cytochrome C

In 1976, Pascher indicated that ceramides may perturb membrane permeability.<sup>63</sup> Based on solid state structures of C16-ceramide **1**, he suggested that ceramide may increase permeability of membranes if the head group hydroxyls participated in hydrogen bonding with water molecules. Pascher postulated that this could destabilize the membrane by either slightly pulling ceramide molecules away from the membrane layer, or by increasing the molecular area at the membrane interface. Additionally, separation into ceramide-rich domains in lipid bilayers was

observed by Huang and coworkers.<sup>64</sup> Using <sup>2</sup>H NMR and deuterated liposomes, Huang observed that ceramide induces lateral phase separation of the bilayers into liquid crystalline phases and ceramide-rich gel phases. More recently, Johnston and coworkers observed these ceramide-rich domains on lipid monolayers using atomic force microscopy.<sup>65</sup> Johnston found that the edges of these ceramide-rich domains are raised above the surrounding monolayer by ~1 nm.

Ceramide has also been shown to cause membrane destabilization through leakage and fusion of vesicles.<sup>6</sup> Aggregation and fusion of ceramide rich liposomes were detected as an increase in light scattering of the liposomal mixture. The cause of membrane destabilization remained unknown until Colombini and Siskind discovered that both C16-ceramide **1** and C2-ceramide **2** form large, stable channels in planar phospholipid membranes.<sup>7</sup> When added to mitochondrial suspensions, ceramide has been shown to induce the release of apoptosis-inducing cytochrome c.<sup>48</sup> The ceramide pores not only allowed the release of the 12 kDa cytochrome c, but increased the permeability of the mitochondrial outer membrane to other small proteins that had a molecular weight of less than 60 kDa.<sup>49</sup>

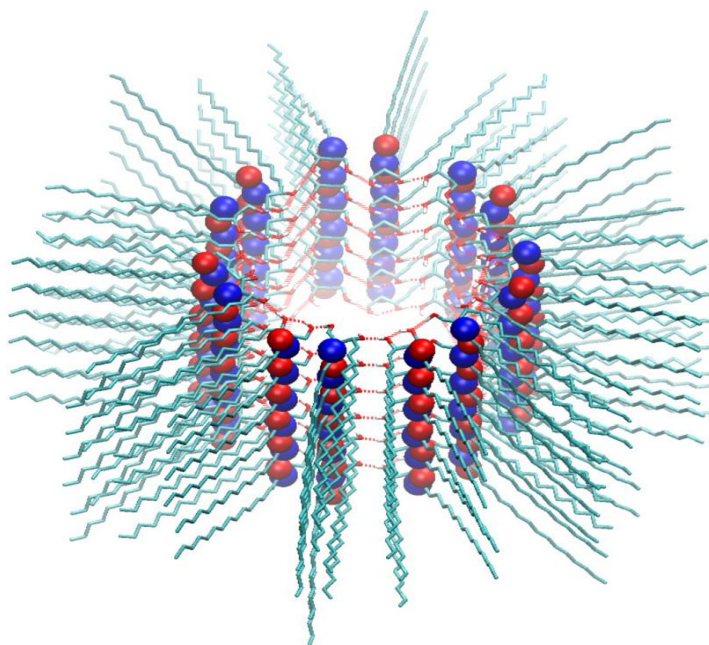


**Figure 2.1.** Molecular dynamics simulation of a C16-ceramide 1 nanopore. Figure used with permission from reference 66.

### **2.3 The Role of Ceramides 1,3-Diol Unit in Pore Formation**

Although it is known that ceramide forms large pores in phospholipid membranes, the actual self-assembled structure of the pore is still unknown. While there is little experimental evidence available, molecular dynamics simulations by Columbini, Sukharev and colleagues suggest a possible membrane-active structure.<sup>66</sup> They propose that barrel-rosette type channels are formed by self-assembly of multiple ceramide subunits, and that these structures are stabilized by hydrogen bonds (**Figure 2.1**). A closer look at the structure of the putative pore reveals that the internal wall of the pore may be composed of a hydrogen bonding array involving the 1,3-diol unit of ceramide (**Figure 2.2a**). This suggests that the 1,3-diol functionality of ceramide plays an integral role in pore self-assembly. Additional stabilization of



these self-assembled pores was proposed to be found in a column of hydrogen bonds between the carbonyl oxygen and the –NH of neighboring amides (**Figure 2.2b**)

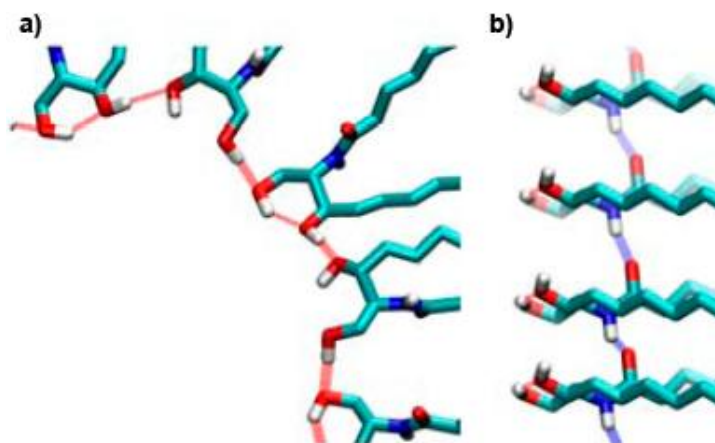
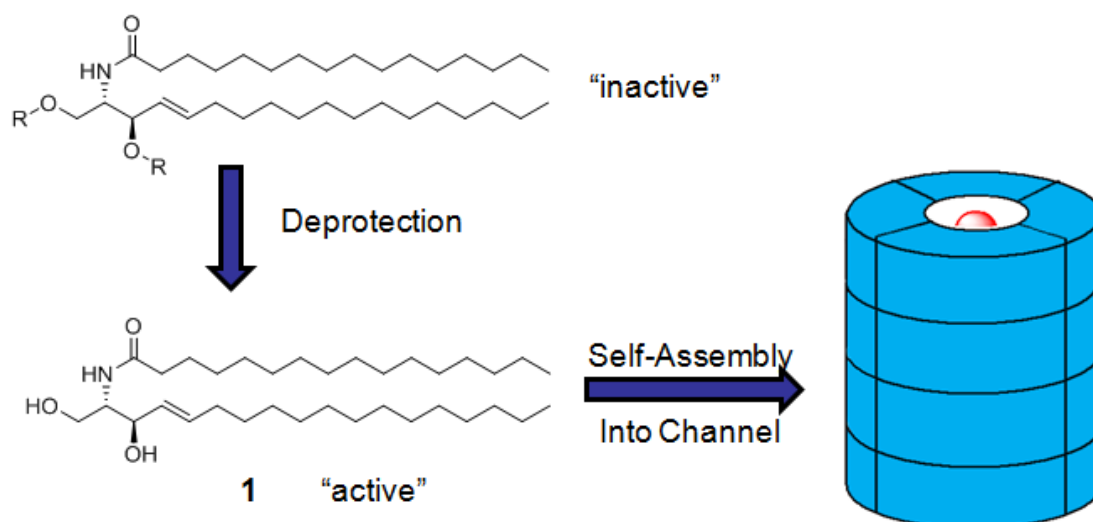


**Figure 2.2.** a) Hydrogen bonding of the 1,3-diol unit of C16-ceramide **1** helps form the inner wall of the pore. b) Vertical columns of ceramides held together by amide hydrogen bonding. Figure used with permission from reference 66.

## 2.4 Protected Ceramide Analogs as Potential Pro-Drugs

One original goal of this project was to prepare C16-ceramide **1** analogs with pH sensitive protecting groups that masked the 1,3-diol unit for potential use as anti-tumor agents. Additionally, these analogs with protected diols could be used to study the role of ceramide's 1,3-diol unit in the self-assembly and stabilization of transmembrane pores. By protecting the 1,3-diol of C16-ceramide **1**, we hoped to render the compound inactive in terms of its ability to self-assemble into functional pores. Upon deprotection, active ceramide would then be free to self-assemble into its membrane active structure (**Scheme 2.1**).

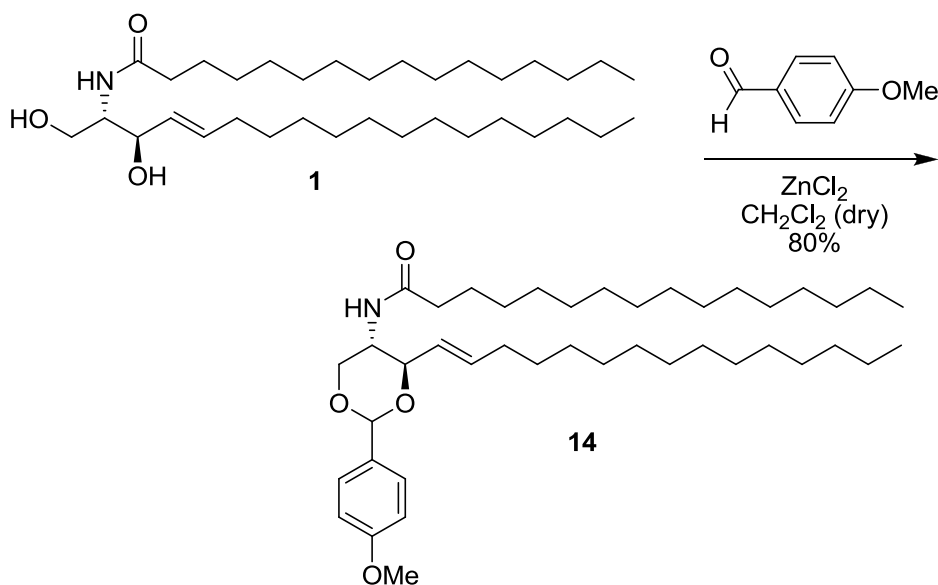


**Scheme 2.1.** General strategy for the development of ceramide pro-drugs.

There are many different strategies being developed to deliver drugs to cancerous cells. These drug delivery vehicles include carbon nanotubes, gold nanoparticles, and liposomes.<sup>67-69</sup> The one thing these all have in common is that the drug delivery vehicles are ingested into the target cell via endocytosis. In the final phase of endocytosis, lysosomes engulf the drug and fuse with the phospholipid membrane of the cell, releasing the contents of the lysosome into the cell.<sup>70</sup> With a pH ~5, the lysosome is relatively acidic when compared to physiological pH (7.4). In fact, folate-conjugated polymer micelles have recently been developed with this in mind.<sup>71</sup> These micelles have increased drug release rates at pH 5. This is why acid labile protecting groups were originally chosen to block the 1,3-diol unit of ceramide. Upon ingestion by the lysosome, we reasoned that deprotection could produce active ceramide, which would then be able to self-assemble into pores and induce apoptosis.

## 2.5 Preparation of a *p*-Methoxybenzylidene C16-Ceramide Analog

In order to block the 1,3-diol unit of C16-ceramide **1**, we first chose to use acid-labile acetal protecting groups. Starting with C16-ceramide **1**, *p*-methoxybenzylidene C16-ceramide (C16-pmb **14**) was prepared in one step. Thus, C16-ceramide **1** was reacted with *p*-anisaldehyde in the presence of a Lewis acid catalyst, ZnCl<sub>2</sub>, giving C16-pmb **14** in 80% yield following purification (**Scheme 2.2**). The <sup>1</sup>H NMR spectrum of C16-pmb **14** in CDCl<sub>3</sub> shows the appearance of the aromatic protons and the –CH<sub>3</sub> of the *p*-methoxybenzylidene protecting group, as well as the loss of the –OH groups and an upfield shift approximately δ 1.30 ppm of the amide –NH proton (**Figure 2.3**). This upfield shift is presumably due to a disruption of intramolecular hydrogen bonding between the amide –NH and the neighboring –OH oxygen due to conformational restriction imposed by the newly formed acetal.



**Scheme 2.2.** Preparation of C16-pmb **14**.

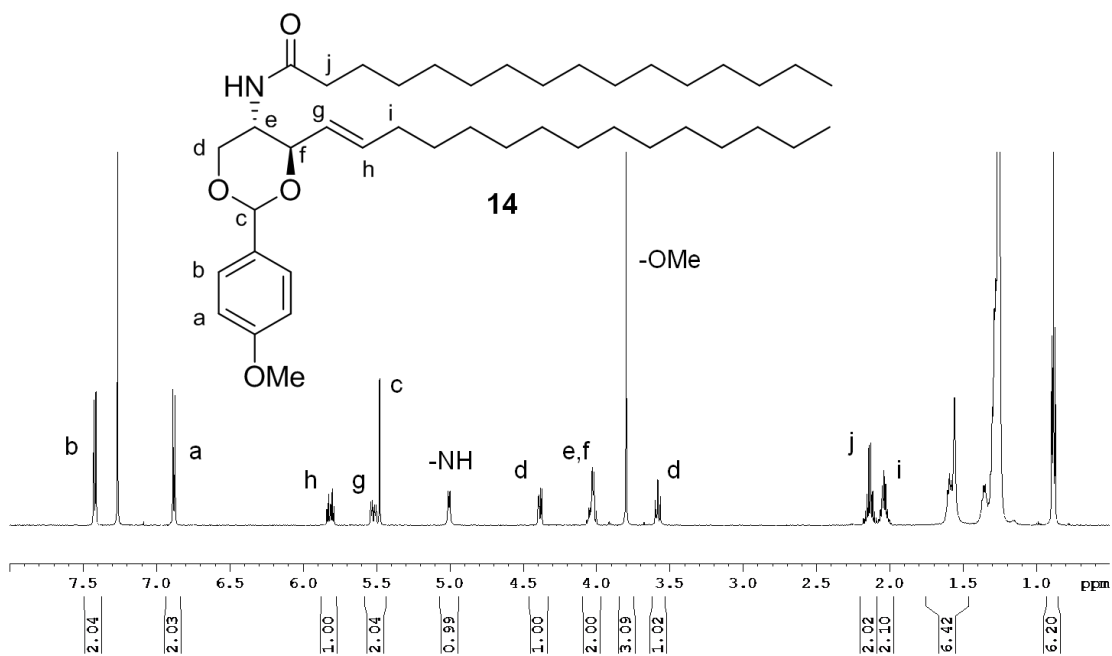


**Figure 2.3.** <sup>1</sup>H NMR spectrum of C16-pmb **14** in CDCl<sub>3</sub>.

## 2.6 Mitochondrial Permeabilization Assay

In order to determine if protecting the 1,3-diol unit of C16-ceramide **1** with a *p*-methoxybenzylidene acetal would render it inactive, C16-pmb **14** was subjected to mitochondrial permeabilization assays.<sup>47,49</sup> These experiments were done in collaboration with Meenu Perera, Kevin Yang and Dr. Marco Colombini in the Department of Biology at the University of Maryland. Purified rat liver mitochondria suspensions were incubated with either C16-ceramide **1** or C16-pmb **14**. Reduced cytochrome c was then added to the mitochondria/ceramide solution. If pores are formed that are large enough to allow the reduced cytochrome c to enter the mitochondria, then the reduced protein becomes oxidized by the cytochrome c oxidase that resides inside the mitochondria. The rate of oxidation of the reduced

cytochrome c is monitored as a decrease in absorbance of the reduced cytochrome c at 550 nm.

**Figure 2.4** compares the ability of C16-ceramide **1** and the protected derivative, C16-pmb **14** to permeabilize mitochondrial membranes to cytochrome c. C16-ceramide **1** allowed cytochrome c to cross the mitochondrial outer membrane, while C16-pmb **14** alone showed significantly less activity in this assay. This suggests that the 1,3-diol unit plays an important role in C16-ceramide **1** self-assembling into a transmembrane pore. Interestingly, when a 1:1 equimolar mixture of the two compounds were added to mitochondrial suspensions, the rate of cytochrome c oxidation was close to that of C16-ceramide **1** alone. This last result suggests that C16-ceramide **1** and C16-pmb **14** may work in a cooperative manner in order to form membrane-active structures. This result was encouraging with regards to using C16-pmb **14** as a potential anti-tumor pro-drug in that only a small amount of the acetal analog may need to be deprotected in order to induce the release of cytochrome c from the mitochondria.

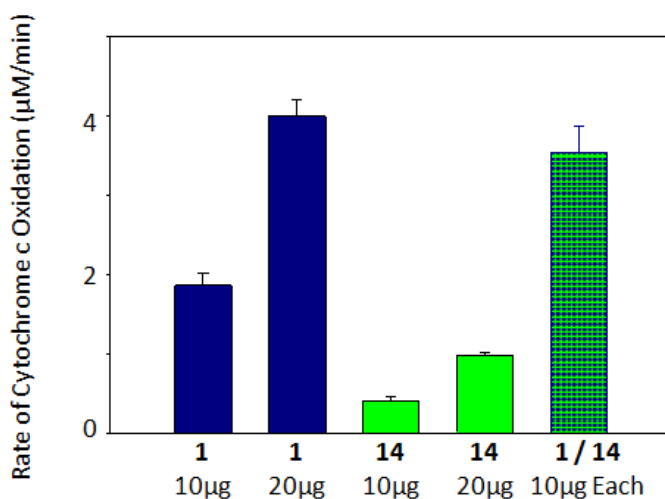


**Figure 2.4.** Mitochondrial permeability assay comparing C16-ceramide **1** and C16-pmb **14**.

While these initial results were encouraging, liposome assays were unable to be carried out using these C16 chain compounds due to solubility issues in many common solvents, including DMSO. In order to develop compounds that were easier to work with, analogs were prepared using the short-chain C2-ceramide **2**. Indeed, these short-chain analogs displayed much better solubility in a variety of solvents.

## 2.7 Preparation of C2-Ceramide 2 Analogs

In order to prepare ceramide analogs that are soluble in DMSO, C2-ceramide **2** was used as the starting material. Using the same preparation as described above for the C16-pmb **14** analog, the *p*-methoxybenzylidene C2-ceramide (C2-pmb **15**) was made in 67 % yield after purification. The X-ray structure for crystals of C2-pmb **15** grown from DMSO can be seen in **Figure 2.5**. Hydrogen bonds are observed between the –NH of one molecule of C2-pmb **15** with the carbonyl oxygen of an adjacent molecule. This solid state evidence of amide hydrogen bonding supports the idea from molecular dynamics simulations by Colombini and Sukharev (**Figure 2.2b**) that columns of hydrogen bonded amides may stabilize the membrane-active structure of ceramide pores.<sup>66</sup>

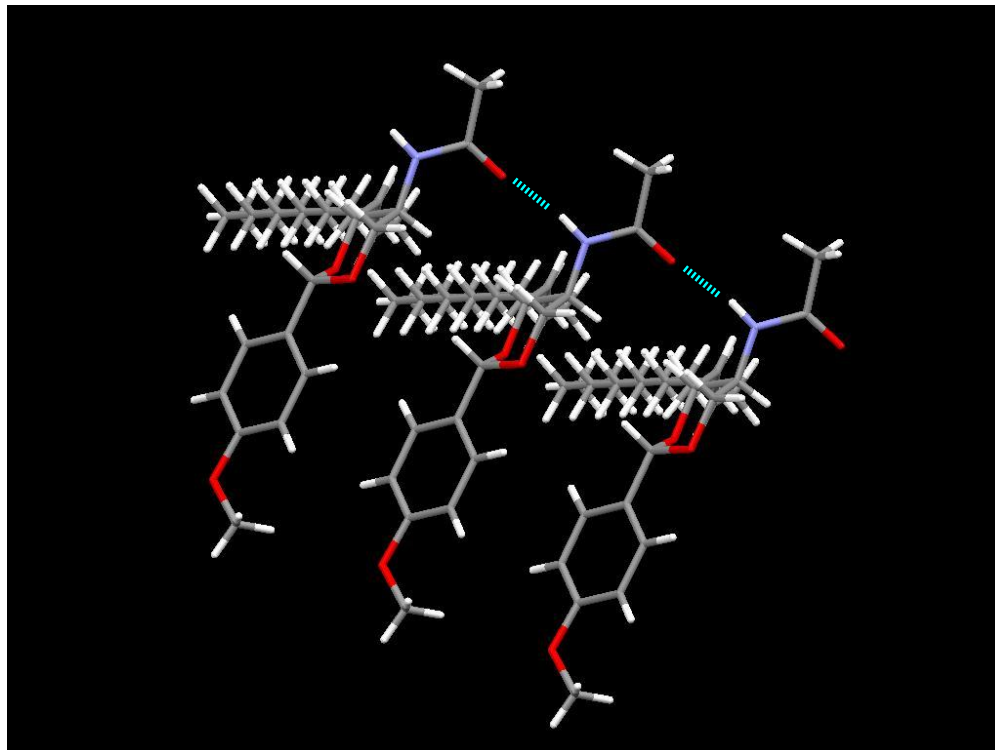
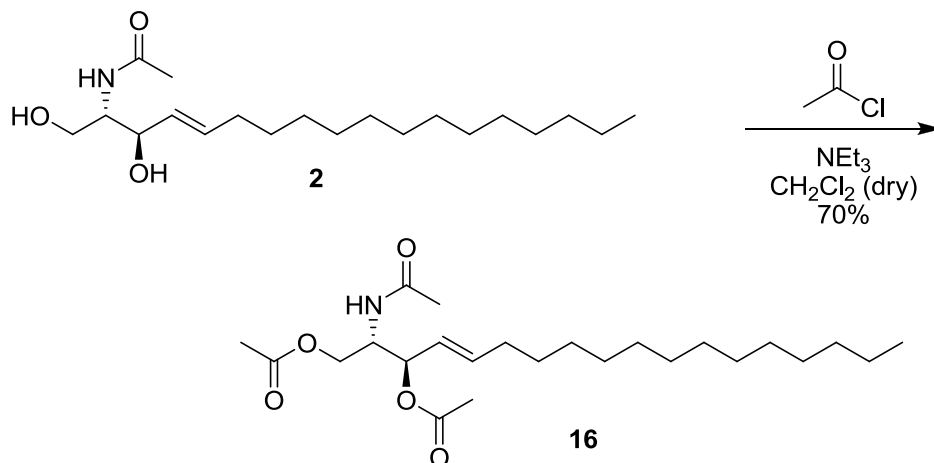


**Figure 2.5.** Crystal structure of C2-pmb **15**.

Additionally, a 1,3-diacetyl C2-ceramide (C2-diacetate **16**) analog was prepared as a possible base/esterase sensitive protected ceramide. Shayman and colleagues have found an enzyme that catalyzes the esterification of short chain ceramides.<sup>72</sup> They discovered a unique transacylase enzyme found in canine and mouse cells that esterifies C2-ceramide **2** to form 1-O-acetylceramide. While there are no studies, to our knowledge, that specifically discuss hydrolysis of O-acylated ceramides, it is reasonable to believe that enzymes exist that may carry out this task. Thus, acetyl chloride was slowly added to a solution of C2-ceramide **2** and triethylamine in  $\text{CH}_2\text{Cl}_2$  to give C2 diacetate **16** in 70 % yield after workup and purification (**Scheme 2.3**). Additionally, in a previous crystal structure study of C2-diacetate **16** by O'Connell and Pascher, hydrogen bonding was also observed between

amide the  $-NH$  of one molecule of C2-diacetate **16** with the amide carbonyl of an adjacent molecule.<sup>73</sup>

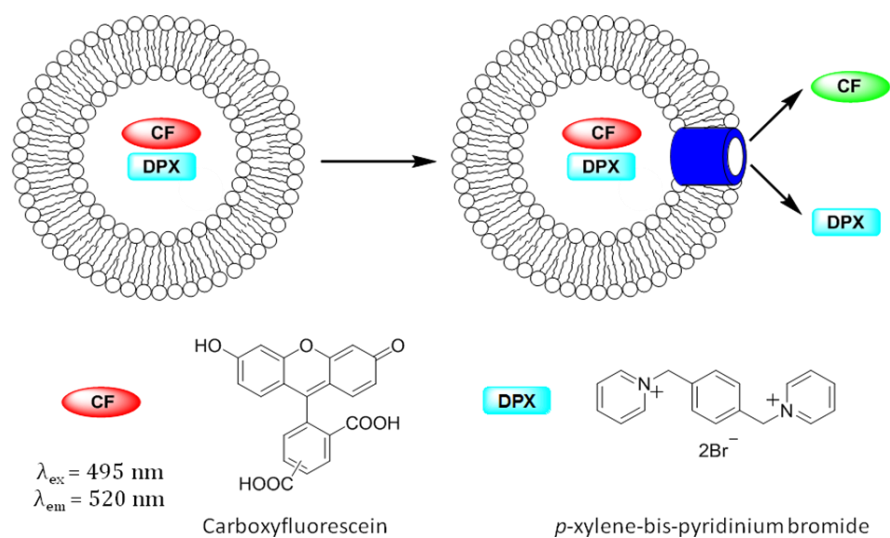


**Scheme 2.3.** Preparation of C2-diacetate **16**.

## 2.8 Carboxyfluorescein (CF) Release Assay for Pore Formation

One purpose of these studies was to determine what role the 1,3-diol unit of ceramide may have in pore formation within phospholipid bilayers. Based on the Colombini and Sukharev molecular dynamics studies,<sup>66</sup> we reasoned that the ceramide analogs C2-pmb **15** and C2-diacetate **16** would be rendered inactive with the removal of the two hydrogen bond donors within the 1,3-diol unit.





**Scheme 2.4.** CF release assay

In order to determine if these ceramide analogs form large pores in phospholipid membranes, we decided to test these analogs in carboxyfluorescein (CF) release assays. CF release assays have been used by a number of groups, including Matile,<sup>74</sup> Colombini,<sup>47</sup> Gokel,<sup>54</sup> and others,<sup>75</sup> to test for compounds that form large pores in phospholipid membranes. Liposomes were prepared containing CF, a fluorescent dye (**Scheme 2.4**). Additionally, a fluorescence quenching agent, *p*-xylene-bis-pyridinium bromide (DPX), was encapsulated in the vesicles along with the CF. In the presence of DPX, CF fluorescence is quenched. If any of these ceramide analogs form pores that are large enough to allow the release of the intravesicular CF and/or DPX, an increase in fluorescence should be observed. Pores observed in these CF release assays are generally thought to have an internal pore diameter of at least 10 Å, corresponding to the approximate diameter of CF.<sup>54</sup>

C2-ceramide **2**, C2-pmb **15**, and C2-diacetate **16** were all tested in this CF release assay. When added at a 15 mol% C2-ceramide **2** to lipid ratio, an increase in CF fluorescence was observed (**Figure 2.6**). As expected, C2-pmb **15**, with the 1,3-diol unit blocked, showed a significant decrease in pore-forming activity when compared to that of C2-ceramide **2**. This is consistent with the cytochrome c mitochondrial release assays performed using the longer chain C16-pmb **15** analog.

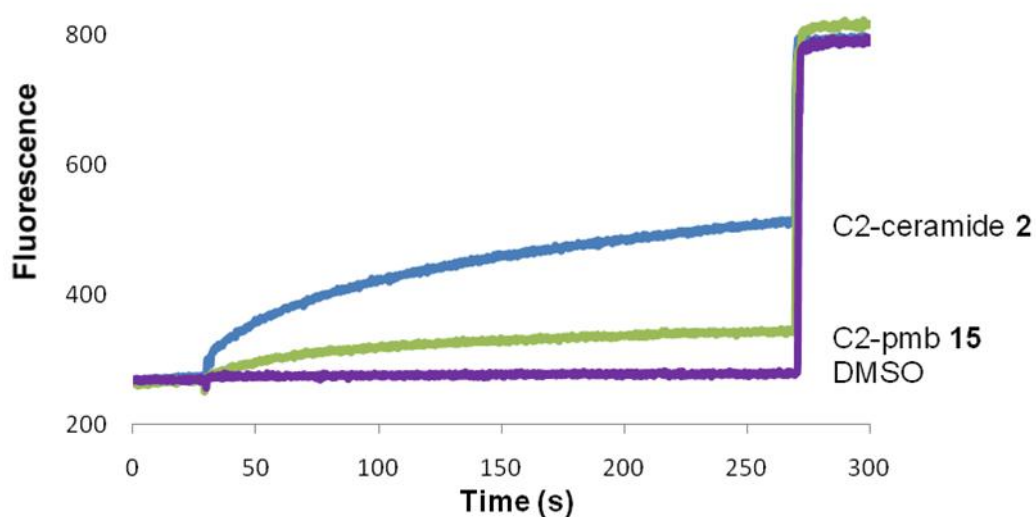


**Figure 2.6.** CF release assay comparing C2-ceramide **2** and C2-pmb **15**.

C2-diacetate **16** was also tested in the CF release assay. This analog has the two hydroxyls of the 1,3-diol blocked, but is less conformationally restricted than the acetal analog C2-pmb **15**. To our surprise, a large increase in the CF release activity of the C2-diacetate **16** was observed when compared to that of the natural C2-ceramide **2** (**Figure 2.7**). These experiments suggest that C2-diacetate **16** readily forms pores that are large enough to allow the release of the 10 Å wide CF from liposomes. While these results are unexpected, they do not prove that the pores formed are large enough to cause apoptosis of cells via the release of cytochrome c.

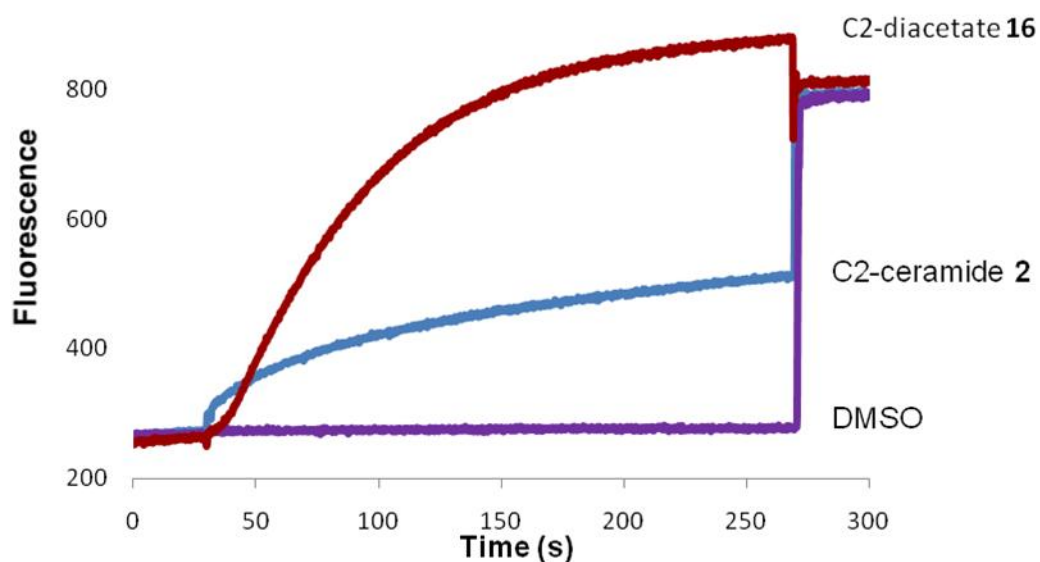


**Figure 2.7.** CF release assay comparing C2-ceramide **2** and C2-diacetate **16**.

## 2.9 Pore Sizing using FITC-Dextran

In an attempt to determine the relative size of the pores formed by C2-diacetate **16**, fluorescent isothiocyanate dextrans (FITC-dextrans) were used as an intravesicular fluorescent probe in liposome experiments. FITC-dextrans are composed of fluorescein derivatives attached to dextran polymers of various sizes (**Figure 2.8a**). FITC-dextrans have been previously used in materials research to determine the relative pore size in microporous films.<sup>76,77</sup> Biological applications include the use of FITC-dextrans as fluorescent probes to measure large molecule flux across epithelial and hepatoma cells.<sup>78-80</sup> In 1986, Stutzin developed a fluorescence assay using FITC-dextrans to monitor the synexin-induced fusion of bovine chromaffin granule ghosts.<sup>81</sup> More recently, FITC-dextrans have been used in liposome experiments to gauge the relative pore size of BAX proteins in phospholipid bilayers.<sup>82</sup>

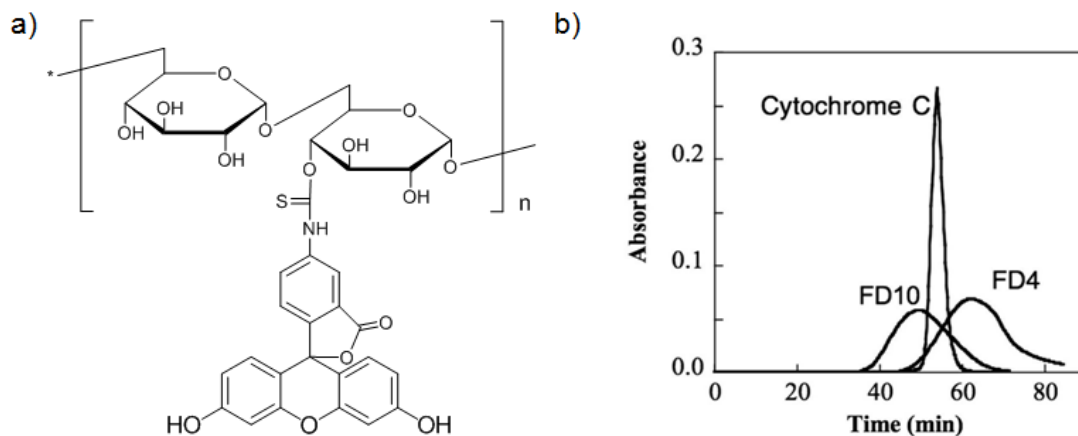
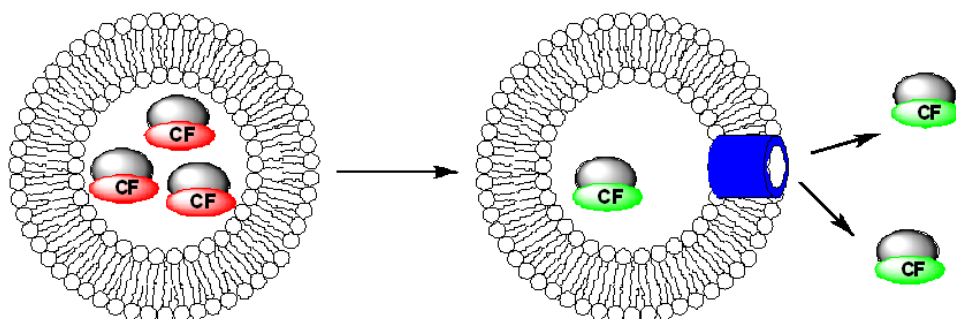


**Figure 2.8.** a) General structure of a FITC-dextran. b) Size-exclusion chromatography showing the sizes of FD4 and FD10 relative to cytochrome c. Figure used with permission from reference 83.

Ceramide is known to form large pores in the mitochondrial outer membrane; pores that are large enough to allow the release of the apoptosis-inducing cytochrome c.<sup>48</sup> In order to determine if pores formed by C2-diacetate **16** are large enough to release proteins as large as cytochrome c, and therefore, potentially induce apoptosis, liposomes were prepared containing FITC-dextran. Commercially available FITC-dextran range in size from FD4 (4 kDa) to FD150 (150 kDa).<sup>84</sup> For these experiments, FD10 (10 kDa) was chosen because its Stokes radius of 33 Å is larger than that of cytochrome c (17 Å).<sup>84,85</sup> Additionally, size exclusion chromatography performed by Sandoval and coworkers determined that the relative hydrodynamic radius of cytochrome c falls between that of dextrans FD4 and FD10 (**Figure 2.8b**).<sup>83</sup> Therefore, if C2-diacetate **16** can form pores large enough to release FD10 from phospholipid liposomes, it is reasonable to believe that these pores should also be large enough to release cytochrome c from the mitochondria.



**Scheme 2.5.** FITC-dextran (FD10) release assay.

EYPC liposomes were prepared in a HEPES buffer containing 7.5 mM of the dextran dye FD10. At these concentrations, the FITC-dextran is moderately self-quenched (**Scheme 2.5**).<sup>83</sup> The amount of self-quenching for FD10 is significantly less than that of CF, due to the increased steric bulk surrounding the fluorophore. If pores are formed in the phospholipid membrane that are large enough to release this 10 kDa FITC-dextran, then an increase in fluorescence should be observed. Upon the addition of C2-ceramide **2**, C2-pmb **15**, and C2-diacetate **16**, we observed fluorescence responses that were remarkably similar to that of previous experiments using the smaller CF dye (**Figure 2.9**). Thus, the acetal C2-pmb **15** gave little response above the DMSO baseline, while the C2-diacetate **16** gives a much larger fluorescence increase than C2-ceramide **2**.

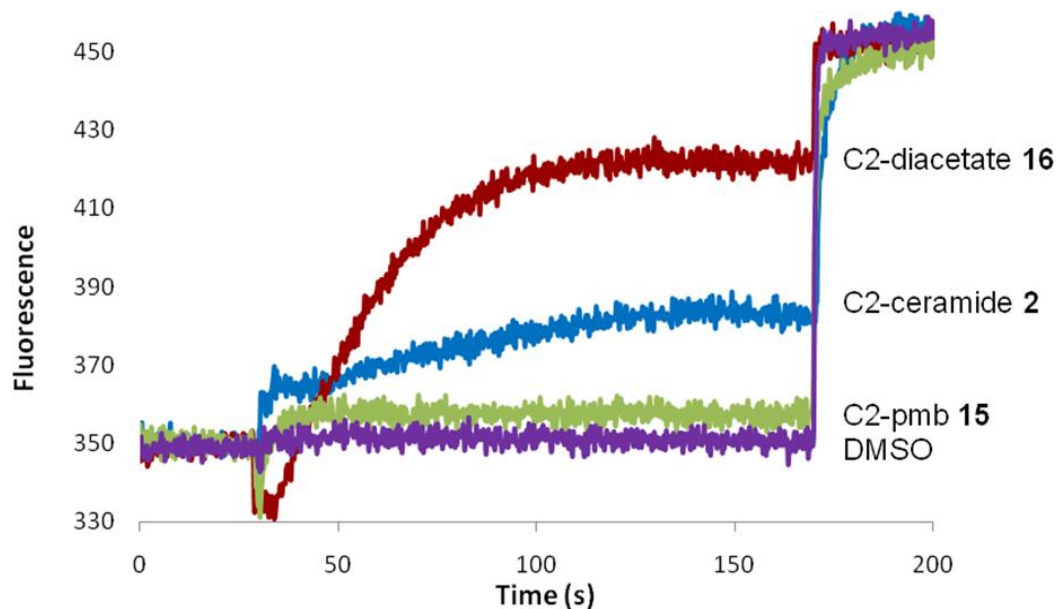


**Figure 2.9.** FITC-dextran release assay results comparing C2-ceramide **2**, C2-pmb **15**, and C2-diacetate **16**.

### 2.10 Mitochondrial Permeabilization Assay using C2-Diacetate **16**

With the knowledge that C2-diacetate **16** forms pores that should be large enough to allow cytochrome c to pass through a phospholipid bilayer, this compound was tested in the mitochondrial permeabilization assay (**Figure 2.10**). Unlike the previous mitochondrial studies with the C16-pmb **14** (**Figure 2.4**), C2-diacetate **16** does retain activity in this assay when compared to C2-ceramide **2**. This assay supports the results from the FITC-dextran release assay in that C2-diacetate **16** does increase the permeability of the mitochondrial outer membrane to small proteins such as cytochrome c.

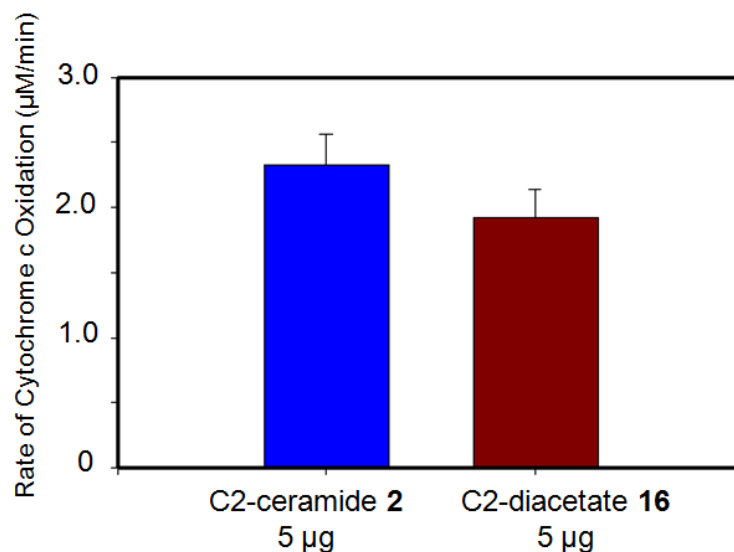


**Figure 2.10.** Mitochondrial permeabilization assay comparing C2-ceramide **2** to C2-diacetate **16**.

## 2.11 Conclusions

In this chapter, we studied the role of the 1,3-diol unit in the self-assembly of ceramide pores using alcohol protecting groups. As expected, blocking the 1,3-diol unit with a *p*-methoxybenzylidene group greatly diminished the ability of C16-ceramide **1** and C2-ceramide **2** to form pores in phospholipid bilayers. To our surprise, the C2-diacetate **16** analog seems to be more active in liposomal dye release assays than that of natural C2-ceramide **2**. These results seemingly go against previous hypotheses suggesting that the hydrogen bonding of the ceramide headgroup is an important factor in self-assembly into membrane-active structures. However, a closer look at the structure of C2-diacetate **16** allows for a possible explanation of these results.

Ceramides located in the stratum corneum layer of the skin are thought to play important roles in skin water barrier homeostasis and water holding capacity.<sup>86-88</sup>

Additionally, the deficiency of skin ceramides is linked to various skin diseases ranging from dermatitis and psoriasis, as well as Gaucher and Niemann-Pick Diseases.<sup>4</sup> Based on the fact that ceramides play important roles in water regulation in the skin, we speculate that water may well play an important role in stabilization of ceramide pores in phospholipid membranes.

Protection of the alcohols of ceramide with ester groups removes two possible hydrogen bond donors from the ceramide headgroup. However, this protection strategy adds two additional hydrogen bond acceptors in the carbonyl oxygen of the ester functionality. Additionally, any pore formed in a phospholipid bilayer would be filled with water. We currently speculate that hydrogen bonding in the ceramide headgroup is integral to pore self-assembly, and that formation of these membrane-active structures may be a cooperative event also involving hydrogen bound water molecules. In the case of C2-diacetate **16**, the partially positive hydrogens of water might well help stabilize the pore structure by hydrogen bonding with the additional hydrogen bond acceptors introduced in the ceramide headgroup.

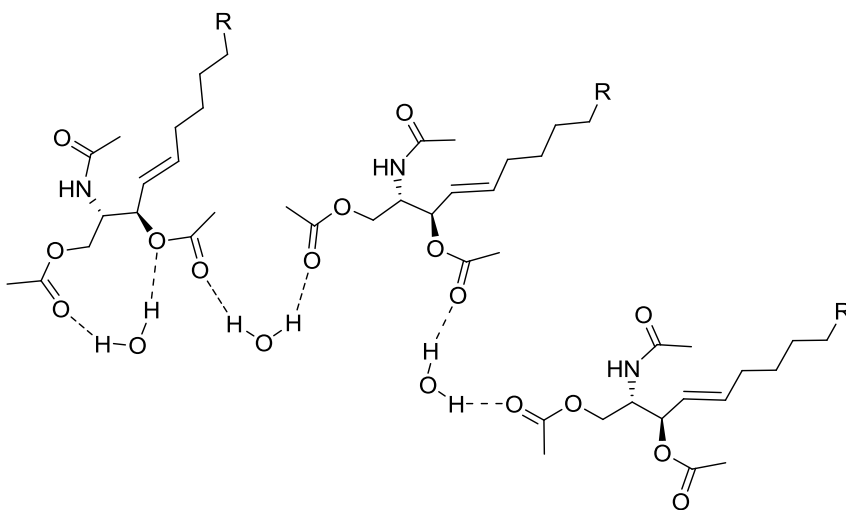


**Figure 2.11.** Schematic representation of a possible water stabilized C2-diacetate **16** pore.



## 2.12 Future Directions

Further experiments are necessary to explore the role of water in the self-assembly of C2-ceramide **2** and C2-diacetate **16** into membrane active structures. Molecular dynamics simulations of these compounds including water molecules could give insight into the role of hydrogen bound water in the stabilization of ceramide pores.

In terms of accomplishing the original goals of this project in the development of anti-tumor pro-drugs, additional blocked analogs are needed. Preliminary results suggest that the use of acetals in blocking the 1,3-diol unit renders ceramide unable to form large pores in phospholipid bilayers. Unfortunately, the C2-pmb **15** analog discussed is likely equipped with a protecting group that is not labile at lysosomal pH of 5 (Green's book "Protective Groups in Organic Synthesis" suggests *p*-methoxybenzylidene acetals are highly labile at pH < 4).<sup>89</sup> However, the preparation of a cyclic ortho ester protected analog should create an inactive analog that is labile at mildly acidic pHs. Cyclic ortho esters are readily cleaved by acidic hydrolysis in phosphate buffer in pH ranges from 4.5-7.5 and should be labile at lysosomal pH.<sup>90</sup>

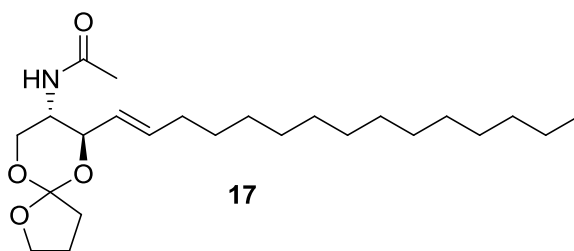


**Figure 2.12.** Cyclic ortho ester protected C2-ceramide analog.

## Chapter 3 : C2-Ceramide Facilitates Anion Exchange across Phospholipid Bilayers

Portions of this chapter have been published in reference 91.

- Harrell, W. A., Jr.; Bergmeyer, M. L.; Zavalij, P. Y.; Davis, J. T. Ceramide-Mediated Transport of Chloride and Bicarbonate Across Phospholipid Membranes. *Chem. Commun.* **2010**, *46*, 3950–3952.

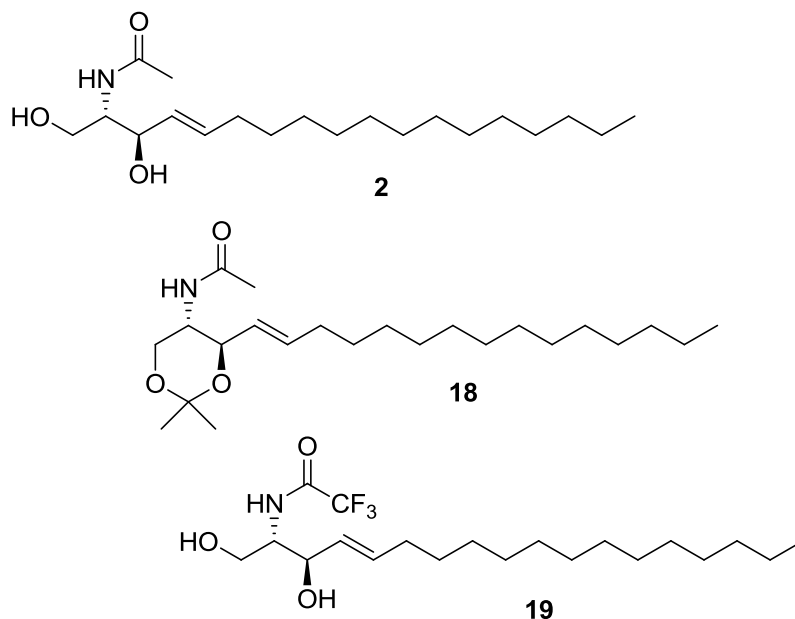
*Some of the experimental work described in this chapter was performed by Ms. Liesel M. Bergmeyer, an undergraduate HHMI fellow working under my supervision. Dr. Peter Y. Zavalij determined the crystal structure of isopropylidene C2-ceramide 18 that is described in this chapter.*

### 3.1 Introduction

The goals of the research in this chapter are two-fold: 1) to investigate the anion transport properties of C2-ceramide **2**; and 2) to prepare analogs of C2-ceramide that might have increased transport activities. These studies are based on the fact that C2-ceramide **2** self-assembles at concentrations >10 mol% within phospholipid membranes to form large pores.<sup>55</sup> However, to our knowledge, no studies exist that have investigated the membrane properties of ceramide at lower concentrations. The major finding in this chapter is the discovery that C2-ceramide **2** transports chloride anions across phospholipid membranes at concentrations that are below known pore forming concentrations. Before describing the new studies on C2-ceramide **2** and some synthetic analogs (**Chart 3.1**), I will first provide a brief

background on natural products that are known anion transporters. I will also provide some background on the use of –OH groups in synthetic anion transporters.

### Chart 3.1



### 3.2 Small Molecule Natural Products that Transport Anions

Numerous natural products facilitate translocation of cations across phospholipid membranes. For example, valinomycin and gramicidin A are probably the best known small molecule natural products that transport cations.<sup>92,93</sup> Recent reviews by Gale,<sup>94</sup> Gokel,<sup>95</sup> A. P. Davis, Sheppard and Smith,<sup>96</sup> and by J. T. Davis and Quesada<sup>97</sup> provide excellent discussions on the large field of synthetic anion transporters. However, there are very few small molecule natural products that are known to transport anions. To our knowledge, only four natural products, duramycin,<sup>98</sup> prodigiosin,<sup>99</sup> amphotericin B,<sup>100</sup> and panamycin-607,<sup>101</sup> have been

implicated in the transmembrane transport of anions, with the prodigiosin and amphotericin B being the most studied.

### 3.2.1 Duramycin

Channel-forming peptides have been studied extensively due to their antibiotic properties, with the cation-selective gramicidin being the most studied.<sup>92</sup> However, examples of peptides that function as anion selective transporters are much more rare. The natural product duramycin **20** is a nonadecapeptide antibiotic isolated from *Streptovercillium cinnamomeus*.<sup>102</sup> Planar membrane studies show that duramycin **20** forms anion selective channels that transport Cl<sup>-</sup> across phospholipid membranes.<sup>98</sup> The authors postulate that multiple molecules of duramycin **20** self-assemble in the lipid bilayer to form the membrane active structure.

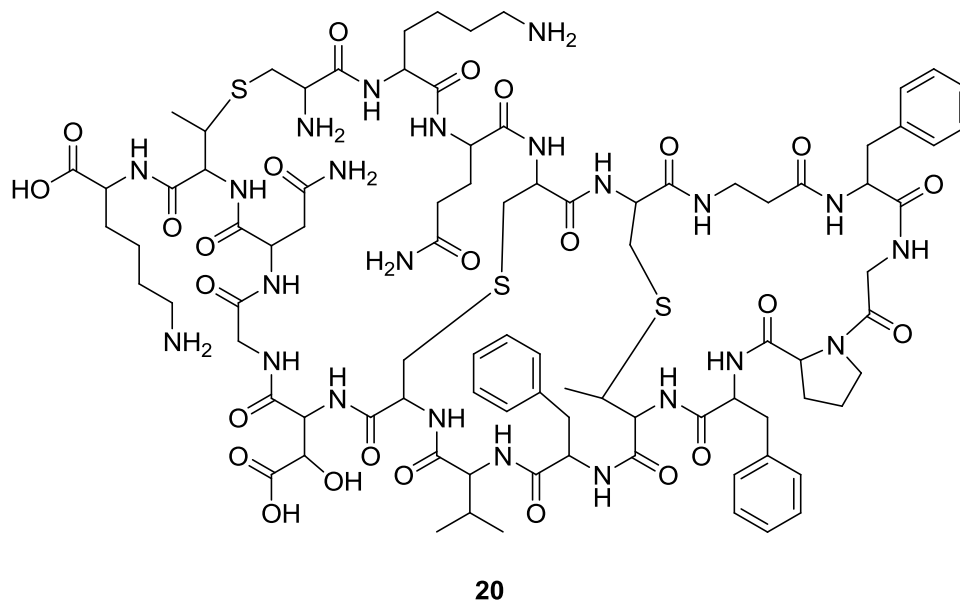


**Figure 3.1.** Structure of duramycin **20**, a natural product anion transporter.

Additionally, duramycin **20** has been found to enhance chloride secretion in airway epithelium.<sup>103</sup> These discoveries have led to duramycin **20** being tested in clinical trials for treatment of cystic fibrosis,<sup>104</sup> a disease caused by defects in the cystic fibrosis transmembrane regulator (CFTR), a protein that facilitates the transmembrane transport of  $\text{Cl}^-$  and  $\text{HCO}_3^-$  anions.<sup>105-108</sup>

### 3.2.2 Prodigiosin

Prodigiosin **21**, first isolated in its pure form in 1929, is a heterocyclic natural product that has a bright red color.<sup>109</sup> However, its structure was only fully elucidated in the early 1960s by separate partial<sup>110</sup> and complete<sup>111</sup> synthesis. Prodigiosins have been shown to possess potent antimicrobial, anticancer, and immunosuppressive activities.<sup>112,113</sup> In 1995, Kataoka and colleagues showed that prodigiosin **21** inhibited the activity of V-ATPase, an enzyme responsible for active transport of protons across intracellular membranes in certain cellular organelles, such as lysosomes and the Golgi apparatus.<sup>114,115</sup> However, these papers did not discuss a specific mechanism for how prodigiosin disrupts the proton pump of V-ATPase.

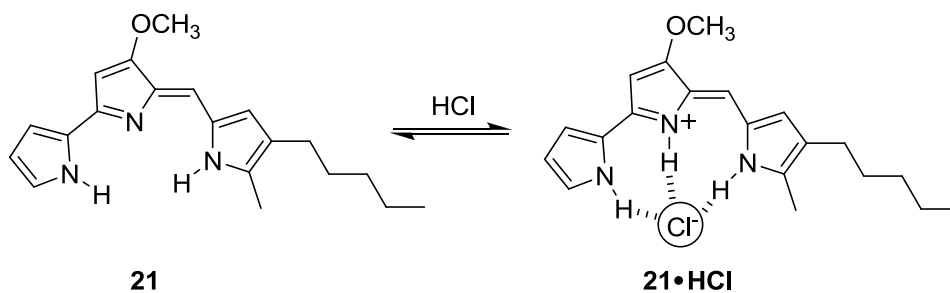


**Figure 3.2.** The structure of prodigiosin **21** and the complex **21·HCl**.

In 1998, Ohkuma, Wasserman and colleagues discovered that prodigiosins uncouple the proton translocation activity of V-ATPase by acting as a  $H^+/Cl^-$  symporter.<sup>116-118</sup> In the presence of HCl, the weakly basic prodigiosin **21** ( $pK_a \sim 7$ ) becomes protonated, forming a binding pocket for the residual  $Cl^-$  anion to bind (**Figure 3.2**). In liposomal solutions containing an excess of extravesicular  $Cl^-$ , they found that the internal pH dropped with the addition of prodigiosin **21**, corresponding to the symport of  $H^+/Cl^-$  to the interior of the liposome.

However, a later study by Seganish and Davis showed that anion transport by prodigiosin **21** does not always occur through a symport mechanism. The authors determined that prodigiosin **21** could also facilitate anion transport through an anion exchange (antiport) mechanism.<sup>119</sup> Liposomes were prepared containing either  $Na_2SO_4$  or  $NaNO_3$  with external NaCl. They monitored both the internal pH of the liposomes and  $Cl^-$  influx using pyranine and lucigenin dyes, respectively. Addition of prodigiosin **21** to the sulfate containing liposomes resulted in immediate acidification inside the liposome with very little concomitant  $Cl^-$  influx. In this case, these results were consistent with the results of Ohkuma and colleagues in that prodigiosin **21** is facilitating  $H^+/Cl^-$  symport (or  $OH^-/Cl^-$  antiport). However, addition of prodigiosin **21** to the nitrate containing liposomes facilitated rapid exchange of  $Cl^-$  and  $NO_3^-$ , with no internal pH change. This study was significant because it demonstrated that prodigiosin **21** can facilitate the transmembrane transport of anions via differing mechanisms, depending on the environmental conditions.

### 3.2.3 Amphotericin B

Amphotericin B (AmB **22**) is an antifungal antibiotic that is used for the treatment of systemic fungal infections.<sup>120</sup> Early work on AmB **22** suggests that its mechanism of action is the generation of ion channels containing 4-12 individual molecules that self-assemble in the membrane of the target cell.<sup>121-123</sup> These channels are known to allow potassium ions and small organic molecules to cross through the phospholipid bilayers.<sup>124,125</sup>

However, recent study planar membrane by Asandei and Luchian discovered some interesting anion transport properties of AmB **22**.<sup>100</sup> Reverse potential planar membrane studies of AmB **22** at pH 7.07 and 11.0 gave positive values of  $8.3 \pm 0.2$  mV and  $28.1 \pm 2.4$  mV, respectively, corresponding to increasing cation ( $K^+$ ) selectivity as the pH of the solution becomes more basic. However, at pH 2.82, AmB **22** gave a negative potential of  $-20.9 \pm 0.7$  mV, corresponding to a strong anion selectivity ( $Cl^-$  in this case). This discovery is unique in that the natural product AmB **22** can act as a pH tunable ion channel.

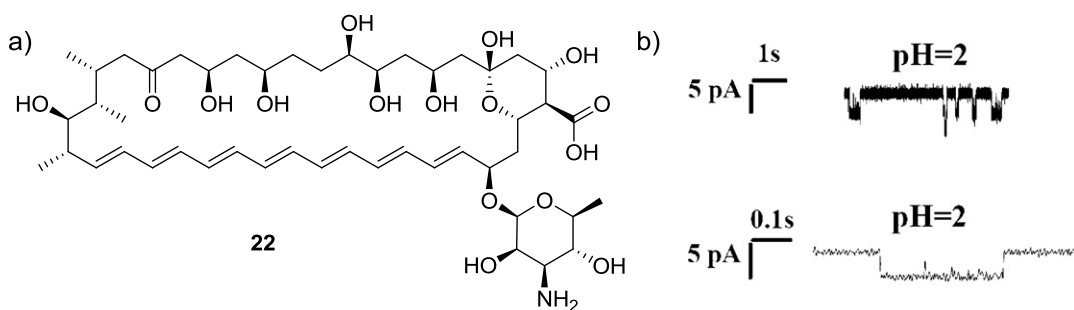


**Figure 3.3.** a) The structure of AmB **22**. b) Results from reverse potential planar membrane studies of AmB **22** at pH = 2 showing a negative potential, corresponding anion selective channel formation. Figure used with permission from reference 100.

Molecular dynamics simulations of AmB **22** channels reveal that –OH groups line the inner wall of the membrane active structure (**Figure 3.4**).<sup>124-126</sup> This suggests that the –OH groups (red) play a vital role in shuttling anions (or cations) across phospholipid membranes. Anion selectivity at low pH is thought to arise from “gating” due to the protonated amines (blue) capping the structure, preventing cations from entering the channel.<sup>100</sup>

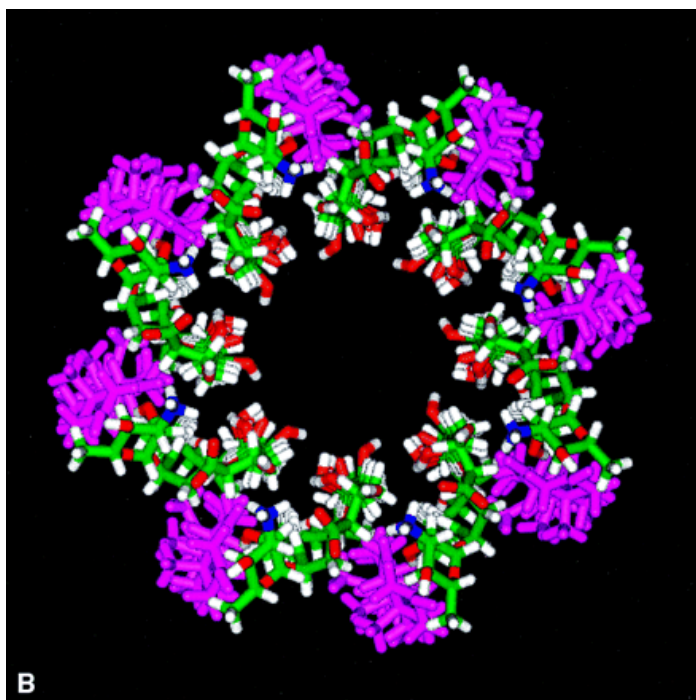


**Figure 3.4.** Molecular dynamics simulation of self-assembled AmB **22** channel. Figure used with permission from reference 124.

### 3.2.4 Pamamycin-607

Pamamycin-607 **23** is a 18-membered macrolide that was originally isolated from *Streptomyces alboniger* in 1987 by Marumo and co-workers.<sup>127</sup> Pamamycin-607 **23** has been of particular interest for its potent activity against the gram-positive bacteria *Mycobacterium tuberculosis*.<sup>128</sup> Pamamycin-607 **23** has been suggested to have supposedly have anionophoric properties,<sup>101,129,130</sup> and has even shown up in the



footnote of review articles as a natural product anion transporter.<sup>96</sup> However, to our knowledge there is absolutely no report in the literature to back up this claim. In fact, the anionophoric properties of pamamycin-607 **23** are suspect, at best. The structure in **Figure 3.5** of Pamamycin-607 **23** reveals that it actually has more in common with a cationophoric crown ether than any anionophore.<sup>131,132</sup>

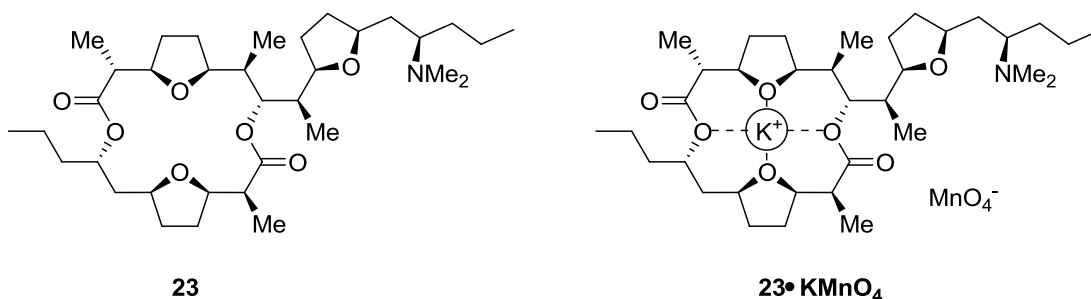


**Figure 3.5.** Structure of pamamycin-607 **23** and an example of a pamamycin-607 **23** lipophilic anion pair with  $\text{KMnO}_4$ .

Pamamycin-607 **23** can bind and transport anionic species from aqueous layers to organic layers through the formation of lipophilic ion pairs.<sup>130</sup> Grafe and colleagues were able to use pamamycin-607 **23** to transport methylorange, a small anionic dye, from a water layer into a toluene layer.<sup>133</sup> Additionally, Marumo and co-workers determined that pamamycin-607 **23** selectively transports anions over cations from aqueous phases to organic layers at neutral and acidic conditions.<sup>129</sup> When  $\text{KMnO}_4$  was partitioned between a water layer and a pamamycin-607 **23** containing benzene layer, only  $\text{MnO}_4^-$  was transferred to the benzene layer, while  $\text{K}^+$  remained in the aqueous layer (presumably bound to pamamycin-607 **23**).

These studies only present evidence that pamamycin-607 **23** can act as a phase transfer catalyst. Pamamycin-607 **23** seems both structurally and functionally similar

to crown ethers in this regard. In my opinion, these studies show that pamamycin-607 **23** no more of an anionophore than the crown ethers. The “binding” of an anion is a secondary electrostatic event that follows the binding of a cation in the pamamycin-607 **23** crown ether like binding pocket.

### 3.3 Synthetic Anion Transporters that Utilize O-H···A<sup>-</sup> Interactions

While most anion-binding ligands use amide –NH groups to coordinate anions,<sup>94,134,135</sup> there are a growing number of receptors that use –OH groups for anion recognition.<sup>136-140</sup> Furthermore, crystal structures of anion binding proteins often show OH side-chains as integral to the active site.<sup>141-143</sup> For instance, Luecke and Quioco discovered that a phosphate buried within the binding pocket of the phosphate-binding protein is held in place by 12 hydrogen-bonds, four of which are –OH groups from two serines and two threonines.<sup>141</sup>

MacKinnon and colleagues were able to obtain a crystal structure for the ClC chloride channel protein from *S. typhimurium*.<sup>143</sup> These studies showed that chloride selectivity is accomplished in the narrowest portion of the channel, the so-called ion filter. In this region (depicted in **Figure 3.6**), chloride is selectively coordinated to multiple hydrogen bond donors, including two –OH groups, one from a serine and one from a tyrosine residue

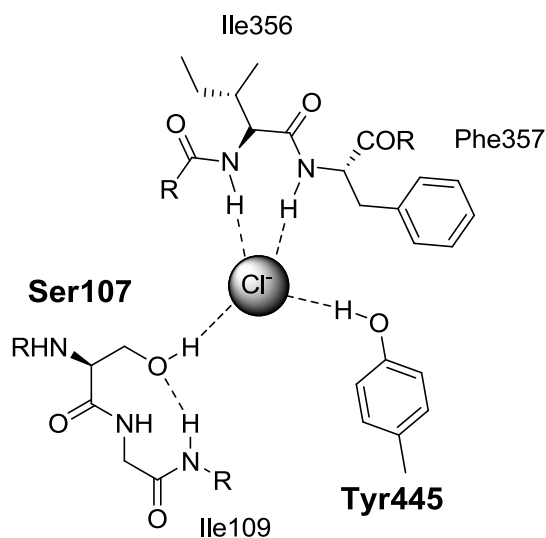
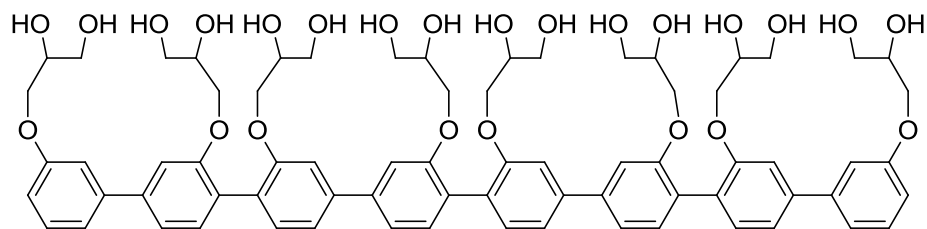


**Figure 3.6.** Schematic representation of the narrowest pore region of the ClC chloride channel.<sup>135</sup>

In another study by Quioco, the crystal structure of the sulfate-binding protein of *Salmonella typhimurium* shows a serine within the binding pocket.<sup>144</sup> Site-directed mutagenesis that changed the serine to a cysteine residue caused a 3200-fold decrease in sulfate binding activity.<sup>142</sup> These three crystal structure studies suggest that –OH containing amino acids play integral roles in the binding and transport of anions in natural systems.

### 3.3.1 Matile's Rigid-Rod Polyol 24 Forms Ion Channels

While natural products like AmB **22** take advantage of –OH functionalities to bind and transport anions, the vast majority of synthetic anion receptors utilize only –NH groups as hydrogen bond donors.<sup>94,134,135</sup> Using this natural product as inspiration, researchers in the lab of Stefan Matile used synthesized an AmB **22** mimic, consisting of eight 1,2-diol functionalities appended to a rigid aromatic backbone.<sup>145</sup>



**24**

**Figure 3.7.** Matile's rigid polyol **24**, an AmB **22** mimic.

Like AmB **22**, Matile's rigid polyol **24** transports different ions under different conditions. Polyol **24** was found to be generally selective for  $H^+$  and other cations over anions. However, when HPTS and chloride containing liposomes were subjected to an external pH change, Matile and coworkers observed an increase in intravesicular pH associated with  $OH^-/Cl^-$  exchange. They also proposed that polyol **24**, which has a length of approximately 34 Å, could span the membrane and act as an ion channel by moving anions (or cations) across phospholipid membranes through a hydrogen-bond chain mechanism. In this case, anions (or cations) would effectively hop from one "binding site" to another until it crossed the lipid bilayer. However, a later voltage-clamp study by the Matile group with polyol **24** gave conductances too large for the ion channel to be comprised of just one unit.<sup>146</sup> They proposed that the membrane-active structure was comprised of four self-assembled polyol **24** subunits.

### 3.3.2 Catechols as Anion Transporters

Catechols have been well studied in the lab of D. K. Smith as receptors for chloride.<sup>139,147,148</sup> Additionally, Miyaji and Sessler found that dyes containing catechols functionalities can be used as colorimetric anion sensors.<sup>149</sup> However, only

recently have catechols been used to facilitate the transmembrane transport of anions. Berezin and Davis developed a bis-catechol **25** receptor that binds and transports anions.<sup>150</sup> The authors appended two catechols to a tren scaffold. A lipophilic carbon tail was attached to the third arm of the tren scaffold in order to help the bis-catechol **25** partition into a phospholipid membrane. Using bis-catechol **25**, Berezin and Davis were able to facilitate the transmembrane transport of a variety of anions including  $\text{Cl}^-$ ,  $\text{Br}^-$ ,  $\text{I}^-$ ,  $\text{NO}_3^-$ ,  $\text{ClO}_4^-$  and  $\text{N}_3^-$ . Additionally, when the hydrogen-bond donor groups were blocked (**26**), no anion transport was observed. This suggests that the  $-\text{OH}$  groups of the catechols functionality play a vital role in these compounds ability to transport anions across phospholipid membranes.

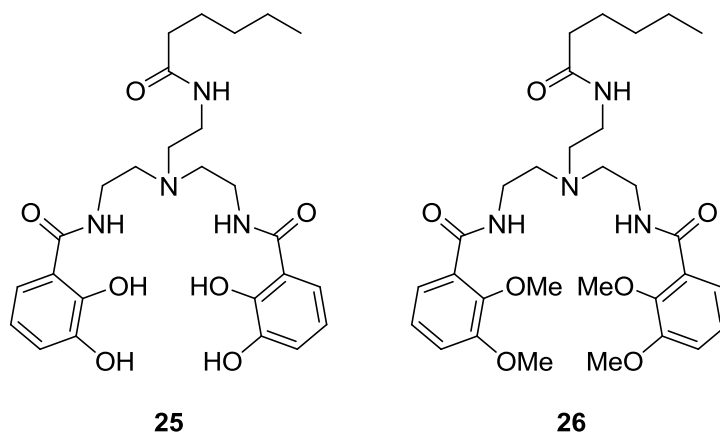


**Figure 3.8.** Bis-catechol **25** facilitates the transmembrane transport of anions, while the protected derivative **26** does not.

### 3.4 Anion Binding Studies of C2-ceramide

In this study we compared the anion binding and anion transport properties of C2-ceramide **2** and its 1,3-isopropylidene protected derivative **18**.<sup>91</sup> These compounds were compared because we wanted to discern the role of ceramide's 1,3-diol in anion recognition and transport.

#### 3.4.1 The C2-Ceramide Tridentate Anion Binding Motif

In this study, we sought to identify membrane-active natural products that might use –OH groups for transporting anions. Our attention turned to the ceramides. We reasoned that the 1,3-diol and neighboring amide –NH functionalities in C2-ceramide **2** might provide an effective tridentate motif for binding anions (**Figure 3.9**). Our rationale was bolstered by reports that ceramides give robust signals for Cl<sup>-</sup> adducts when analyzed by electrospray mass spectrometry.<sup>151,152</sup>

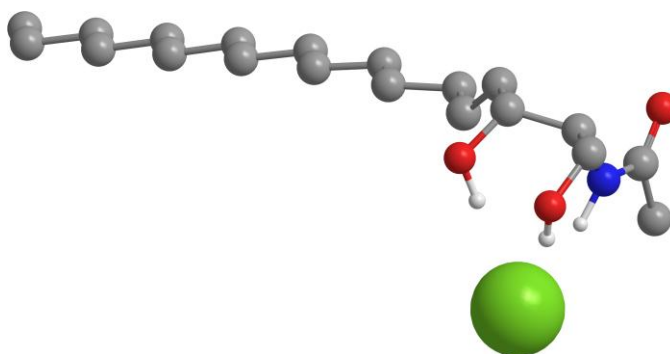
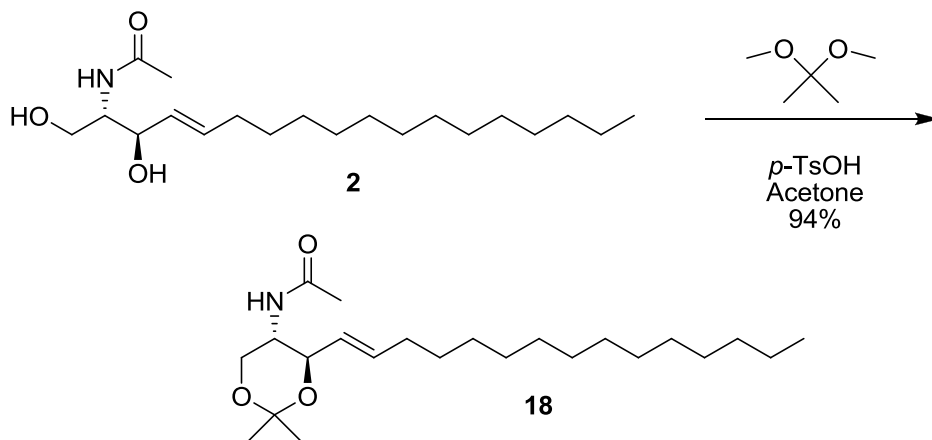


**Figure 3.9.** Model showing the binding of Cl<sup>-</sup> by C2-ceramide **2**.

### 3.4.2 Preparation and Characterization of Isopropylidene C2-Ceramide **18**

In order to determine the role of the 1,3-diol unit in the ability of C2-ceramide **2** to bind anions, isopropylidene C2-ceramide **18** was prepared in one step. C2-ceramide **2** was reacted with 2,2-dimethoxypropane in the presence of an acid catalyst, giving isopropylidene C2-ceramide **18** in 94 % yield (**Scheme 3.1**). The  $^1\text{H}$  NMR spectrum of isopropylidene C2-ceramide **18** shows the loss of the  $-\text{OH}$  protons of ceramide, as well as an upfield shift of the  $-\text{NH}$  proton (**Figure 3.10**). Additionally, the NMR also shows the clear presence of the diastereotopic methyl groups of the newly formed isopropylidene group. To our knowledge, this is the first literature example of the preparation of isopropylidene C2-ceramide **18**.



**Scheme 3.1.** Preparation of isopropylidene C2-ceramide **18**.

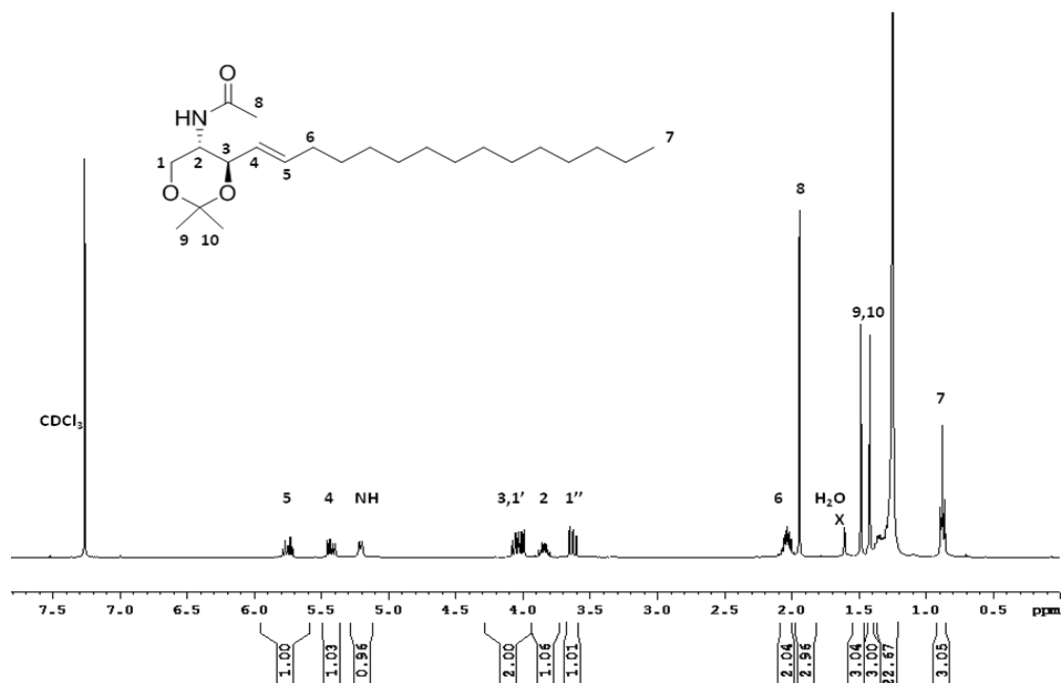


**Figure 3.10.**  $^1\text{H}$  NMR spectrum (in  $\text{CDCl}_3$ ) of isopropylidene C2-ceramide **18** distinguished by the loss of the broad  $-\text{OH}$  signals at 2.5 ppm and the appearance of protons 9 and 10 of the isopropylidene functionality. Additionally, a 1 ppm upfield shift of the  $-\text{NH}$  proton is observed when compared to C2-ceramide **2**.

Additionally, we were able to obtain an X-ray crystal structure for isopropylidene C2-ceramide **18**. Interestingly, four symmetrically independent molecules make up the unit cell. While the  $-\text{OH}$  groups in this analog are blocked from participating as hydrogen bond donors, hydrogen-bonding is observed between the amide  $-\text{NH}$  and the carbonyl of a neighboring isopropylidene C2-ceramide **18** molecule.



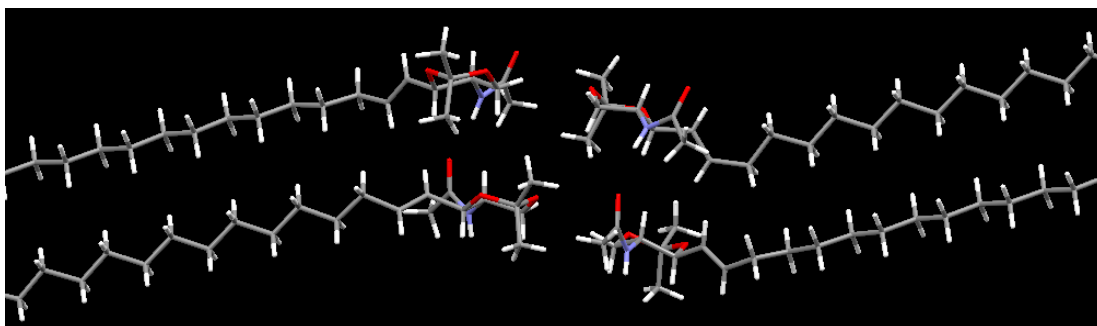


**Figure 3.11.** Depiction of the crystal structure of isopropylidene C2-ceramide **18**. The ends of the lipophilic tails have been removed for clarity.

### 3.4.3 ESI-MS Evidence that C2-Ceramide **2** Binds Anions

We initially obtained evidence for anion binding by C2-ceramide **2** from mass spectrometry (**Figure 3.12**). Previous mass spectrometry studies on longer chain ceramides in negative mode have allowed for the detection of a C16-ceramide **1**·Cl<sup>-</sup> adduct.<sup>151,152</sup> ESI-MS analysis in negative mode of a solution of C2-ceramide **2** and tetrabutylammonium chloride (TBACl) in CH<sub>2</sub>Cl<sub>2</sub> showed a strong signal for the adduct at  $m/z = 376.21$  (ESI-MS [M+Cl]<sup>-</sup> calculated for C<sub>20</sub>H<sub>39</sub>ClNO<sub>3</sub><sup>-</sup>,  $m/z = 376.26$ ). Isopropylidene C2-ceramide **18**, which lacks the 1,3-diol, did not form any such detectable Cl<sup>-</sup> adduct under identical conditions (ESI-MS [M+Cl]<sup>-</sup> calculated for C<sub>23</sub>H<sub>43</sub>ClNO<sub>3</sub><sup>-</sup> was  $m/z = 416.29$ , no such signal was detected for this adduct). This comparative mass spectrometry data was the first indication to us that the 1,3-diol unit was essential for anion binding.

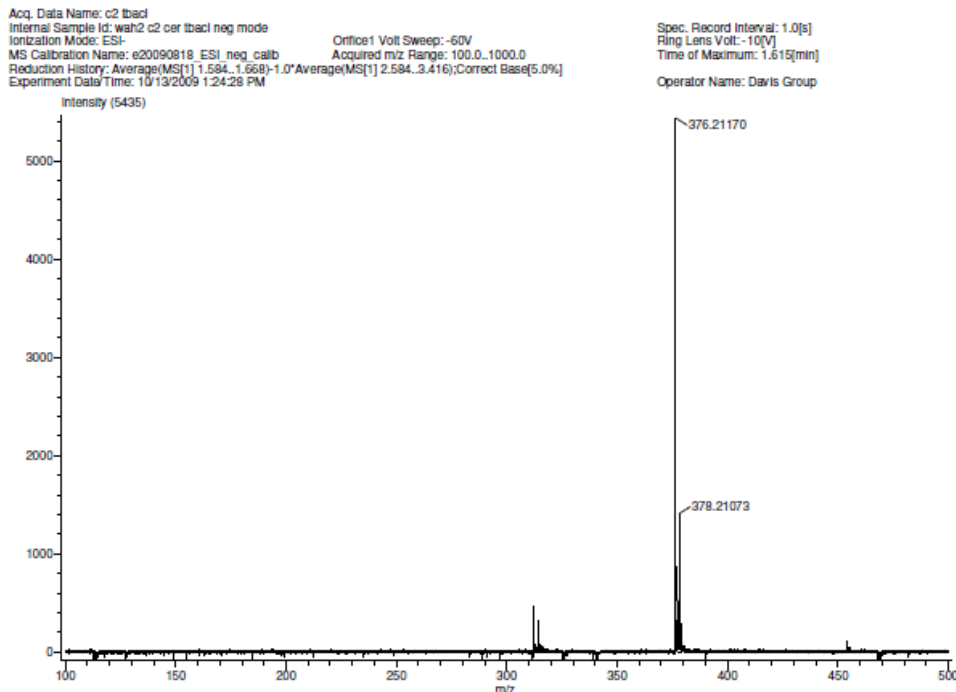


**Figure 3.12.** ESI-MS (negative mode) of C2-ceramide **2**·Cl<sup>-</sup> adduct. A solution of C2-ceramide **2** (2 mM) and TBACl (6 mM) in CD<sub>2</sub>Cl<sub>2</sub> was injected using MeOH as the eluant. ESI-MS [M+Cl]<sup>-</sup> calculated for C<sub>20</sub>H<sub>39</sub>ClNO<sub>3</sub><sup>-</sup> 376.26, found 376.21. Experimental variables are listed above the spectrum.

### 3.4.4 <sup>1</sup>H NMR Evidence that C2-Ceramide **2** Binds Anions

NMR spectroscopy provided more details about the ability of C2-ceramide **2** to bind Cl<sup>-</sup> in solution. Changes in chemical shifts of the -NH and/or -OH protons upon addition of anions to a solution of C2-ceramide **2** confirmed that the ceramide head-group is a potent anion binder. In dry CD<sub>2</sub>Cl<sub>2</sub>, the two -OH resonances for C2-ceramide **2** appeared together as a broad signal at δ 2.68. Importantly, the <sup>1</sup>H NMR signals for the 1-OH and 3-OH were separated in water-saturated CD<sub>2</sub>Cl<sub>2</sub>, allowing us to follow changes in chemical shifts during anion titrations (**Figure 3.13**). This information is in agreement with previous studies of C2-ceramide **2** showing that the head group is strongly hydrated (however, in these studies, separation of the -OH

groups by  $^1\text{H}$  NMR spectroscopy was only achieved using a combination of low concentrations and temperatures in  $\text{CDCl}_3$ .<sup>153</sup>

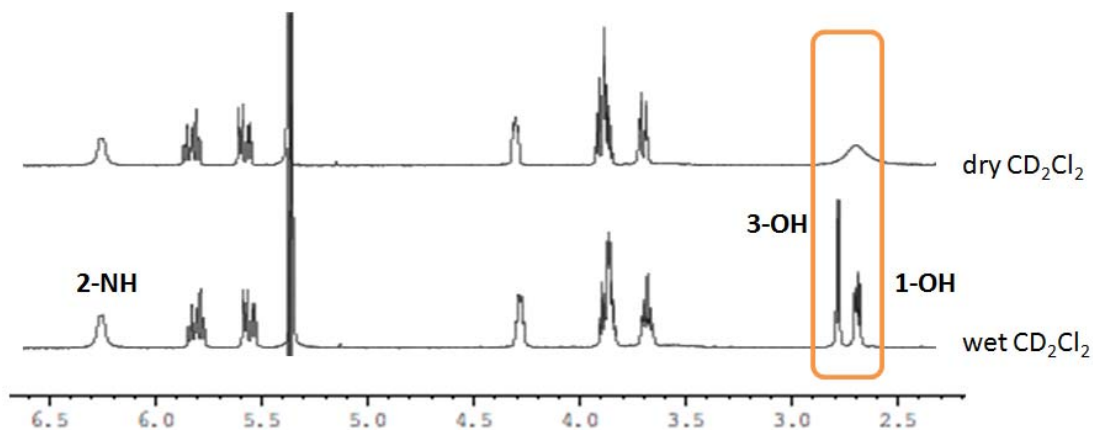


**Figure 3.13.**  $^1\text{H}$  NMR of C2-ceramide **2** in dry and wet  $\text{CD}_2\text{Cl}_2$  showing resolution of the hydroxyl protons in the water saturated  $\text{CD}_2\text{Cl}_2$  solution.

Addition of TBACl to a solution of C2-ceramide **2** in wet  $\text{CD}_2\text{Cl}_2$  resulted in large downfield shifts for the  $-\text{NH}$  ( $\Delta\delta = 1.9$  ppm) and  $-\text{OH}$  signals ( $\Delta\delta = 2.3$  ppm and 2.6 ppm for 1-OH and 3-OH), consistent with formation of hydrogen bonds between  $\text{Cl}^-$  and these 3 acidic hydrogen atoms (**Figure 3.14**). By evaluating chemical shift changes for the  $-\text{NH}$  proton we determined a  $\text{Cl}^-$  binding constant of  $K_a = 1734 \pm 82 \text{ M}^{-1}$  for C2-ceramide **2** in wet  $\text{CD}_2\text{Cl}_2$  using WinEQNMR2.<sup>154</sup> Similar binding constants were determined for the 1-OH ( $K_a = 1935 \pm 65 \text{ M}^{-1}$ ) and 3-OH ( $K_a = 1877 \pm 54 \text{ M}^{-1}$ ) protons in  $\text{CD}_2\text{Cl}_2$ . A Job plot analysis from  $^1\text{H}$  NMR spectra taken in  $\text{CD}_2\text{Cl}_2$  shows that C2-ceramide **2** binds chloride in a 1:1 ratio (**Figure 3.15**).

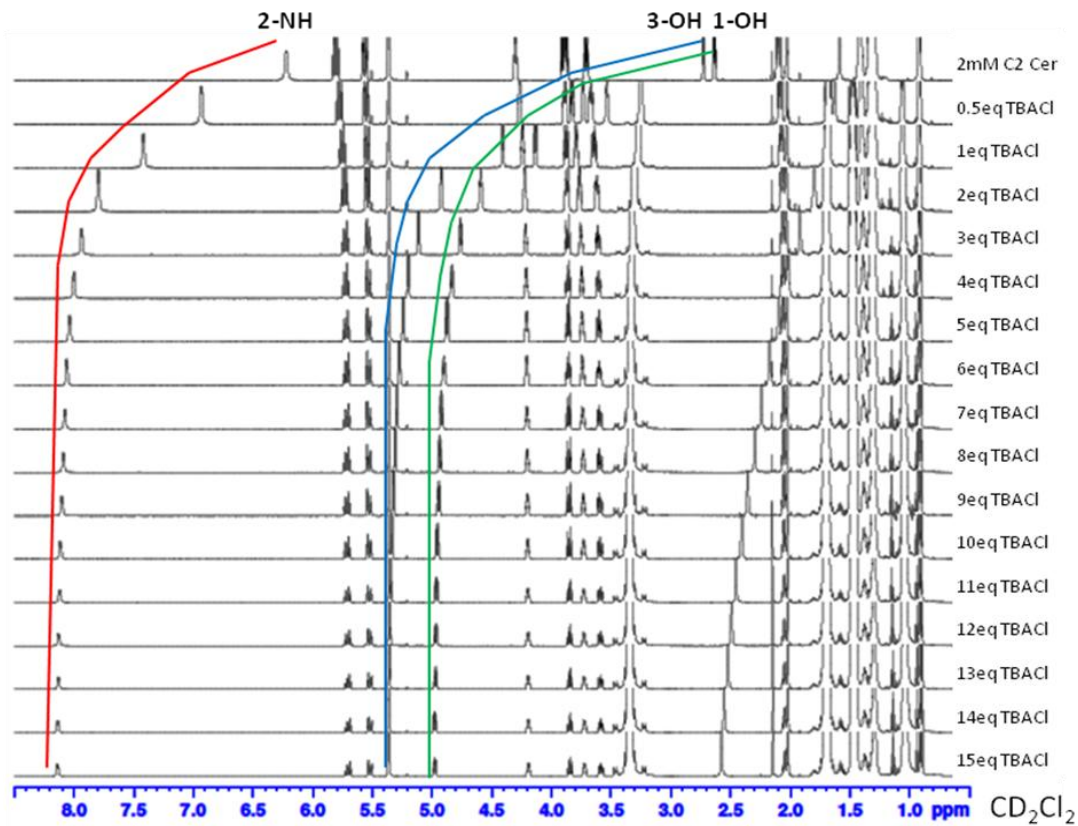


**Figure 3.14.** Stack plot from  $^1\text{H}$  NMR titrations of C2-ceramide **2** (2 mM) with increasing concentrations of tetrabutylammonium chloride (TBACl) in  $\text{CD}_2\text{Cl}_2$ .

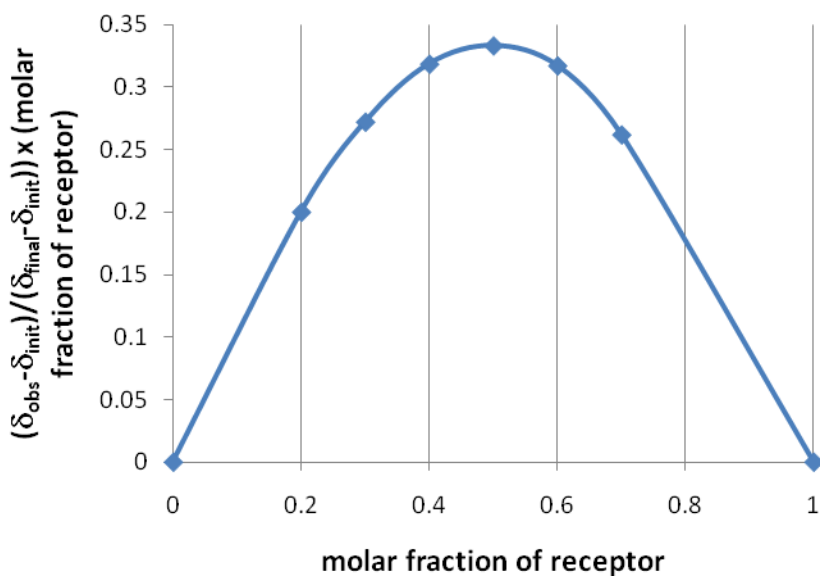


**Figure 3.15.** Job plot of C2-ceramide **2** with TBACl showing 1:1 binding.

To demonstrate the importance of the ceramide's 1,3-diol –OH groups in anion recognition, we conducted NMR binding experiments with isopropylidene C2-ceramide **18** (Figure 3.16). Isopropylidene C2-ceramide **18** had a much weaker affinity for Cl<sup>-</sup> ( $K_a = 27 \pm 0.6 \text{ M}^{-1}$ ) than did C2-ceramide **2**. These results are consistent with Hamilton's synthetic receptor that utilizes four amide –NH and two –OH functionalities to bind carboxylate anions.<sup>136</sup> In his system, removal of the two –OH groups leads to an 800 fold decrease in  $K_a$ . Together the MS and NMR data showed that the ceramide head group binds chloride in non-polar CD<sub>2</sub>Cl<sub>2</sub>.

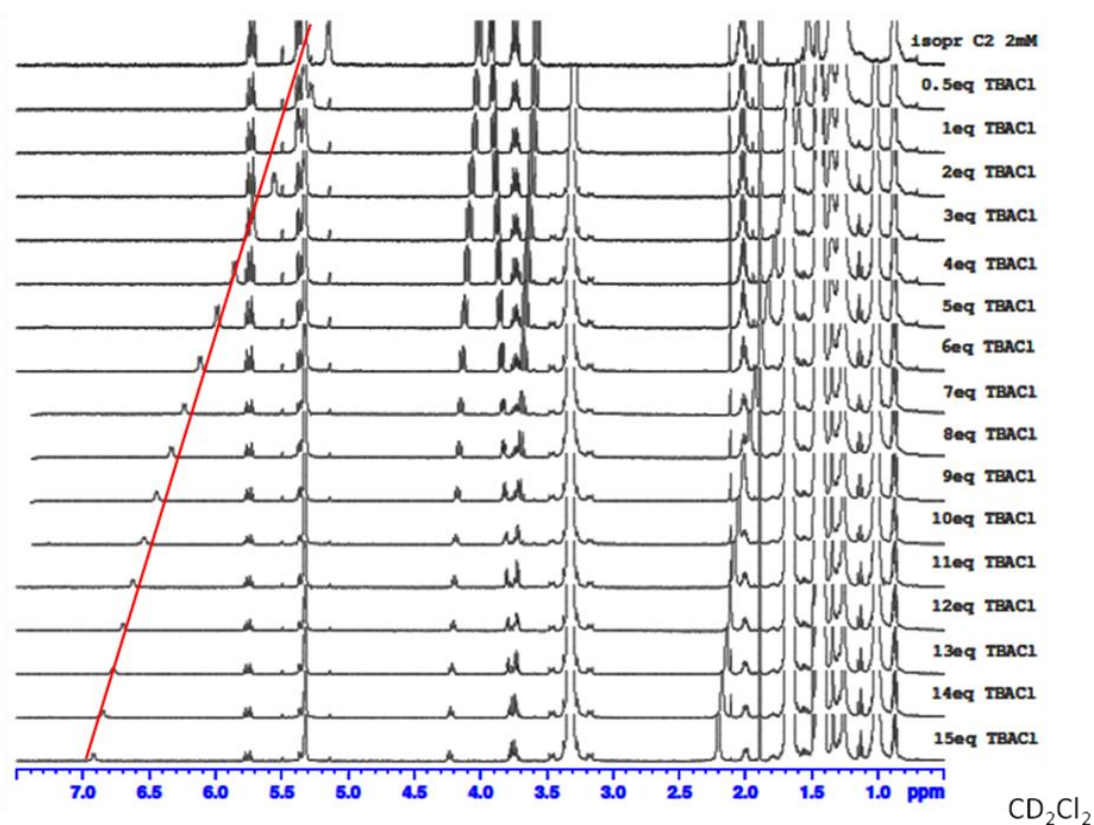


**Figure 3.16.** Stack plot from <sup>1</sup>H NMR titrations of isopropylidene C2-ceramide **18** (2 mM) with TBACl in CD<sub>2</sub>Cl<sub>2</sub>.

### 3.5 Transmembrane Anion Transport by C2-Ceramide 2

Since C2-ceramide **2** readily flip-flop within lipid bilayers ( $\tau_{1/2} \sim 1$  min at 20 °C),<sup>155,156</sup> we envisioned that the amphiphilic C2-ceramide **2** might function well as a transmembrane anion carrier.<sup>157</sup> Ceramides form nm-sized pores in liposomes when added at high concentrations (>10 mol%).<sup>158</sup> We wanted to determine if C2-ceramide **2** could transport anions across lipid membranes when present at lower concentrations, concentrations where transmembrane pores are not formed. Thus, we carried out carboxyfluorescein (CF) release assays to ensure that large channels were not formed by C2-ceramide **2** at concentrations of 1 mol%.<sup>159,160</sup> EYPC liposomes were prepared containing 1.5 mM CF and 6 mM *p*-xylene bis-pyridinium bromide (DPX). In the presence of DPX, CF fluorescence is quenched. If ceramide pores were formed that were large enough to allow release of either the intravesicular CF or DPX, then an increase in fluorescence should be observed. When 1 mol% concentrations of either C2-ceramide **2** or isopropylidene C2-ceramide **18** were added to these CF liposomes we observed no increase in fluorescence (**Figure 3.17**), indicating that large transmembrane pores were not formed at this particular ceramide concentration. Importantly, we found that higher concentrations of C2-ceramide **2** (15 mol%) did enable release of CF from EYPC liposomes (**Figure 3.18**).

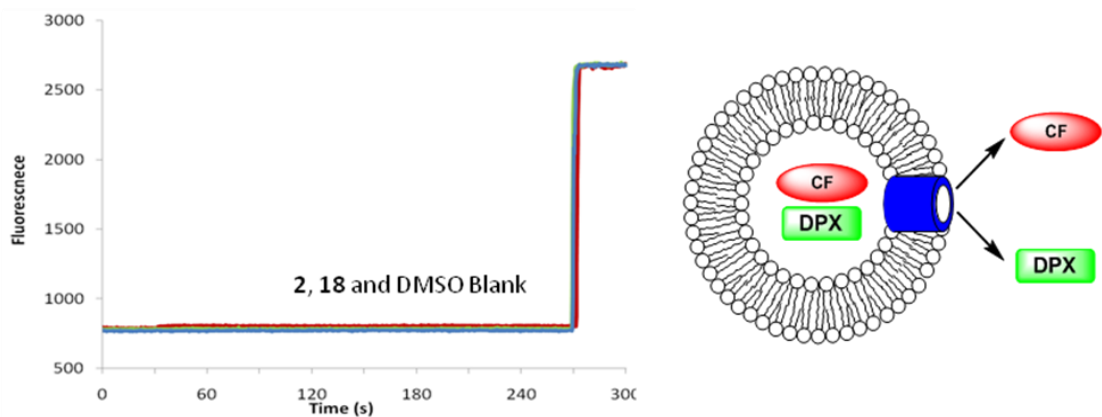


**Figure 3.17.** C2-ceramide **2** and isopropylidene C2-ceramide **18** were added at a 1 mol% compound to lipid ratio to a buffered solution of liposomes containing CF and DPX. At these concentrations, no large pores are formed by either compound.

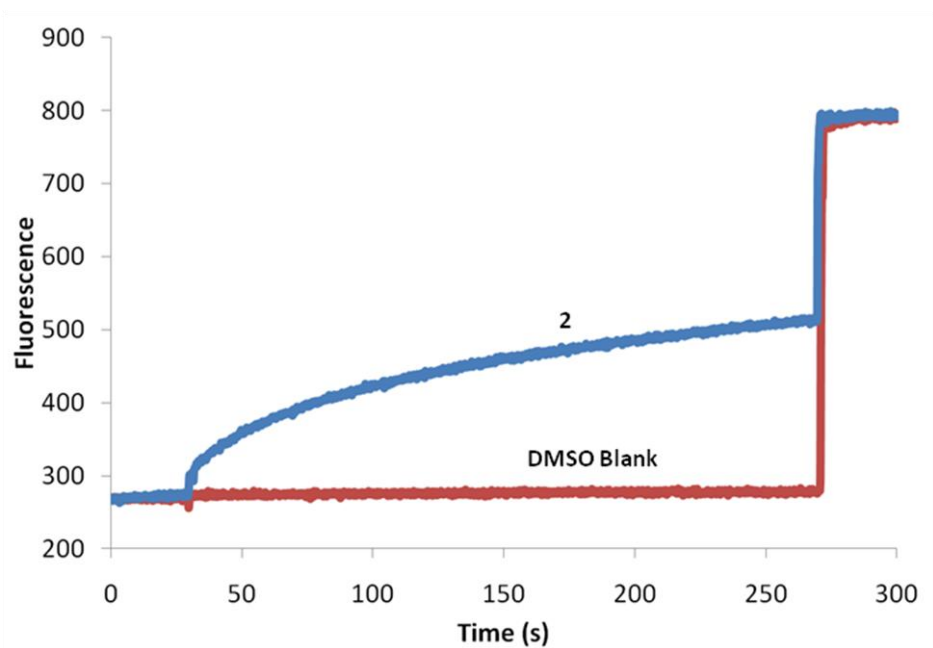


**Figure 3.18.** C2-ceramide **2** was added at a 15 mol% compound to lipid ratio to a buffered solution of liposomes containing CF and DPX. At this concentration, C2-ceramide forms pores in the phospholipid membrane large enough for to allow the escape of CF and/or DPX.

To evaluate the ability of C2-ceramide **2** to move  $\text{Cl}^-$  anions across membranes we used EYPC liposomes containing 100 mM NaCl and 2 mM lucigenin, a chloride-sensitive dye,<sup>161</sup> added to an extravesicular buffer containing nitrate

anions. Since  $\text{Cl}^-$  quenches lucigenin fluorescence, the facilitated efflux of  $\text{Cl}^-$  from liposomes, with concomitant influx of  $\text{NO}_3^-$ , can be monitored by an increase in fluorescence. Compounds **2** and **18** were added to liposomal solutions at 1 mol%, so as to stay below pore-forming concentrations. Only C2-ceramide **2**, and not isopropylidene C2-ceramide **18**, promoted release of chloride from the liposomes in the presence of external nitrate (**Figure 3.19**). The contrast in  $\text{Cl}^-$  transport for C2-ceramide **2** and its blocked derivative **18** demonstrates that ceramide's 1,3-diol is necessary for transporting  $\text{Cl}^-$  across the bilayer. This is, to our knowledge, the first demonstration that low concentrations of ceramides are capable of promoting exchange of anions across lipid membranes.

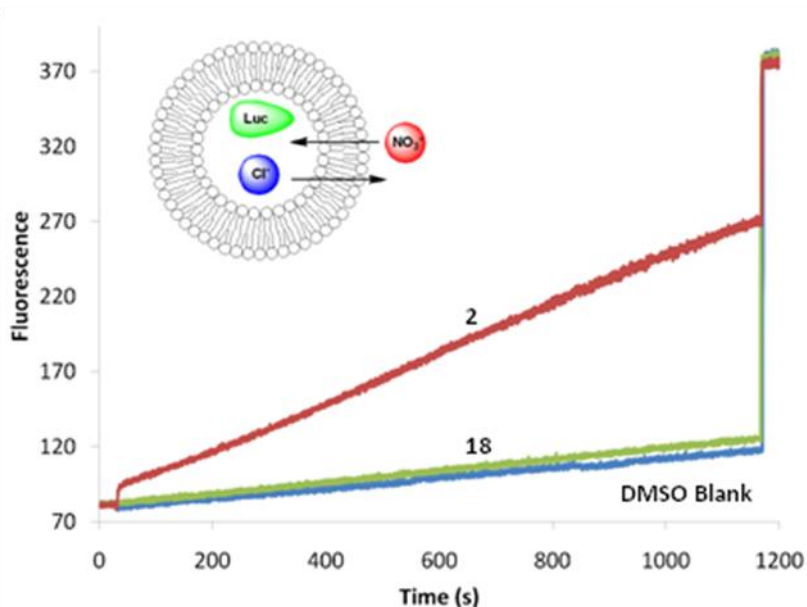


**Figure 3.19.** Chloride transport assay using EYPC liposomes (100 nm, 200  $\mu\text{M}$ ) with external nitrate (100 mM  $\text{NaNO}_3$ ) in 20 mM HEPES buffer (pH = 7.4). Upon addition of C2-ceramide **2** (2  $\mu\text{M}$ , 1 mol%), the increase in lucigenin fluorescence indicates  $\text{Cl}^-$  efflux. Only C2-ceramide **2** promoted the anion exchange of  $\text{Cl}^-/\text{NO}_2^-$ .

To gain some initial insight into the mechanism by which C2-ceramide **2** transports anions across lipid membranes, we measured  $\text{Cl}^-$  efflux in the presence of



different extravesicular anions. Thus, EYPC liposomes (100 mM NaCl, 2 mM lucigenin, 20 mM HEPES pH 7.4) were added to extravesicular buffers containing sulfate anions. Importantly, when sulfate was the extravesicular anion, little  $\text{Cl}^-$  efflux above the DMSO baseline was observed following addition of C2-ceramide **2** (or isopropylidene C2-ceramide **18**) (**Figure 3.20**). These results are consistent with ceramide-facilitated exchange of chloride for the singly charged nitrate anion. Sulfate, with its -2 charge and a much higher dehydration energy ( $\Delta G = -1080$  kJ/mol) than  $\text{Cl}^-$  ( $\Delta G = -340$  kJ/mol) or  $\text{NO}_3^-$  ( $\Delta G = -300$  kJ/mol),<sup>162</sup> is obviously more difficult to transport across a bilayer than either of the singly-charged anions. That minimal  $\text{Cl}^-$  transport was observed for solutions containing extravesicular  $\text{SO}_4^{2-}$  supports an anion-exchange mechanism mediated by C2-ceramide **2**. The lack of change in lucigenin fluorescence in the presence of extravesicular sulfate also provides further evidence that C2-ceramide **2** does not form large pores under these condition, as lucigenin would have been released from the vesicle if nM-sized pores had been formed by C2-ceramide **2**.

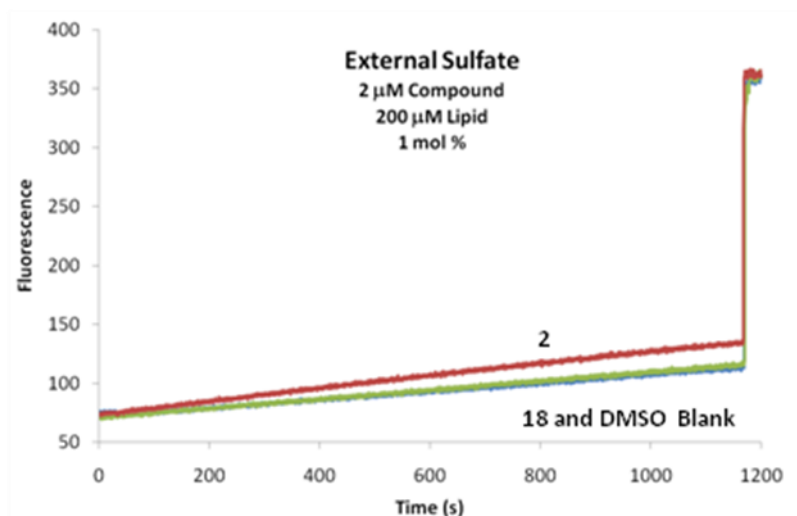


**Figure 3.20.** Chloride transport assay using EYPC liposomes (100 nm, 200  $\mu$ M) with external sulfate (75 mM  $\text{Na}_2\text{SO}_4$ ) in 20 mM HEPES buffer (pH = 7.4). Very little activity is observed for either compound.

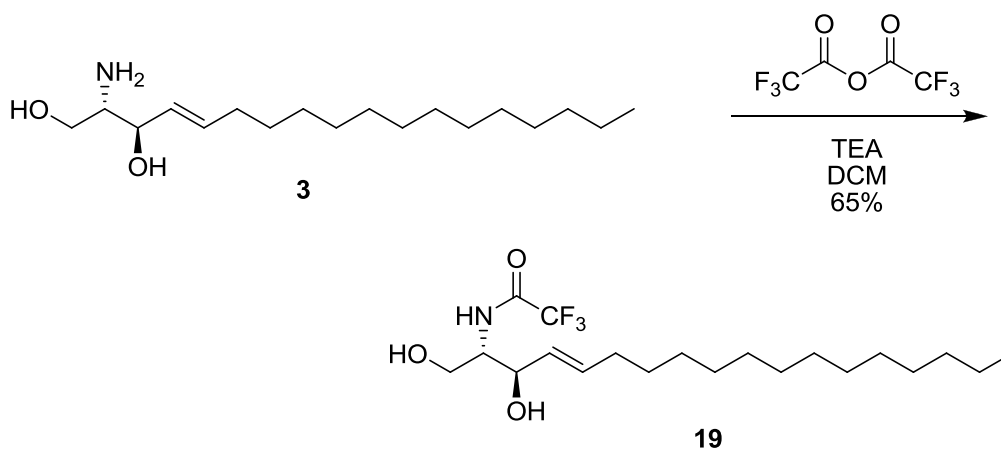
### 3.6 Anion Binding and Transport Studies of a C2-Ceramide Derivative with Modifications to the Amide Side-Chain

Following the discovery that C2-ceramide **2** facilitates the transport of monovalent anions, we decided to make modifications to the amide chain portion in an attempt to test structure-function relationships. We replaced the  $-\text{CH}_3$  group of the amide side-chain with a trifluoroacetyl group. The rationale behind this change was that the addition of an electron withdrawing group to the corresponding trifluoroacetyl C2-ceramide **19** analog should increase the acidity, and therefore the hydrogen bond donor ability of the amide  $-\text{NH}$ . In fact, equilibrium studies by Bordwell on acidities of simple methyl and trifluoro amides in DMSO give  $\text{pK}_a$ 's of 25.5 and 17.2, respectively for the  $-\text{NH}$  proton.<sup>163</sup> Using this trifluoroacetyl C2-ceramide **19** analog, we hope to find out whether there is a correlation between the amide  $-\text{NH}$  binding strength and anion transport. Hopefully this change would allow

for an increase in the binding and transport properties of this trifluoroacetyl C2-ceramide **19** derivative.

### 3.6.1 Preparation of a Trifluoroacetyl C2-Ceramide Analog

The preparation of trifluoroacetyl C2-ceramide **19** involved one step using D-erythro-sphingosine **3** as the starting material (**Scheme 3.2**). Trifluoroacetic anhydride was added to a dry CH<sub>2</sub>Cl<sub>2</sub> solution containing sphingosine **3** and triethylamine (TEA). The mixture was allowed to stir overnight at room temperature to give trifluoroacetyl C2-ceramide **19** in 65 % yield following purification via column chromatography. Spectroscopic characterization data is in good agreement with the two previous literature preparations of trifluoroacetyl C2-ceramide **19**.<sup>164,165</sup> In these two cases, trifluoroacetyl C2-ceramide **19** was used as a synthetic intermediate in the total synthesis of sphingosine **3**, where the trifluoroacetyl protecting group was removed under basic conditions. This study is the first, to our knowledge where trifluoroacetyl C2-ceramide **19** has been studied as a C2-ceramide **2** analog.



**Scheme 3.2.** Preparation of trifluoroacetyl C2-ceramide **19**.

### 3.6.2 $^1\text{H}$ NMR Evidence that Trifluoroacetyl C2-Ceramide **19** Binds Anions

Addition of TBACl to a solution of trifluoroacetyl C2-ceramide **19** in  $\text{CD}_2\text{Cl}_2$  resulted in smaller downfield shifts (NH  $\Delta\delta = 1.0$  ppm) in comparison to that observed for C2-ceramide **2** (NH  $\Delta\delta = 1.9$  ppm). However, the two OH signals of trifluoroacetyl C2-ceramide **19** have larger downfield shifts by approximately  $\Delta\delta=0.5$  ppm when compared to C2-ceramide **2** (**Figure 3.21**). By evaluating chemical shift changes for the NH proton of trifluoroacetyl C2-ceramide **19**, we determined a  $\text{Cl}^-$  binding constant of  $K_a = 3361 \pm 120 \text{ M}^{-1}$ , roughly twice that found for C2-ceramide **2** (See **Table 3.1** for a full list of binding constants). Addition of the  $-\text{CF}_3$  does seem to enhance the hydrogen bonding ability of C2-ceramide **2**.

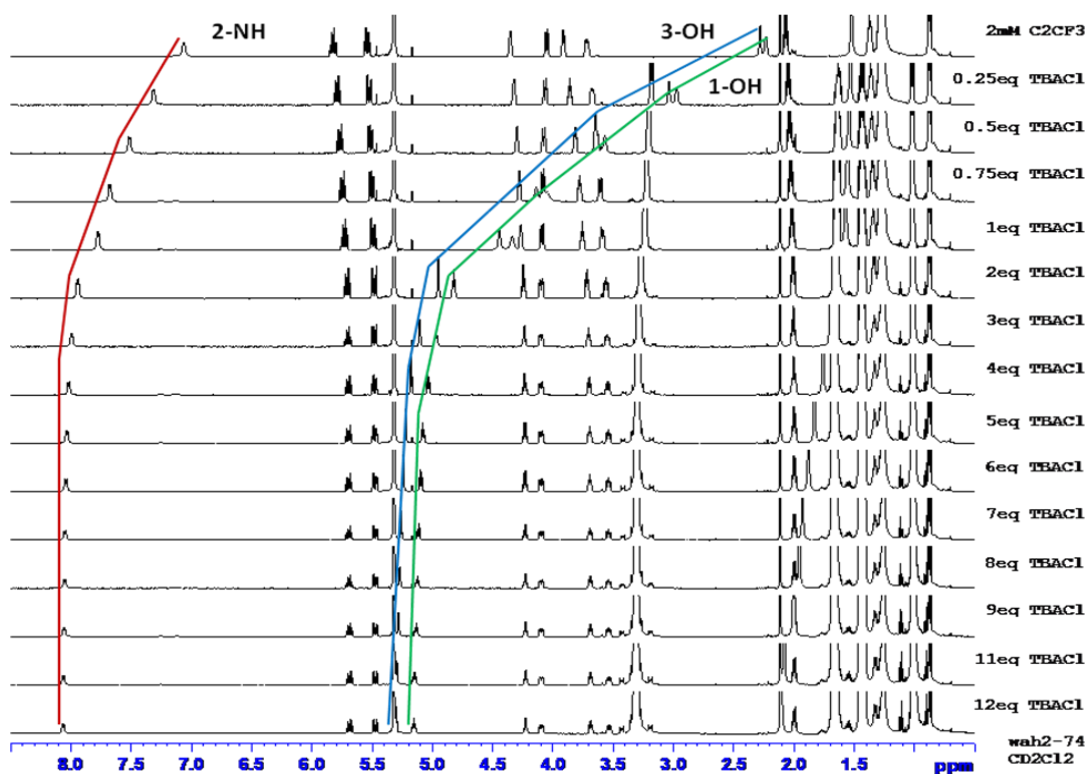


**Figure 3.21.** Stack plot from  $^1\text{H}$  NMR titrations of trifluoroacetyl C2-ceramide **19** (2 mM) with increasing concentrations of TBACl in  $\text{CD}_2\text{Cl}_2$ .

**Table 3.1.** Binding constants ( $K_a$ ) of C2-ceramide **2** and trifluoroacetyl C2-ceramide **19** with TBACl in  $CD_2Cl_2$ .

| Compound                              | $K_a$ ( $M^{-1}$ ) 2-NH | $K_a$ ( $M^{-1}$ ) 1-OH | $K_a$ ( $M^{-1}$ ) 3-OH |
|---------------------------------------|-------------------------|-------------------------|-------------------------|
| C2-ceramide <b>2</b>                  | $1734 \pm 82$           | $1935 \pm 65$           | $1877 \pm 54$           |
| trifluoroacetyl C2-ceramide <b>19</b> | $3361 \pm 120$          | $3817 \pm 386$          | $3628 \pm 278$          |

### 3.6.3 Anion Transport Activity of Trifluoroacetyl C2-Ceramide **19**

To evaluate the ability of trifluoroacetyl C2-ceramide **19** to transport anions across phospholipid membranes, we again used EYPC liposomes containing 100 mM NaCl and 2 mM lucigenin in the presence of various external anions. C2-ceramide **2** and trifluoroacetyl C2-ceramide **19** both facilitated the release of intravesicular chloride from the liposomes in the presence of nitrate. However, C2-ceramide **2** showed more activity in this chloride release assay when nitrate was the external anion (**Figure 3.22**). This result is somewhat surprising due to the fact that the binding constants of the trifluoroacetyl C2-ceramide **19** derivative with chloride were roughly double that of C2-ceramide **2**.

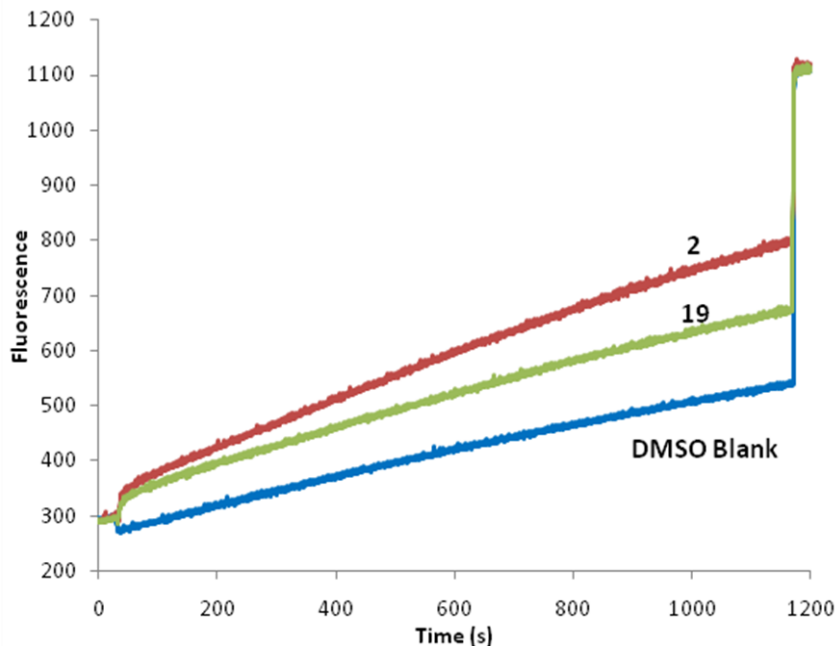


**Figure 3.22.** Chloride transport assay using EYPC liposomes (100 nm, 50  $\mu$ M) with external nitrate (100 mM  $\text{NaNO}_3$ ) in 20 mM HEPES buffer (pH = 7.4). The compounds were added at a concentration of 2  $\mu$ M (4 mol%). An increase in lucigenin fluorescence indicates  $\text{Cl}^-$  efflux.

In the next set of experiments, we used the same lucigenin containing EYPC liposomes, using bicarbonate as the external anion (**Figure 3.23**). Interestingly, the trifluoroacetyl C2-ceramide **19** derivative was more active than C2-ceramide **2** when bicarbonate was the external anion. Importantly, when sulfate was used as the external anion, little  $\text{Cl}^-$  efflux above background was observed (**Figure 3.24**). These results correspond to the trifluoroacetyl C2-ceramide **19** derivative facilitating anion exchange of chloride for either nitrate or bicarbonate.

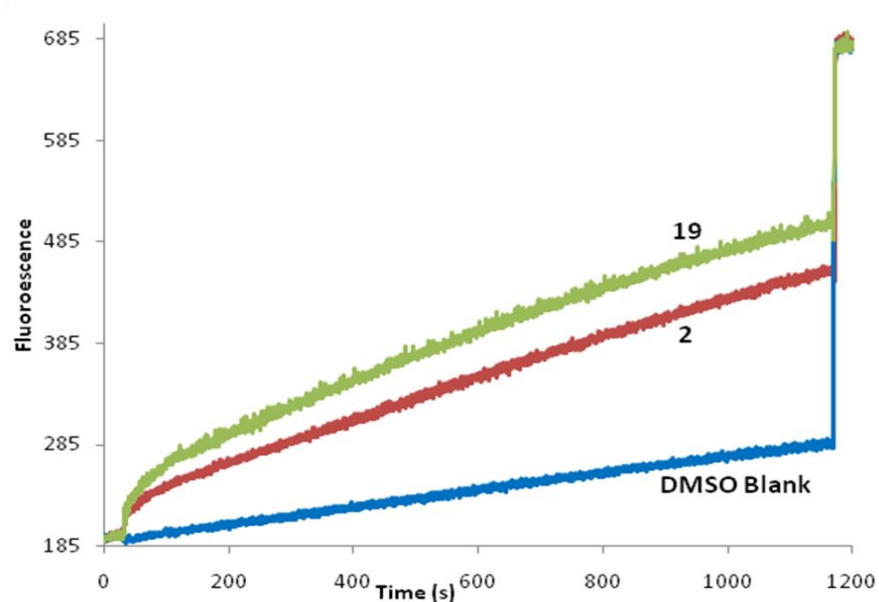


**Figure 3.23.** Chloride transport assay using EYPC liposomes (100 nm, 50  $\mu\text{M}$ ) with external bicarbonate (100 mM  $\text{NaHCO}_3$ ) in 20 mM HEPES buffer (pH = 7.4). The compounds were added at a concentration of 2  $\mu\text{M}$  (4 mol%). An increase in lucigenin fluorescence indicates  $\text{Cl}^-$  efflux.

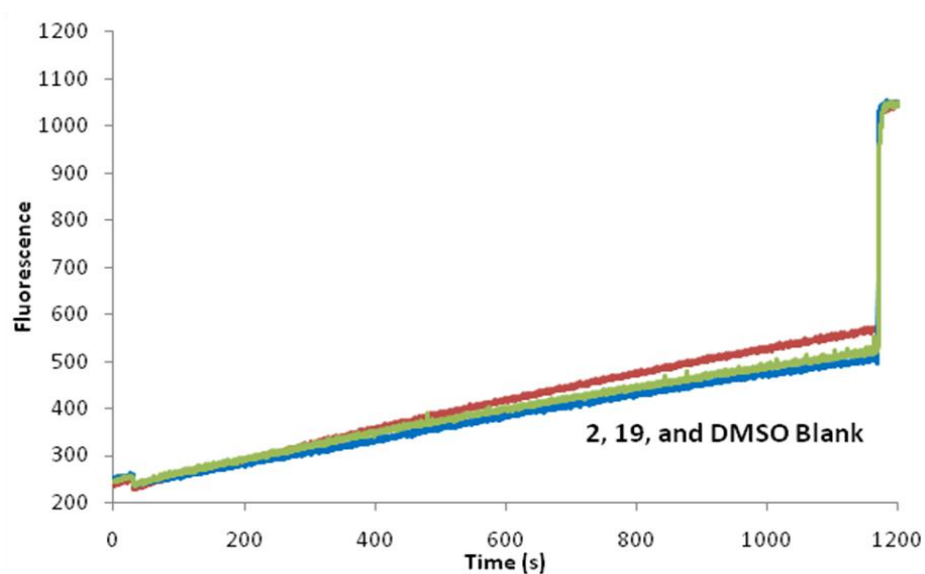


**Figure 3.24.** Chloride transport assay using EYPC liposomes (100 nm, 50  $\mu\text{M}$ ) with external sulfate (75 mM  $\text{Na}_2\text{SO}_4$ ) in 20 mM HEPES buffer (pH = 7.4). The compounds were added at a concentration of 2  $\mu\text{M}$  (4 mol%). Little activity was observed for any of compounds tested.

To ensure we were working below concentrations where ceramide forms large pores, we tested these three compounds in CF dye release assays. EYPC liposomes were prepared containing 20 mM CF, a concentration in which CF self-quenches.<sup>160</sup> If pores are formed that are large enough to allow the release of CF, an increase in fluorescence is observed. When 4 mol% concentrations of C2-ceramide **2** or trifluoroacetyl C2-ceramide **19** were added to these CF liposomes, we observe no increase in fluorescence (**Figure 3.25a**). This indicates that large transmembrane pores were not formed at the concentrations used in the lucigenin assays. Upon the addition of these compounds at 50 mol%, an increase in fluorescence is observed corresponding to the formation of pores in the phospholipid bilayer (**Figure 3.25b**). At these concentrations, trifluoroacetyl C2-ceramide **19** is more active at forming large pores than is C2-ceramide **2**.

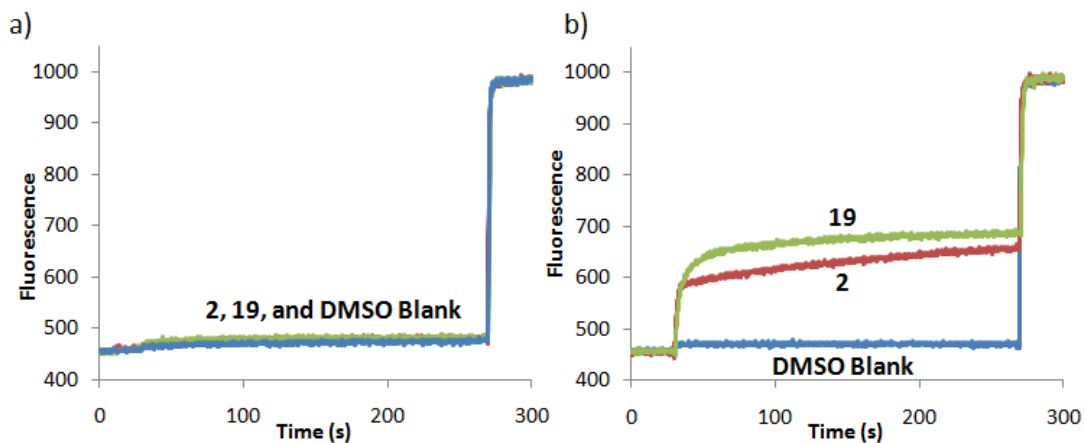


**Figure 3.25.** CF dye release assays. C2-ceramide **2** and trifluoroacetyl C2-ceramide **19** were added EYPC liposomes containing 20 mM CF in a 10 mM HEPES buffer at pH =7. Compounds were added at a) 4 mol% and b) 50 mol%.



### 3.7 Conclusions

One significant finding in this chapter is the observation that ceramide can permeabilize membranes in different ways. For instance, Colombini and colleagues have shown that high concentrations of ceramide lead to the formation of large transmembrane pores capable of allowing proteins to cross membranes.<sup>158,166</sup> In this chapter, we have shown that C2-ceramide **2** functions as a transmembrane anion transporter at concentrations below those where it self-associates to form the large transmembrane pores. Additionally, we have shown that the trifluoroacetyl C2-ceramide **19** analog functions as a transmembrane anion transporter that can facilitate the exchange of  $\text{Cl}^-/\text{HCO}_3^-$  better than that of C2-ceramide **2**. Ceramide's head group, with its 1,3-diol and its neighboring amide  $-\text{NH}$ , is well suited for binding biologically essential anions such as  $\text{Cl}^-$  and  $\text{HCO}_3^-$ . It may be that ceramide's ability to transport these physiologically relevant anions across lipid membranes is also important *in vivo*.

## Chapter 4 : Natural and Synthetic Small Molecules that Bind and Transport Bicarbonate

Portions of this chapter have been published in references 167-169.

- Harrell, W. A., Jr.; Bergmeyer, M. L.; Zavalij, P. Y.; Davis, J. T. Ceramide-mediated transport of chloride and bicarbonate across phospholipid membranes. *Chem. Commun.* **2010**, *46*, 3950-3952.
- Busschaert, N.; Gale, P. A.; Haynes, C. J.; Light, M. E.; Moore, S. J.; Tong, C. C.; Davis, J. T.; Harrell, W. A., Jr. Tripodal transmembrane transporters for bicarbonate. *Chem. Commun.* **2010**, *46*, 6252-6254.
- Andrews, N. J.; Haynes, C. J. E.; Light, M. E.; Moore, S. J.; Tong, C. C.; Davis, J. T.; Harrell, W. A., Jr.; Gale, P. A. Structurally simple lipid bilayer transport agents for chloride and bicarbonate. *Chem. Sci.* **2011**, *2*, 256-260.

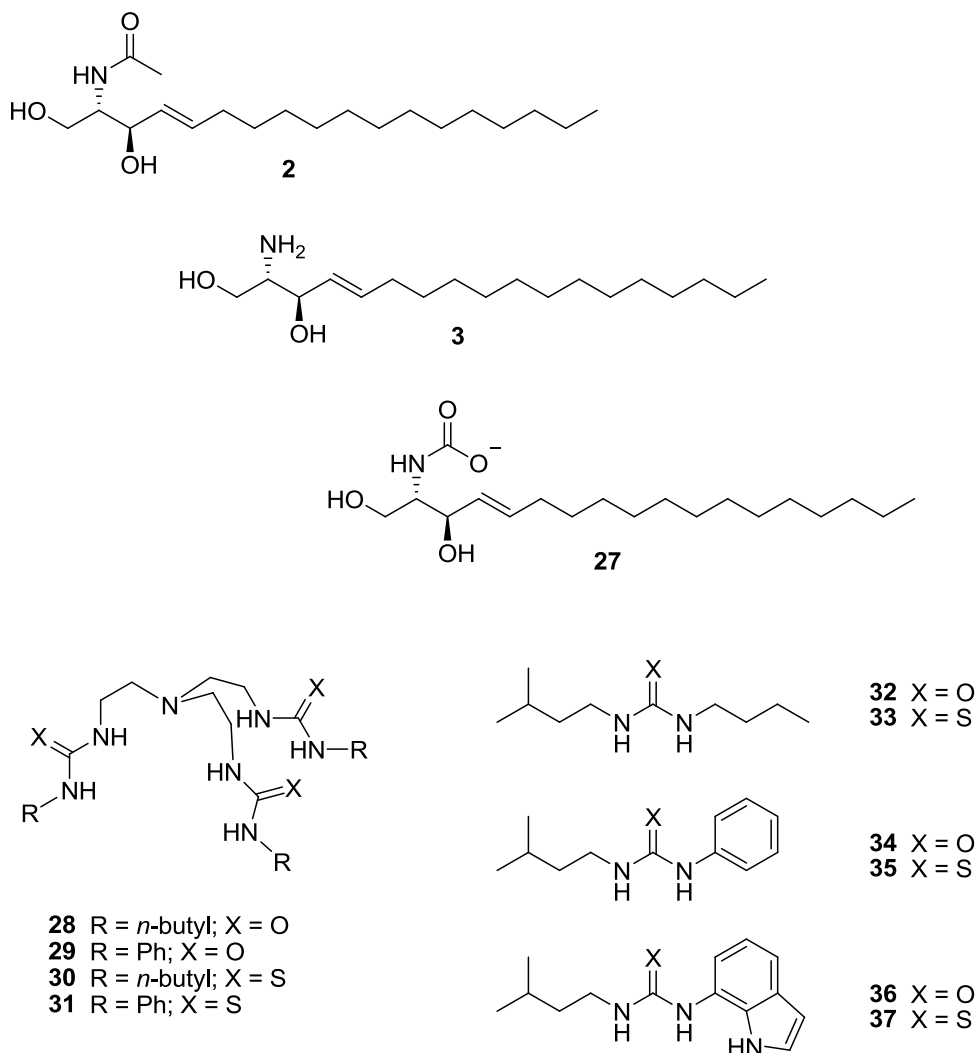
### 4.1 Introduction

The goal of the research in this chapter was to study the interactions of sphingolipids and small synthetic molecules with bicarbonate anion ( $\text{HCO}_3^-$ ). This chapter will be divided into two parts. In the first half of this chapter, I will discuss work that shows that C2-ceramide **2** and synthetic urea and thiourea-based small molecules (**28-37**) facilitate the transmembrane transport of  $\text{HCO}_3^-$  (see **Chart 4.1** for structures). Preceding this I will give a brief introduction on the biochemistry of bicarbonate anions, highlighting the importance of  $\text{HCO}_3^-$  to human health issues. I

will also describe other small molecules known to specifically facilitate the transmembrane transport of  $\text{HCO}_3^-$ .

We have also discovered that D-erythro-sphingosine **3** forms a carbamate (**27**) in the presence of  $\text{HCO}_3^-$  and  $\text{CO}_2$ . The second half of this chapter will begin with a brief discussion on the chemistry and biochemistry of  $\text{CO}_2$ . Since we elucidated that sphingosine **3** forms carbamates in the presence of  $\text{HCO}_3^-$  and  $\text{CO}_2$ , recent research on some other supramolecular carbamate-forming systems will be briefly discussed.

**Chart 4.1**

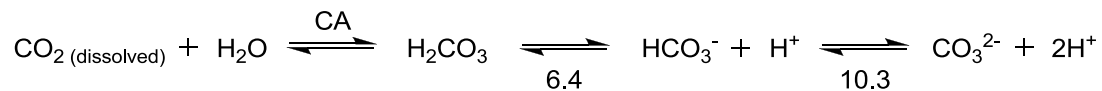


### 4.1.1 Chemistry and Biochemistry of Bicarbonate Anion and Carbon Dioxide

Bicarbonate is an organic anion that is relatively small (thermochemical radius  $r_c = 1.56 \text{ \AA}$ ) and more basic ( $\text{p}K_a$  [conjugate acid] = 6.4) when compared to other biologically relevant anions such as  $\text{NO}_3^-$  ( $r = 1.96 \text{ \AA}$ ,  $\text{p}K_a$  [conjugate acid] = -1.3) and  $\text{Cl}^-$  ( $r = 1.72 \text{ \AA}$ ,  $\text{p}K_a$  [conjugate acid] = -8.0).<sup>106,170</sup> As depicted in **Scheme 4.1**, an important chemical and biochemical property of the bicarbonate anion is that it is both the conjugate acid of carbonate ( $\text{CO}_3^{2-}$ ) and the conjugate base of carbonic acid ( $\text{H}_2\text{CO}_3$ ). These equilibrium processes make bicarbonate particularly difficult to study in terms of binding and transport, in that proper experiments must be designed in order to insure that binding, and not acid-base reactions are being observed.

Additionally, the amphoteric nature of  $\text{HCO}_3^-$  makes it an important buffering agent in biological systems. At physiological pH (~7.2-7.4), both  $\text{HCO}_3^-$  and  $\text{CO}_2$  are present in significant levels within the body (~95:5 ratio of  $\text{HCO}_3^- / \text{CO}_2$ ).<sup>171</sup> This equilibrium is important in the  $\text{CO}_2 / \text{HCO}_3^-$  buffer system that helps maintain cellular pH, as well as for larger systems in the body.<sup>172</sup>

Due to the negative charge associated with bicarbonate anions, they are unable to readily pass through a phospholipid bilayer without the assistance of a transporter.<sup>171</sup> In living cells, membrane-bound transport proteins are required to facilitate the movement of  $\text{HCO}_3^-$  across cell membranes.<sup>106</sup>



**Scheme 4.1.** Equilibrium reaction starting with  $\text{CO}_2$ , moving through  $\text{HCO}_3^-$  and ending with carbonate. The  $\text{p}K_a$  values are located below the equilibrium arrows. Carbonic anhydrases (CA) enhance the rate of the  $\text{CO}_2$  hydration and  $\text{HCO}_3^-$  dehydration reactions.

### 4.1.2 Why Study Bicarbonate Transport?

Bicarbonate is implicated in a number of important biological processes including regulation of physiological pH and respiration.<sup>173</sup> **Table 4.1** lists a few additional biological implications of  $\text{HCO}_3^-$ . For example, the inability to properly regulate the transmembrane transport of  $\text{HCO}_3^-$  and  $\text{Cl}^-$  can lead to conditions such as cystic fibrosis and heart disease.<sup>106,107,174</sup>

**Table 4.1.** Bicarbonate plays a key role in multiple biological functions

| Major Role       | Target  | Function                         | Ref.        |
|------------------|---|----------------------------------|-------------|
| Enzyme Substrate | Rubisco                                       | Photosynthesis                   | 175         |
|                  | Carbonic Anhydrase                            | Cell Respiration / Metabolism    | 106,176,177 |
|                  | Biotin Carboxylase                            | Biosynthesis / Metabolism        | 178         |
|                  | Acetyl-CoA Carboxylase                        | Fatty Acid Biosynthesis          | 179         |
| Enzyme Co-factor | Leucine Aminopeptidase                        | Protein Metabolism               | 180         |
|                  | Plant Cyclopropane Oxidase                    | Ethylene Biosynthesis            | 181         |
| Cellular Signal  | cAMP Synthase                                 | Sperm Activation                 | 182,183     |
| Homeostasis      | Anion Exchange Proteins                       | $\text{HCO}_3^-$ Transport       | 106,184     |
|                  | $\text{Na}^+$ / $\text{HCO}_3^-$ Symporters   | Pancreas and Kidney              | 185-187     |
| Disease / Health | CFTR $\text{Cl}^-$ / $\text{HCO}_3^-$ Channel | Cystic Fibrosis                  | 107         |
|                  | DNA Cis-Platin Complex                        | Cancer Chemotherapy              | 106,188     |
|                  | Carbonic Anhydrase                            | Memory / Alzheimer's Disease     | 189         |
|                  | Bone Markers                                  | Osteoporosis / Bone Resorption   | 190         |
|                  | Anion Exchange Proteins                       | Epilepsy / Cardiovascular Health | 106,174,191 |

### 4.1.3 Chloride / Bicarbonate Exchange Proteins

Carbon dioxide is produced during cellular respiration as a metabolic waste product. Acetyl-CoA is oxidized to  $\text{CO}_2$  in the Krebs cycle, which is the primary source of energy production in the mitochondria. However,  $\text{CO}_2$  is poorly soluble in aqueous media such as the blood.<sup>106</sup> Carbon dioxide released during respiration diffuses through blood plasma into red blood cells. Carbonic anhydrases (CAs) then catalyze the reversible conversion of  $\text{CO}_2$  to  $\text{HCO}_3^-$ , providing a more soluble species of  $\text{CO}_2$  in the blood plasma.<sup>191,192</sup> The  $\text{HCO}_3^-$  is carried to the lungs where it is transported back into red blood cells. In the lungs, CAs then convert bicarbonate back to  $\text{CO}_2$ , which is then exhaled through the lungs. The transport of  $\text{HCO}_3^-$  in and out of red blood cells is facilitated by specific bicarbonate transport proteins.

Anion exchange (AE) proteins, a class of chloride / bicarbonate exchangers, facilitate the transport of bicarbonate into and out of red blood cells during respiration. First isolated and studied in 1985, the AE family of chloride / bicarbonate exchangers all function through an electroneutral ion exchange mechanism.<sup>193,194</sup> AE proteins work by reversibly exchanging  $\text{Cl}^-$  and  $\text{HCO}_3^-$  in a process that is driven by gradient differences across cell membranes.<sup>195</sup> Due to their important role in respiration, AE proteins represent the most studied class of bicarbonate transporters.

A second group of bicarbonate transport proteins belong to the SLC26 class of proteins. Misregulation of anions in the kidneys due to faulty SLC26 proteins can lead to the formation of kidney stones.<sup>196,197</sup> Originally determined to function as sulfate transport proteins, some members of SLC26 family also function as chloride /

bicarbonate exchangers.<sup>198-200</sup> The SLC26 class of proteins also use an electroneutral ion exchange mechanism, exchanging one  $\text{Cl}^-$  for every  $\text{HCO}_3^-$ .<sup>201,202</sup>

#### **4.1.5 Small Molecules that Facilitate the Transmembrane Transport of $\text{HCO}_3^-$**

Bicarbonate anions are incredibly important to biological systems. However, there has been surprisingly little research on small molecules that facilitate the transmembrane transport of  $\text{HCO}_3^-$ , and little before 2009.<sup>203</sup> Currently, there are only five papers that specifically discuss this topic; and I am a co-author on three of these papers.

In **Chapter 3**, I described research showing that C2 ceramide **2** belongs to a small group of natural products that have been shown to facilitate transmembrane anion transport.<sup>167</sup> In this chapter I will present evidence that C2-ceramide **2** also belongs to a small group of compounds that are known to specifically transport  $\text{HCO}_3^-$  across phospholipid membranes. Prodigiosin **21** is another natural product that falls into this category. Prodigiosin **21** is known to facilitate the symport of  $\text{H}^+/\text{Cl}^-$  and the antiport of  $\text{Cl}^-/\text{NO}_3^-$  across phospholipid membranes.<sup>204,205</sup> In 2009, Oluyomi Okunola and Jeffery Davis, in collaboration with Philip Gale and Roberto Quesada, published research determining that prodigiosin **21** can also transport bicarbonate anions across lipid bilayers.<sup>206</sup> This was the first paper describing a small molecule natural product that can facilitate the transmembrane transport of  $\text{HCO}_3^-$ .

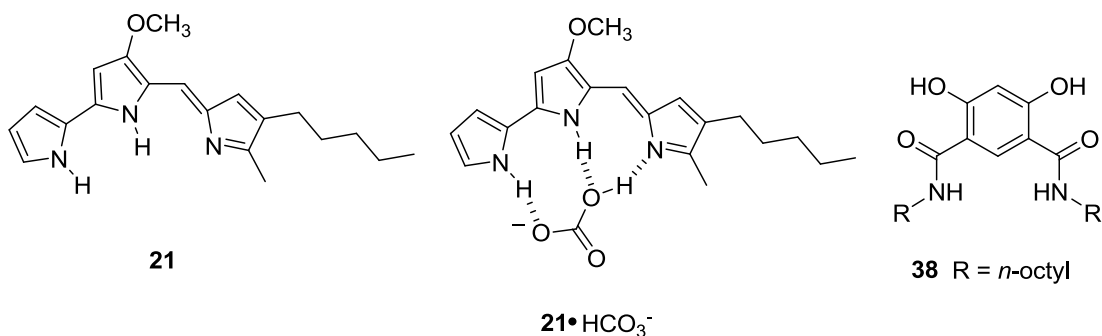


**Figure 4.1.** Structure of prodigiosin **21**, a proposed structure of a prodigiosin **21•HCO<sub>3</sub><sup>-</sup>** complex, and the structure of isophthalamide **38**.

Using NMR spectroscopy, the authors showed that prodigiosin **21** and the synthetic isophthalamide **38** bind HCO<sub>3</sub><sup>-</sup> in non-polar solvents, such as CD<sub>2</sub>Cl<sub>2</sub>. In one set of experiments, chloride containing liposomes were suspended in a buffer containing sulfate. A Cl<sup>-</sup> selective electrode was used to monitor the efflux of Cl<sup>-</sup> from the liposomes. Prodigiosin **21** or isophthalamide **38** were added to the liposomal solution, and allowed a two minute incubation time to incorporate into the liposomes. During this time, no appreciable amount of Cl<sup>-</sup> was observed to be released from the liposomes. Upon the addition of HCO<sub>3</sub><sup>-</sup> to the liposomal solution, an increase in extravesicular chloride was observed, suggesting that prodigiosin **21** and isophthalamide **38** can facilitate the exchange of Cl<sup>-</sup>/HCO<sub>3</sub><sup>-</sup> across phospholipid membranes.

However, these experiments only provided indirect evidence of bicarbonate transport. In order to monitor the transport of bicarbonate directly, the authors introduced a new <sup>13</sup>C NMR assay using H<sup>13</sup>CO<sub>3</sub><sup>-</sup>. Liposomes were prepared containing H<sup>13</sup>CO<sub>3</sub><sup>-</sup>, with sulfate as the external anion. Internal and external H<sup>13</sup>CO<sub>3</sub><sup>-</sup> peaks gave distinct signals in the <sup>13</sup>C NMR spectrum. In order to verify this, a



paramagnetic  $\text{Mn}^{2+}$  line broadening agent was used to bleach the signal of any external  $\text{H}^{13}\text{CO}_3^-$  into the baseline. These experiments show that both prodigiosin **21** and isophthalamide **38** can facilitate the anion exchange of  $\text{Cl}^-/\text{HCO}_3^-$  across phospholipid membranes (**Figure 4.2**).

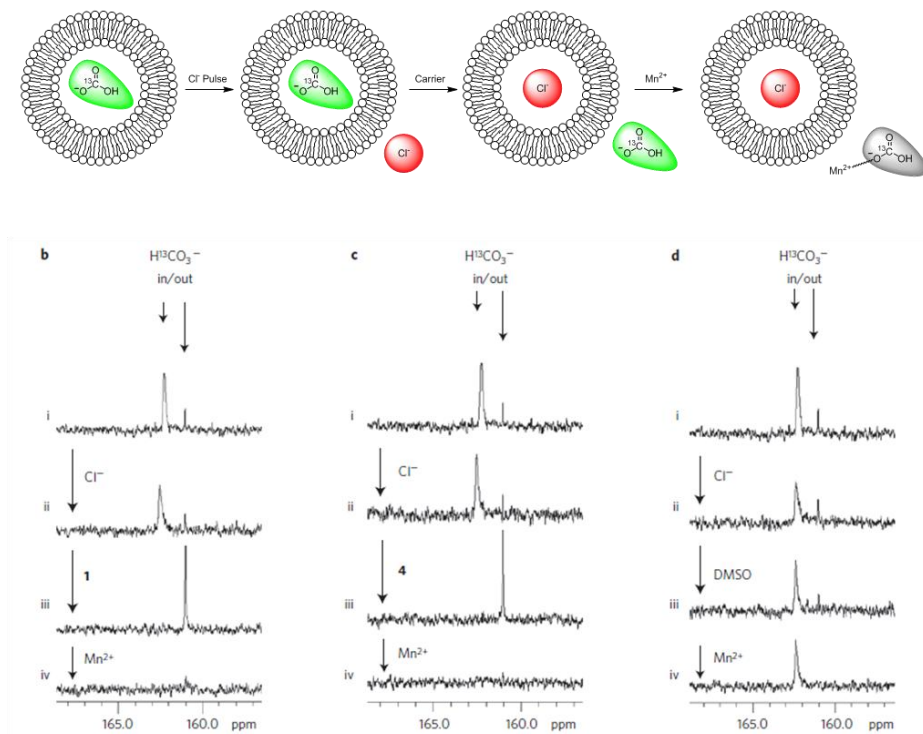


**Figure 4.2.**  $^{13}\text{C}$ -NMR experiments showing that prodigiosin **21** is able to facilitate  $\text{Cl}^-/\text{HCO}_3^-$  exchange. The titration sequence for monitoring the transmembrane transport of bicarbonate ions is as follows:  $^{13}\text{C}$  NMR spectra (i) before and (ii) after the addition of the chloride pulse to EYPC vesicles containing  $\text{H}^{13}\text{CO}_3^-$ ; (iii) after the addition of prodigiosin **21**, isophthalamide **38** or DMSO blank; (iv) after the addition of  $\text{Mn}^{2+}$ . Figure used with permission from reference 206.

Another small molecule that was recently determined to transport bicarbonate across lipid bilayers is octafluorocalix[4]pyrrole **39** (**Figure 4.3**).<sup>207</sup> In contrast to the non-fluorinated calixpyrrole, which had limited anion transport properties, Sessler, Gale, and Quesada discovered that the fluorinated derivative had a much higher affinity for anions. This is presumably due to the electron withdrawing fluorine

substituents that increase the acidity, and therefore, the hydrogen bond donor ability of the pyrrole units. The authors found that octafluorocalix[4]pyrrole **39** allows for the anion exchange of  $\text{Cl}^-$  and  $\text{HCO}_3^-$  using the same ion sensitive electrode liposome experiments as described above.

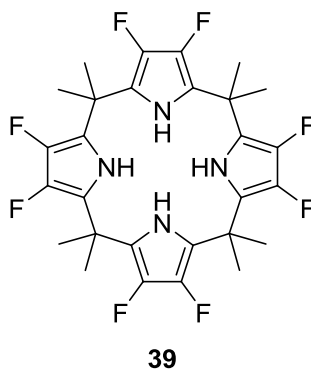


**Figure 4.3.** Octafluorocalix[4]pyrrole **39** facilitates  $\text{Cl}^-/\text{HCO}_3^-$  exchange.

In two recent collaborative papers, the Davis and Gale groups identified two classes of thiourea-based compounds that facilitate exchange of  $\text{Cl}^-$  and  $\text{HCO}_3^-$  across phospholipid membranes (**Figure 4.4**).<sup>168,169</sup> Both urea and thiourea derivatives were able to bind anions, but only the thiourea analogs were able to transport anions in ion sensitive electrode and  $^{13}\text{C}$  NMR assays. My contributions to these papers will be explained in greater detail later in this chapter.

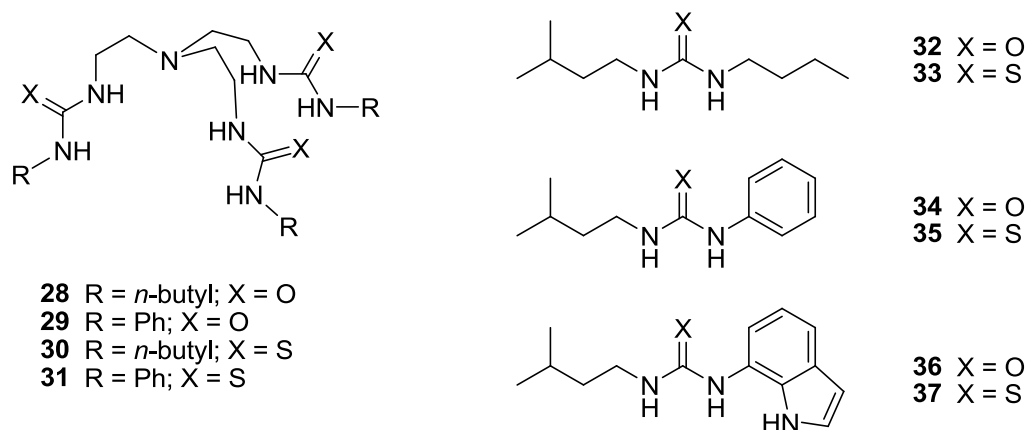


**Figure 4.4.** Urea- and thiourea-based compounds for the study of  $\text{HCO}_3^-$  transport.

#### 4.2 C2-Ceramide **2** Binds and Transports $\text{HCO}_3^-$

To determine that C2-ceramide **2** binds bicarbonate anions, 2 mM solutions of C2-ceramide **2** in  $\text{CD}_2\text{Cl}_2$  were prepared with increasing amounts of tetraethylammonium bicarbonate ( $\text{TEAHCO}_3$ ). Large downfield shifts of the  $-\text{NH}$  proton ( $\Delta\delta = 1.8$  ppm) were observed (**Figure 4.5**). Unfortunately, we could not follow the shift of the  $-\text{OH}$  protons as addition of  $\text{TEAHCO}_3$  to solutions of C2-ceramide **2** led to the disappearance of the  $-\text{OH}$  signals. Additionally, these spectra were further complicated by the appearance of small signals at  $\delta$  4.4, 4.8, and 6.9 ppm. While it is unclear exactly what gives rise to these signals, we believe they may correspond to the binding of C2-ceramide **2** to a small amount of carbonate in solution. By evaluating the chemical shift changes for the  $-\text{NH}$  proton, we determined a  $\text{HCO}_3^-$  binding constant of  $K_a = 1933 \pm 58 \text{ M}^{-1}$  for C2-ceramide **2** in  $\text{CD}_2\text{Cl}_2$ , using the WinEQNMR2 program.<sup>154</sup> The binding constant for  $\text{HCO}_3^-$  is consistent with that found for C2-ceramide **2** and  $\text{Cl}^-$  ( $K_a = 1734 \pm 82 \text{ M}^{-1}$ ).

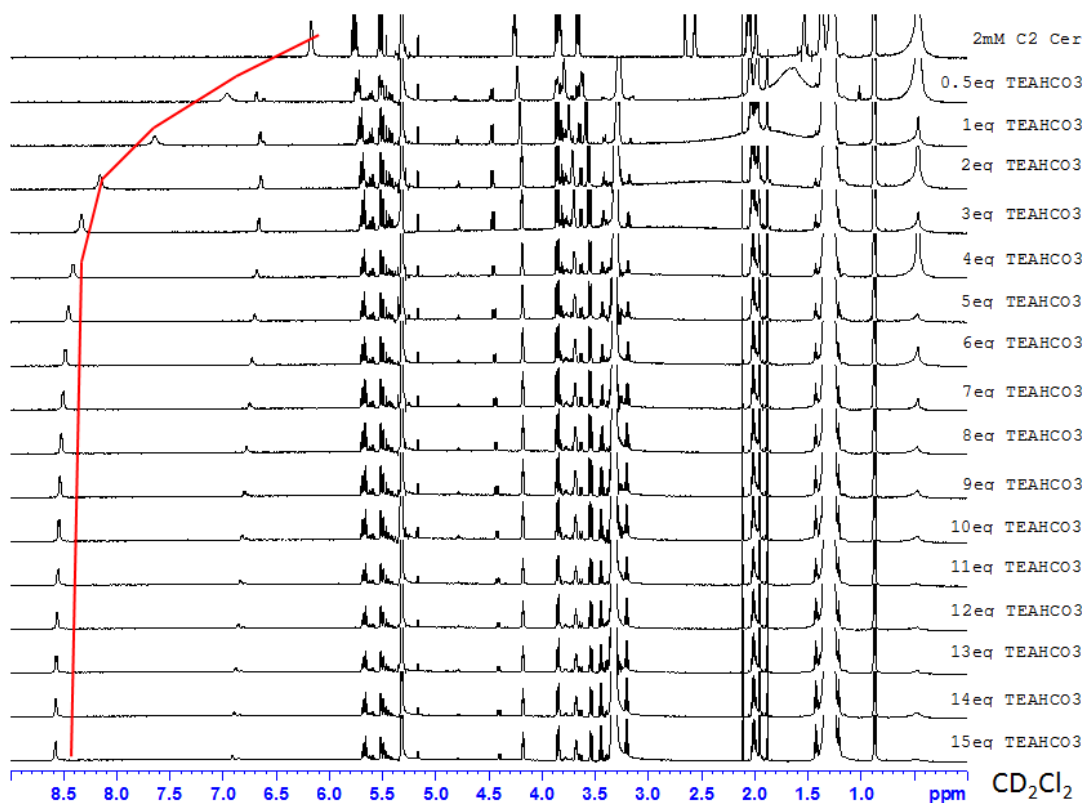


**Figure 4.5.** Stack plot from  $^1\text{H}$  NMR titrations of 2 mM solutions of C2-ceramide **2** with  $\text{TEAHCO}_3$  in  $\text{CD}_2\text{Cl}_2$ . The line shows the change in the chemical shift of the C2-ceramide **2** amide  $-\text{NH}$  signal with increasing concentration of  $\text{TEAHCO}_3$ .

To evaluate the ability of C2-ceramide **2** to facilitate the transport of bicarbonate anions across phospholipid bilayers, EYPC liposomes were prepared containing 100 mM NaCl and 2 mM lucigenin, a chloride-sensitive dye.<sup>208</sup> The liposomes were suspended in an extravesicular buffer containing bicarbonate anions. Since  $\text{Cl}^-$  quenches the fluorescence of lucigenin, the facilitated exchange of  $\text{Cl}^-$  with extravesicular  $\text{HCO}_3^-$  can be monitored by an increase in fluorescence.

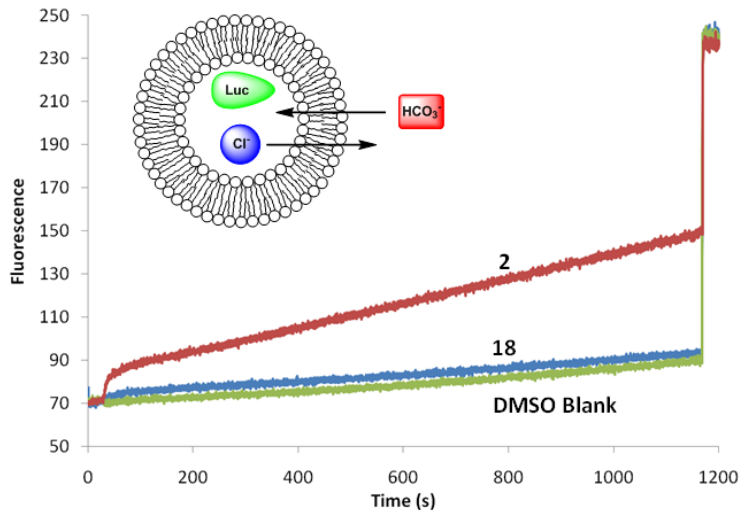


**Figure 4.6.** Chloride transport assay using EYPC liposomes (100 nm, 200  $\mu$ m) containing  $\text{Cl}^-$  and lucigenin, with external bicarbonate (100 mM) in a 20 mM HEPES buffer (pH = 7.4). C2-ceramide **2** and isopropylidene C2-ceramide **18** were added at concentrations of 1 mol % (relative to phospholipid concentration).

Following the addition of C2-ceramide **2** (2  $\mu$ M, 1 mol %) to liposomes suspended in a bicarbonate buffer, an increase in the fluorescence of lucigenin was observed (**Figure 4.6**). If the external bicarbonate was replaced with sulfate anions, little fluorescence increase was observed (**Figure 4.7**). This result is consistent with ceramide-facilitated exchange of chloride and bicarbonate. Addition of the protected isopropylidene C2-ceramide **18** did not allow for  $\text{Cl}^-/\text{HCO}_3^-$  exchange across the liposomal membrane. For comparison purposes, **Figure 4.7** shows fluorescence data from the chloride transport assays with various external anions using C2-ceramide **2**. C2-ceramide **2** facilitated the exchange of intravesicular chloride when either bicarbonate or nitrate was the external anion. When sulfate was the external anion, no anion exchange was observed.

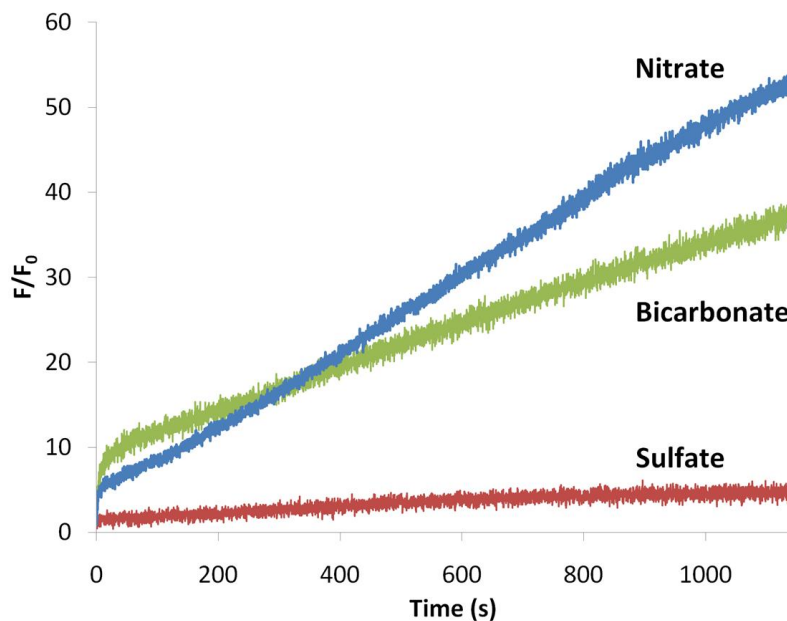


**Figure 4.7.** For comparison purposes, fluorescence data from the chloride transport assays using C2-ceramide **2** is plotted as a function of initial fluorescence ( $F_0$ ).

These results put C2-ceramide **2** into a small group of naturally-occurring small molecules that facilitate transmembrane bicarbonate transport, with prodigiosin **21** being the only other natural product shown to transport bicarbonate. Additionally, this suggests that ceramide could play a role in the transport of  $\text{Cl}^-/\text{HCO}_3^-$  in natural systems. For instance, cystic fibrosis (CF) is caused by mutations in the CF transmembrane conductance regulator (CFTR). Mutations in the CFTR leads to misregulation of  $\text{Cl}^-$  and  $\text{HCO}_3^-$  transport across lung epithelial cell membranes.<sup>107</sup> Recently, Worgall and colleagues found that cells with defective CFTR show an increase in production of sphingolipids, including various ceramides.<sup>209</sup> Our results suggest that this increase in ceramide accumulation may be the cells' attempt to regain some level of anion conductance across the epithelial cell membrane.

### 4.3 Tren-Based Small Molecules: A New Class of Bicarbonate Transporters

Bicarbonate is a biologically important anion. In a collaboration between the Davis and Gale labs, we set out to determine if tris(2-aminoethyl)amine (tren) based compounds could facilitate the transport of  $\text{HCO}_3^-$  across phospholipid membranes.<sup>168</sup> Previous studies have shown that tren-based compounds can have various membrane activities. For instance, D. K. Smith and co-workers have shown that tren-based tris-amides facilitate  $\text{H}^+/\text{Cl}^-$  symport across  $\text{CH}_2\text{Cl}_2$  “membranes” in U-tube experiments.<sup>210</sup> In Smith’s experiments, two aqueous layers were separated by an organic layer. The water layer on one side was doped with HCl. Transport of HCl by tren **40** was monitored by a change in pH in the water layer on the other side.

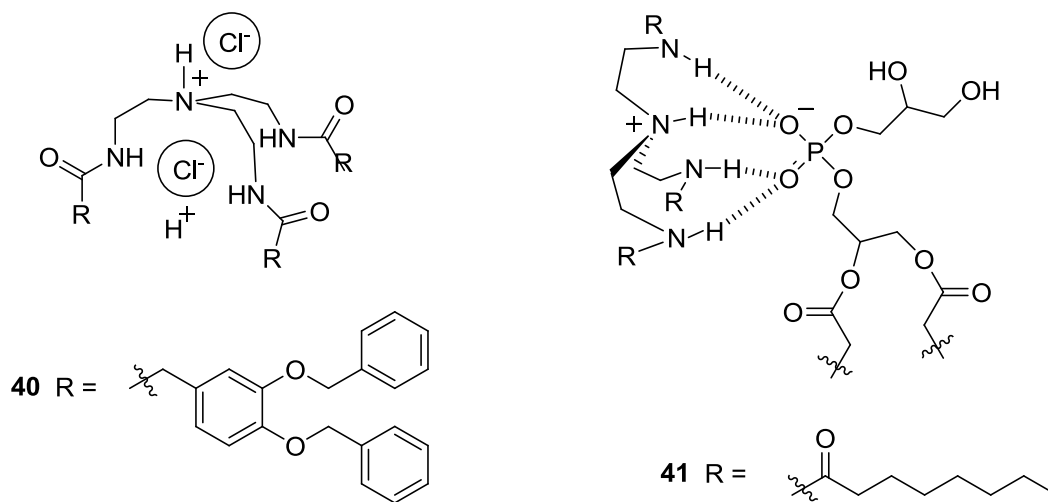


**Figure 4.8.** Examples of membrane active tren-based amides.

In another example, Brad Smith has demonstrated that tren-based amides can act as synthetic phospholipid flippases.<sup>211</sup> Smith was able to show that tren **41** was able to facilitate the translocation of anionic phospholipid mimics across surface differentiated vesicles. He proposed that tren **41** binds with the negatively charged phosphate group of anionic phospholipids. When tren **41** crosses the membrane, it

carries the head group along with it, causing the phospholipid to move from the outer leaflet of the phospholipid bilayer to the inner leaflet.

Additionally, Sofia Berezin in the Davis lab has shown that a bis-catechol tren based receptor **25** is capable of transmembrane chloride transport.<sup>150</sup> For a more detailed description of this work, see **Section 3.3.2**.

#### **4.4 Thiourea Tren-Based Receptor Facilitates the Transport of HCO<sub>3</sub><sup>-</sup>**

In collaboration with the Gale group, we have discovered a new class of bicarbonate transporters.<sup>168</sup> Synthesized by members of the Gale group, these compounds are based on a tren scaffold, containing either tris-urea or tris-thiourea functionalities (**Figure 4.9a**). NMR titrations in d<sub>6</sub>-DMSO/0.5% H<sub>2</sub>O with tetrabutylammonium chloride gave binding constants of 658, 830, 447, and 191 M<sup>-1</sup> for compounds **28-31**, respectively. Additionally, single crystals of a carbonate complex of tren **31** were grown by slow evaporation of DMSO/water solution in the presence of excess tetraethylammonium bicarbonate. The solid state structure revealed that two equivalents of tren **31** bind to a single carbonate anion via 12 hydrogen bonds (**Figure 4.9b**).



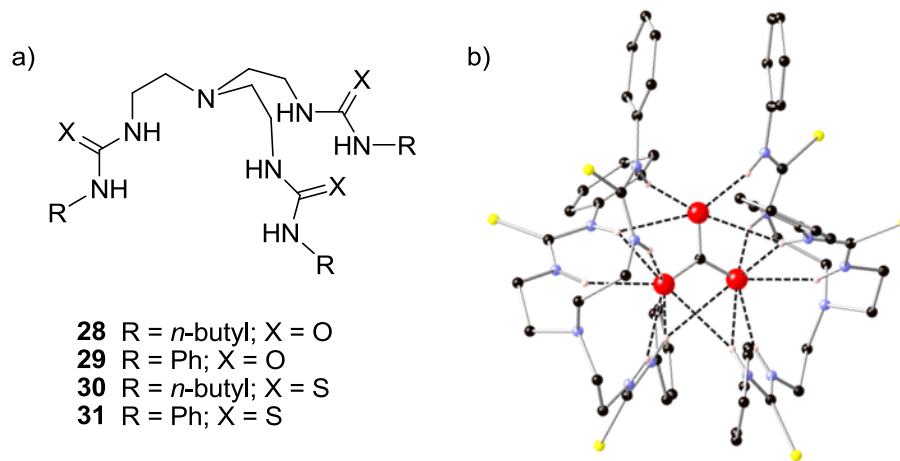


**Figure 4.9.** a) Tren-based anion receptors **28-31** synthesized by the Gale group. b) Crystal structure of two tren **31** molecules with a single bound carbonate anion.

The Gale group studied the transport capabilities of these tren analogs via ion sensitive electrode experiments. Chloride containing liposomes were suspended in a buffer containing sulfate. A chloride-sensitive electrode was used to monitor the efflux of  $\text{Cl}^-$  from the liposome. In separate runs, each of the tren-based receptors were added to the liposomal suspensions and allowed to incubate for two minutes. Upon the addition of  $\text{HCO}_3^-$  to the liposomal solution, an increase in extravesicular chloride was observed for compounds that can facilitate  $\text{Cl}^-/\text{HCO}_3^-$  exchange. Tren **28**, which contains butylurea groups, did not transport chloride under these conditions (**Figure 4.10**). Tren **29**, which has three phenyl urea groups, allowed for a small amount of chloride to be released from the liposome. However, the thiourea appended tren receptors **30** and **31** were the most active in this assay, suggesting that these two compounds are the best at facilitating  $\text{Cl}^-/\text{HCO}_3^-$  exchange.

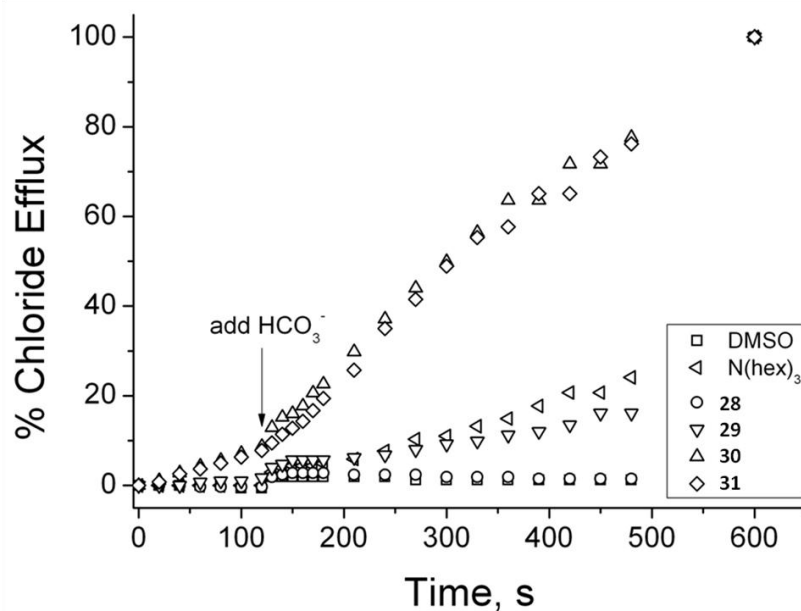


**Figure 4.10.** Chloride sensitive electrode studies with tren receptors **28-31**.

However, these experiments only provided indirect evidence of bicarbonate transport, as this experiment monitors the movement of  $\text{HCO}_3^-$  as a consequence of  $\text{Cl}^-$  efflux. The most commonly used methods for monitoring anion transport are those that use chloride-sensitive electrode<sup>168,207</sup> or fluorescence based assays using the chloride sensitive dye lucigenin (previously described in **Section 3.5**).<sup>54,167,208,212,213</sup> In both cases, the anion that is monitored is chloride, giving only indirect evidence of the transmembrane movement of  $\text{HCO}_3^-$ .

In order to observe the transport of bicarbonate directly, I tested the tren compounds **28-31** in a  $^{13}\text{C}$  NMR liposome assay that monitors the transmembrane movement of  $\text{H}^{13}\text{CO}_3^-$ . Liposomes were prepared containing  $\text{H}^{13}\text{CO}_3^-$ , with sulfate as the initial external anion. Peaks for free and liposome encapsulated  $\text{H}^{13}\text{CO}_3^-$  give distinct signals in the  $^{13}\text{C}$  NMR spectrum (**Figures 4.11** and **4.12**). In the final step of this experiment,  $\text{MnCl}_2$  is added to the NMR tube. When  $\text{MnCl}_2$  binds with the external bicarbonate, the carbonyl signal is broadened into the baseline. However,

this line broadening agent cannot cross the phospholipid membrane, therefore leaving the signal for encapsulated bicarbonate unaffected.

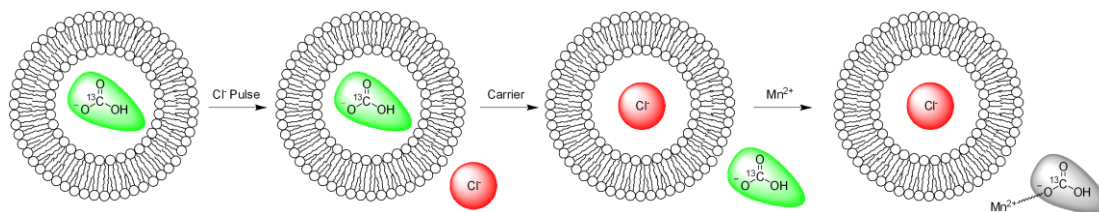


**Figure 4.11.**  $^{13}\text{C}$  NMR liposome assay directly monitoring the release of  $\text{H}^{13}\text{CO}_3^-$ .

To directly evaluate the ability of tren **28-31** to transport bicarbonate, EYPC liposomes containing 100 mM  $\text{H}^{13}\text{CO}_3^-$  were prepared in HEPES buffer at  $\text{pH} = 7.4$ . The liposome solution was then dialyzed to replace the external  $\text{H}^{13}\text{CO}_3^-$  with  $\text{SO}_4^{2-}$ .

**Figure 4.12** shows the  $^{13}\text{C}$  NMR of this liposome solution a) before and b) after addition of a NaCl pulse that brings the final concentration of  $\text{Cl}^-$  to 50 mM. Tren **28-29** (4 mol%) or a DMSO blank were added to the liposome solution (**Figure 4.12c**) and another  $^{13}\text{C}$  NMR spectra was obtained. The final spectra were taken following the addition of  $\text{MnCl}_2$  (0.5 mM final concentration), a paramagnetic line broadening agent that only affects external bicarbonate.

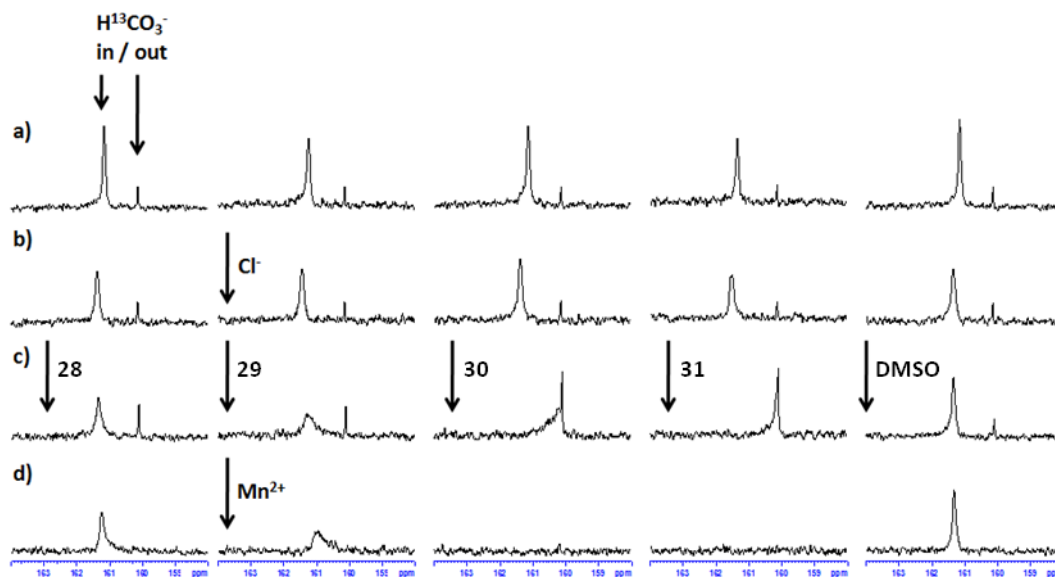


**Figure 4.12.**  $^{13}\text{C}$  NMR evidence of  $\text{H}^{13}\text{CO}_3^-/\text{Cl}^-$  exchange promoted by 4 mol% of receptors **28-31** a) before and b) after addition of a 50 mM NaCl pulse to EYPC vesicles containing 100 mM  $\text{NaH}^{13}\text{CO}_3$  buffered to pH 7.4 with 20 mM HEPES, dispersed in 75 mM  $\text{Na}_2\text{SO}_4$  buffered to pH 7.4 with 20 mM HEPES; c) following addition of **28-31** or DMSO; d) following addition of 0.5 mM  $\text{MnCl}_2$ , a paramagnetic line broadening agent that only affects external bicarbonate.

These  $^{13}\text{C}$  NMR experiments provide direct evidence that the tren thioureas **30** and **31** readily transport bicarbonate across phospholipid membranes in the presence of external chloride. Additionally, in results consistent with chloride sensitive electrode experiments, in that tren urea **28** showed no transport activity, while tren urea **29** showed only modest activity. No changes were noted in the  $^{13}\text{C}$  NMR spectrum when sulfate was the external anion. This information supports a  $\text{H}^{13}\text{CO}_3^-/\text{Cl}^-$  anion exchange mechanism facilitated by tren thioureas **30** and **31**.

#### 4.5 Structurally Simple Thiourea-Based Bicarbonate Transporters

With the knowledge that thiourea-based tren receptors transport bicarbonate across phospholipid membranes, we set out to prepare other, more structurally simple

thiourea-based transporters.<sup>169</sup> In another collaborative effort with the Gale group, simple urea and thiourea receptors **32-37** were prepared (**Figure 4.13**).

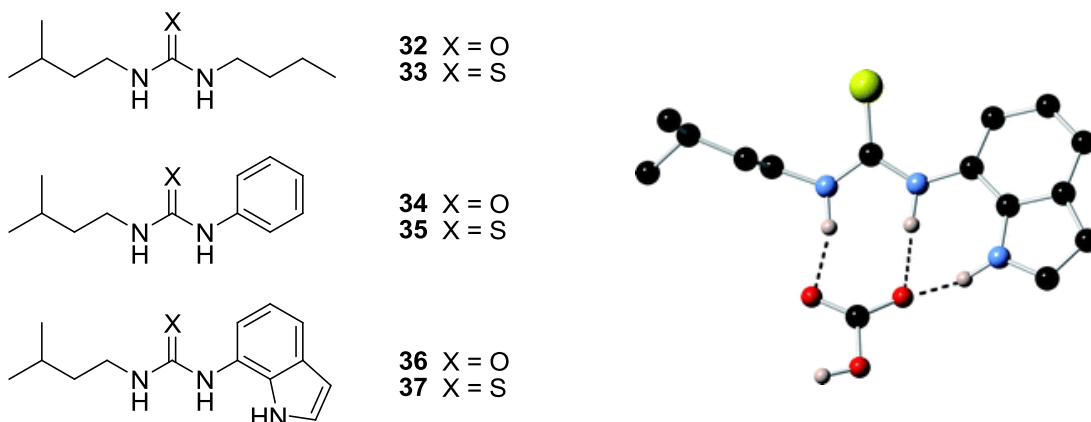


**Figure 4.13.** a) Structurally simple urea- and thiourea-based receptors. b) Model illustrating possible complex between thiourea **37** and bicarbonate.

The Gale group studied the transport capabilities of these simple urea and thiourea analogs via ion sensitive electrode experiments. Chloride containing liposomes were suspended in a buffer containing sulfate. A chloride sensitive electrode was used to monitor the efflux of  $\text{Cl}^-$  from the liposome. In separate runs, each of the receptors were added to the liposomal suspensions and allowed to incubate for two minutes. Upon the addition of  $\text{HCO}_3^-$  to the liposomal solution, an increase in extravesicular chloride was observed for compounds that can facilitate  $\text{Cl}^-/\text{HCO}_3^-$  exchange. Results from these experiments showed that only the thiourea compounds **33**, **35**, and **37** are capable of bicarbonate transport, while the urea receptors exhibited little activity above the DMSO baseline (**Figure 4.14**). Again, the chloride sensitive electrode experiments only indirectly monitor bicarbonate transport.

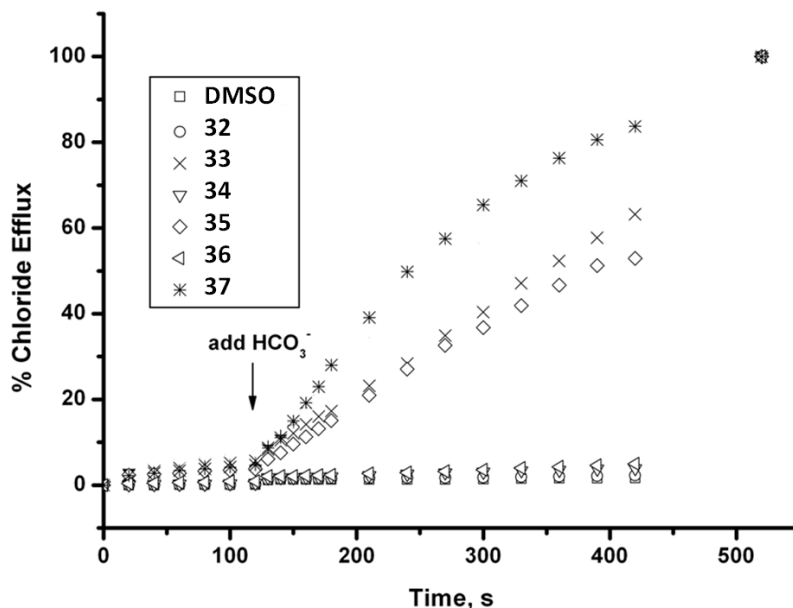


**Figure 4.14.** Chloride sensitive electrode studies using compounds **32-37**.

To directly evaluate the ability of urea and thiourea receptors **32-37** to transport bicarbonate, EYPC liposomes containing 100 mM  $\text{H}^{13}\text{CO}_3^-$  were prepared in HEPES buffer at pH = 7.4. The liposome solution was then dialyzed to replace the external  $\text{H}^{13}\text{CO}_3^-$  with  $\text{SO}_4^{2-}$ . **Figure 4.15** shows the  $^{13}\text{C}$  NMR of this liposome solution a) before and b) after addition of a NaCl pulse that brings the final concentration of  $\text{Cl}^-$  to 50 mM. Compounds **32-37** (4 mol%) or a DMSO blank were added to the liposome solution (**Figure 4.15c**) and another  $^{13}\text{C}$  NMR spectra was obtained. The final spectra were taken following the addition of  $\text{MnCl}_2$  (0.5 mM final concentration), a paramagnetic line broadening agent that only affects external bicarbonate.

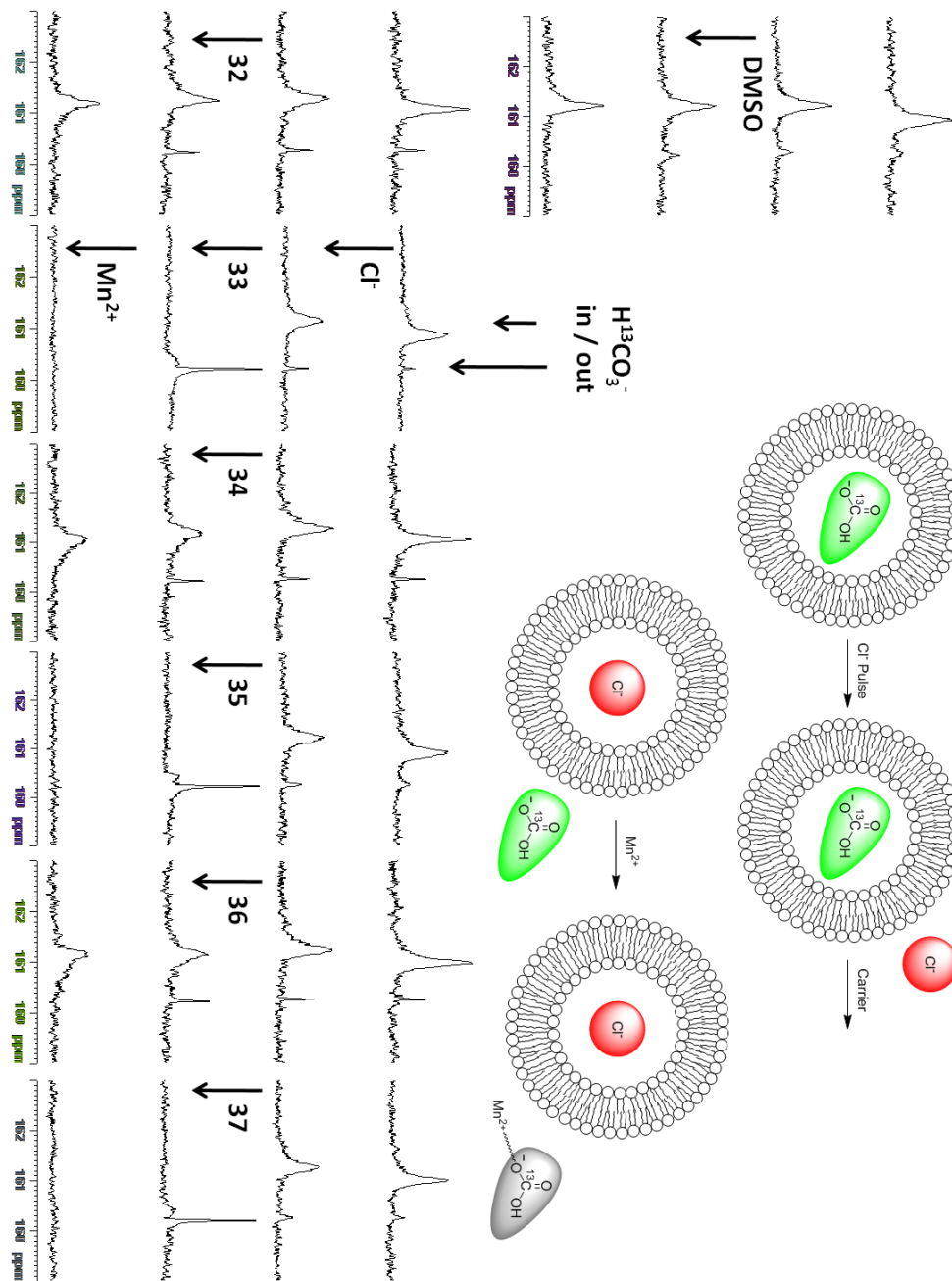


**Figure 4.15.**  $^{13}\text{C}$  NMR evidence of  $\text{H}^{13}\text{CO}_3^-/\text{Cl}^-$  exchange promoted by 4 mol% of receptors **32-37** a) before and b) after addition of a 50 mM NaCl pulse to EYPC vesicles containing 100 mM  $\text{NaH}^{13}\text{CO}_3$  buffered to pH 7.4 with 20 mM HEPES, dispersed in 75 mM  $\text{Na}_2\text{SO}_4$  buffered to pH 7.4 with 20 mM HEPES; c) following addition of **32-37** or DMSO; d) following addition of 0.5 mM  $\text{MnCl}_2$ , a paramagnetic line broadening agent that only affects external bicarbonate.

These  $^{13}\text{C}$  NMR experiments provide direct evidence that the thiourea receptors **33**, **35**, and **37** readily transport bicarbonate across phospholipid membranes in the presence of external chloride. These results suggest a  $\text{H}^{13}\text{CO}_3^-/\text{Cl}^-$  anion exchange mechanism facilitated by the thiourea analogs. Additionally, in results consistent with chloride sensitive electrode experiments, the urea receptors **32**, **34**, and **36** showed little activity in the  $^{13}\text{C}$  NMR assay.

In conclusion, in collaboration with the Gale group we have discovered new thiourea-based small molecules that facilitate the transmembrane transport of the biologically important bicarbonate anion. Through both indirect and direct liposome assays, we have determined that these thiourea analogs operate through a  $\text{H}^{13}\text{CO}_3^-/\text{Cl}^-$  anion exchange mechanism, while the urea receptors show little to no activity. Our results clearly show that the thiourea analogs are significantly better at transporting bicarbonate anions than the corresponding ureas. While Davis and Smith have seen similar effects on chloride transport using functionalized cholapods,<sup>214</sup> the studies presented here are the first time such trends have been noted for bicarbonate transport. To our knowledge, these results represent two of only five papers on small molecule bicarbonate transporters.

#### **4.6 Biological and Environmental Impacts of Carbon Dioxide**

Carbon dioxide is a neutral gas that can diffuse across phospholipid membranes.<sup>106</sup> However, its low solubility in aqueous environments can slow this process. Carbon dioxide is much more soluble in organic / lipophilic solvents.



Henry's Law states that at a constant temperature, the concentration ( $c$ ) of a dissolved gas is proportional to the partial pressure ( $p$ ) of the gas in equilibrium with the liquid.

$$k_H = \frac{p}{c}$$

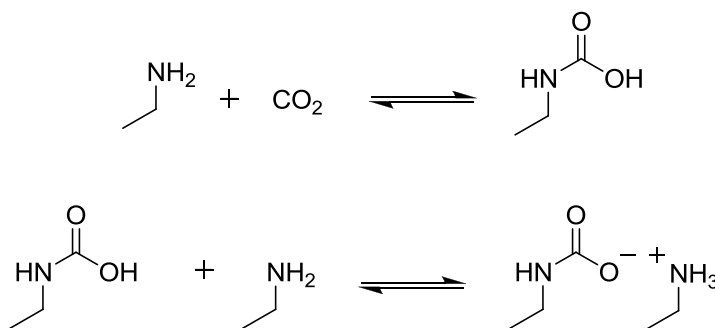
Solubility of a gas in a particular solvent can be given as Henry's law constant ( $k_H$ ). For comparison purposes, **Table 4.2** lists  $k_H$  for CO<sub>2</sub> in H<sub>2</sub>O, DMSO, and CH<sub>2</sub>Cl<sub>2</sub>. Lower  $k_H$  values indicate that the concentration of dissolved gas is higher with lower partial pressures of gas above the solvent. In this case, CO<sub>2</sub> is the most soluble in CH<sub>2</sub>Cl<sub>2</sub> as the  $k_H$  value is the smallest, and the least soluble in H<sub>2</sub>O.

**Table 4.2.** Henry's Constants ( $k_H$ ) for CO<sub>2</sub> in Select Solvents

| Solvent                         | $k_H$ (L·atm/mol) | Ref.               |
|---------------------------------|-------------------|--------------------|
| CH <sub>2</sub> Cl <sub>2</sub> | 0.2252            | <sup>215</sup>     |
| DMSO                            | 1.996             | <sup>216</sup>     |
| H <sub>2</sub> O                | 29.15             | <sup>217,218</sup> |

In certain instances, evidence suggests that aquaporin (AQP) water channels may also facilitate the transport of CO<sub>2</sub> across phospholipid membranes.<sup>219</sup> Research from the Gros group shows that human red blood cells lacking AQP-1 have a 60 % decrease in transmembrane CO<sub>2</sub> transport.<sup>220</sup> Recently, the Gros group also identified the RBC Rhesus complex protein, RhAG as an additional protein in red blood cells that also functions as a CO<sub>2</sub> channel.<sup>221</sup> This suggests that AQP-1 and RhAG work together with the bicarbonate transport proteins of red blood cells to play important roles in cellular respiration through the removal of waste HCO<sub>3</sub><sup>-</sup>/CO<sub>2</sub>.

Carbon dioxide is one of the major greenhouse gases and is the major product of combustion of organic matter.<sup>222</sup> Some of the main sources of atmospheric CO<sub>2</sub> are energy production through the combustion of fossil fuels, decaying plant matter, and a respiratory waste product of animals. An important method used for greenhouse gas reduction from fossil fuel based energy production is a process known as post-combustion capture. Aqueous amine solutions or polymer bound amines are used in scrubbers to remove CO<sub>2</sub> waste before it enters the atmosphere.<sup>223-227</sup> These take advantage of a reversible reaction between amines and CO<sub>2</sub> to form carbamates.<sup>228</sup>



**Scheme 4.2.** Reversible carbamate formation between two primary amines and one molecule of CO<sub>2</sub>.

#### 4.7 Supramolecular Carbamate-Forming Systems

Research in the lab of Dmitry Rudkevich took advantage of carbamate formation to drive the self-assembly of supramolecular structures. During the early portions of this decade, his work focused on the use of supramolecular containers such as hemicarcerands and calixarenes to encapsulate gases such as He, H<sub>2</sub>, N<sub>2</sub>, NO, N<sub>2</sub>O, and CO<sub>2</sub>.<sup>229-232</sup> Following this work, Rudkevich began to use gases, such as SO<sub>2</sub> and CO<sub>2</sub>, to drive the assembly of functional supramolecular polymers.<sup>233</sup>

Under physiological conditions, the N-terminus of peptides have been shown to form carbamates in the presence of CO<sub>2</sub>.<sup>234</sup> Using the amino acid lysine, Rudkevich developed a small dipeptide **38** that takes advantage of carbamate chemistry to form reversible linear supramolecular polymers.<sup>235</sup> Bubbling CO<sub>2</sub> through a solution of this lysine peptide in DMSO gave rise to carbamate formation, as the amino group of lysine reacts with CO<sub>2</sub>. The carbamate anion formed on one of the amino groups forms a hydrogen bond with an RNH<sub>3</sub><sup>+</sup> group on a neighboring peptide to produce a linear polymer **39**. The labile nature of carbamate chemistry allows this reaction to be reversible. Simply heating the solution forces the equilibrium in the opposite direction, as CO<sub>2</sub> is released and the lysine peptide returns to its monomeric form.

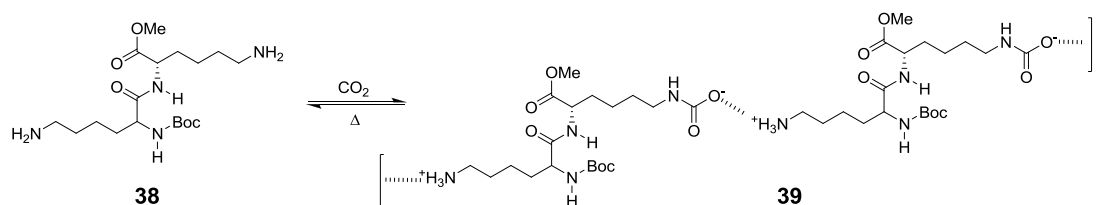


**Figure 4.16.** Linear supramolecular polymer that traps CO<sub>2</sub> via carbamate formation.

In order to more closely study carbamate formation of this molecular assembly, Rudkevich also prepared a simple mono-lysine analog **40**. Since this analog contained one free amine per subunit, only dimers, as opposed to long polymers, could be formed. Upon bubbling CO<sub>2</sub> into a 1 M solution of **40** in CDCl<sub>3</sub>, carbamate formation was observed by <sup>13</sup>C and <sup>1</sup>H NMR spectroscopy. In the <sup>13</sup>C NMR spectrum, a new signal at  $\delta$  161 ppm was observed, corresponding to the carbonyl carbon of the newly formed carbamate. However, the <sup>1</sup>H NMR spectra gave more insight into the type of structures being formed in solution. In this case, only 50

% of the mono-lysine **40** formed a carbamate. The other half became protonated at the primary amine of lysine, and the ammonium carbamate **41** was formed. The  $^1\text{H}$  NMR spectrum of ammonium carbamate **41** showed two 1:1 signals at  $\delta$  2.74 ppm and  $\delta$  2.94 ppm, corresponding to the  $\alpha\text{-CH}_2\text{NH}$  of the ammonium and carbamate halves, respectively. Additionally, the peak corresponding to the methylene protons of the ammonium half shifted downfield approximately  $\delta$  0.25 ppm from that of the same methylene protons of the neutral mono-lysine **40** precursor. Interestingly, when  $\text{d}_6\text{-DMSO}$  was used as the solvent, no signals were observed for the protonated amine half. In this case,  $\text{CO}_2$  quantitatively reacted with mono-lysine **40** to form the corresponding carbamic acid.

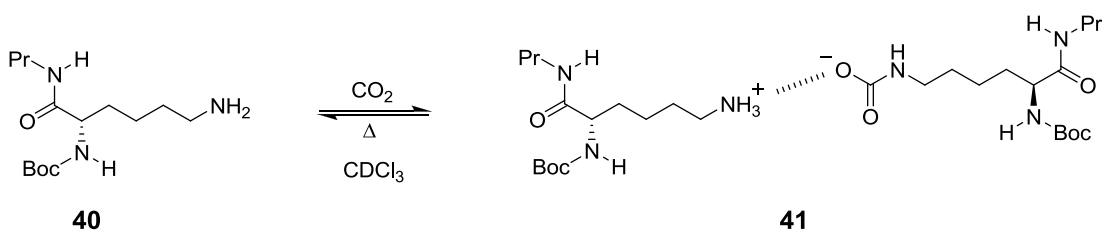


**Figure 4.17.** Mono-lysine **40** forms an ammonium carbamate salt **41** upon bubbling with  $\text{CO}_2$  in  $\text{CDCl}_3$ .

The solvent dependence of carbamate formation between amines and carbon dioxide has also been thoroughly studied by Yoshikatsu Ito and colleagues.<sup>236</sup> In this study, the authors test carbamate formation of 3-(1-naphthyl)propylamine **42** and  $\text{CO}_2$  in a variety of solvents. The results of these studies are similar to the solvent dependence observed by Rudkevich.<sup>237,238</sup> Upon bubbling  $\text{CO}_2$  into a solution of **42** in polar aprotic solvents such as  $\text{d}_7\text{-DMF}$ ,  $\text{d}_5\text{-pyridine}$ , and  $\text{d}_6\text{-DMSO}$ ,  $^1\text{H}$  and  $^{13}\text{C}$  NMR evidence suggests quantitative conversion of **42** to the corresponding carbamic acid **43**. In the  $^1\text{H}$  NMR spectrum in  $\text{d}_6\text{-DMSO}$ , only one set of signals was observed,

with the  $\alpha$ -CH<sub>2</sub>NH shifted downfield approximately  $\delta$  0.40 ppm from that of the free amine. A signal at approximately  $\delta$  163 ppm was observed in the <sup>13</sup>C NMR spectrum corresponding to the carbonyl of the carbamic acid **43**.

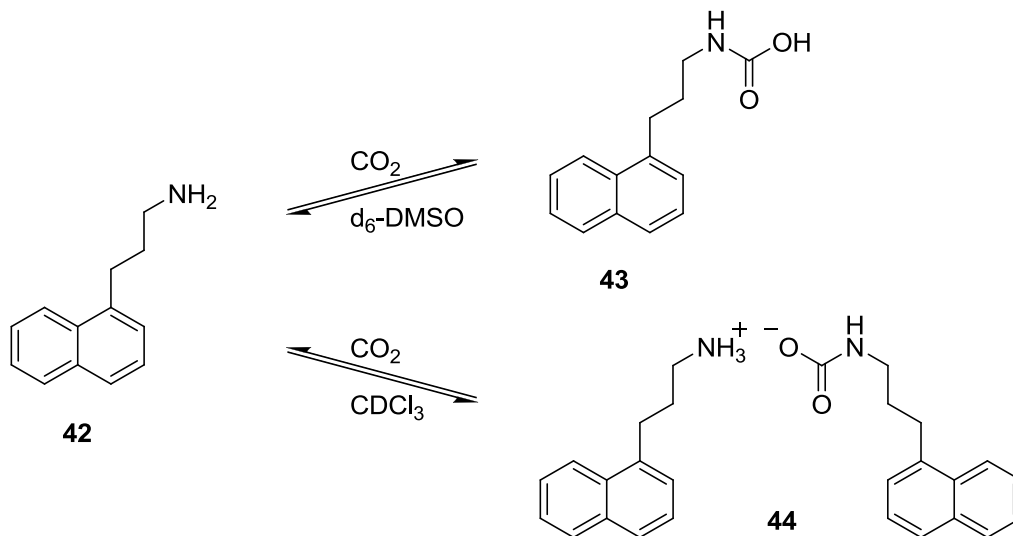


**Figure 4.18.** Ito's 3-(1-naphthyl)propylamine **42** forms carbamic acid **43** or ammonium carbamate **44** in a solvent dependent manner.

Upon bubbling CO<sub>2</sub> through solutions of **42** in CDCl<sub>3</sub> or *d*<sub>8</sub>-isopropanol, the ammonium carbamate **44** was observed. The <sup>1</sup>H NMR spectrum of **44** in CDCl<sub>3</sub> showed a doubling of signals corresponding to the  $\alpha$ -CH<sub>2</sub>NH protons of the carbamate half and the ammonium half. A signal corresponding to the carbonyl of the carbamate was observed at  $\delta$  163 in the <sup>13</sup>C NMR spectrum.

The authors also note that the carbamic acid and the carbamate are indistinguishable via NMR spectroscopy. However, the neutral carbamic acid is assumed to be the major product in solvents such as *d*<sub>6</sub>-DMSO, as no ammonium counterion is observed to stabilize a negative charge associated with a carbamate.

#### 4.8 Anion Binding and Transport Properties of Sphingosine 3

With the knowledge that C2-ceramide **2** binds and transports anions, we sought to determine if its precursor, sphingosine **3**, would do the same. Sphingosine **3** differs from C2-ceramide **2** in that it contains a primary amine instead of the amide functionality at the ceramide C2 position.

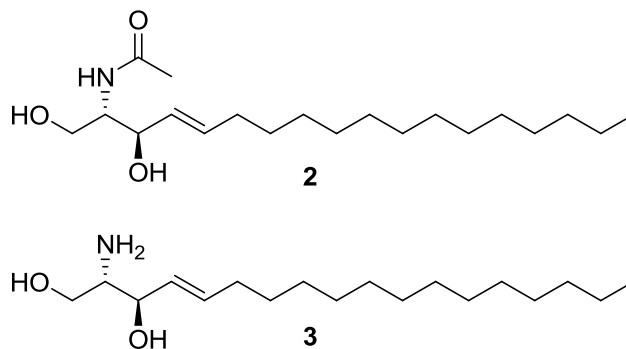


**Figure 4.19.** C2-ceramide **2** and sphingosine **3**.

In order to determine if sphingosine **3** binds chloride, we used NMR spectroscopy. Thus, 2 mM solutions of sphingosine **3** were prepared in CD<sub>2</sub>Cl<sub>2</sub> with increasing amounts of TBACl added to the solution. Unfortunately, unlike C2-ceramide **2**, the signals corresponding to the hydroxyl protons of sphingosine **3** were not observed in CD<sub>2</sub>Cl<sub>2</sub>. Upon adding increasing concentrations of TBACl to the solution, some clear changes were observed for the protons in the head group of sphingosine **3** (**Figure 4.20**). The signals corresponding to the protons alpha to the -NH<sub>2</sub> and secondary -OH moved downfield approximately  $\delta$  0.19 ppm. Additionally, the signals for the diastereotopic protons adjacent to the primary -OH changed significantly upon addition of TBACl to the solution. We attribute these shifts to conformational changes associated with sphingosine **3** binding Cl<sup>-</sup>.

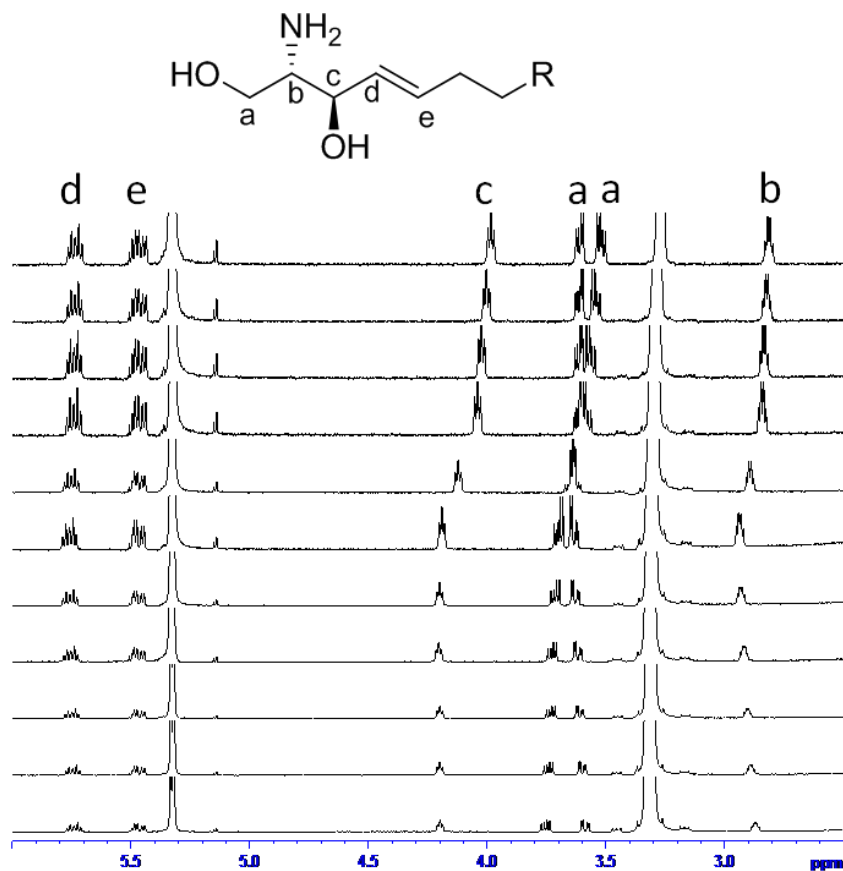


**Figure 4.20.** Titrations of sphingosine **3** with TBACl in  $\text{CD}_2\text{Cl}_2$  give rise to small shifts in the head group protons.

With the knowledge that sphingosine **3** can bind  $\text{Cl}^-$  in  $\text{CD}_2\text{Cl}_2$ , we wanted to determine if sphingosine **3** could facilitate anion transport across phospholipid membranes. To do this, we utilized the  $^{13}\text{C}$  NMR assay previously described in **Section 4.4**. EYPC liposomes containing 100 mM  $\text{H}^{13}\text{CO}_3^-$  were prepared in 20 mM HEPES buffer at pH = 7.4. The liposome solution was then dialyzed to replace the external  $\text{H}^{13}\text{CO}_3^-$  with  $\text{SO}_4^{2-}$ . **Figure 4.21** shows the  $^{13}\text{C}$  NMR of this liposome solution a) before and b) after addition of a NaCl pulse that brings the final concentration of  $\text{Cl}^-$  to 50 mM. Sphingosine **3** (4 mol%) or a DMSO blank were added to the liposome solution (**Figure 4.21c**) and another  $^{13}\text{C}$  NMR spectra was

obtained. The final spectra was taken following the addition of  $\text{MnCl}_2$  (0.5 mM final concentration), a paramagnetic line broadening agent that only affects external bicarbonate.

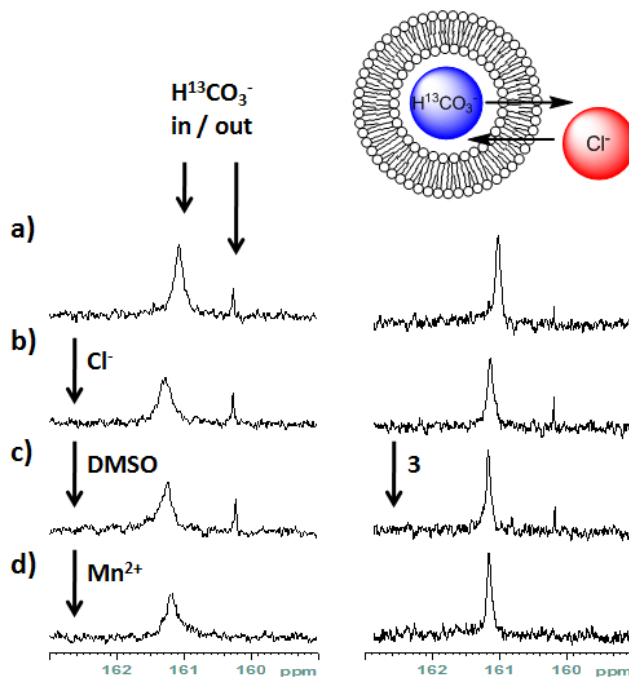


**Figure 4.21.** Initial  $^{13}\text{C}$  NMR experiments to determine if sphingosine **3** promotes  $\text{H}^{13}\text{CO}_3^-/\text{Cl}^-$  exchange. Sphingosine **3** does not facilitate the exchange bicarbonate with chloride under these conditions.

Under these conditions, sphingosine **3** does not facilitate  $\text{Cl}^-/\text{H}^{13}\text{CO}_3^-$  exchange across the liposomal membrane. The spectra obtained during the sphingosine **3** tests look the same as the DMSO blank. The signal at approximately  $\delta$  161 ppm corresponding to intravesicular  $\text{H}^{13}\text{CO}_3^-$  remains unchanged upon addition of sphingosine **3** (or the DMSO blank) to the liposomal solution. Upon the addition of  $\text{MnCl}_2$  (**Figure 4.21d**), the external  $\text{H}^{13}\text{CO}_3^-$  was broadened into the baseline leaving a prominent signal for the internal bicarbonate that was not transported out of the liposomes by sphingosine **3**. Following this negative transport result, we sought



to find a possible explanation for the lack of anion transport by sphingosine **3**. Since this assay also relies on the ability of sphingosine **3** to bind and transport bicarbonate, we wanted to determine if sphingosine **3** could bind  $\text{HCO}_3^-$  in organic solvents.

#### 4.9 Sphingosine **3** forms Carbamates in the Presence of $\text{HCO}_3^-$ in $\text{CD}_2\text{Cl}_2$

Having shown that sphingosine **3** binds  $\text{Cl}^-$ , but does not facilitate the anion exchange of chloride with bicarbonate, we sought to determine if sphingosine **3** would bind  $\text{HCO}_3^-$ . Titration of a 2 mM solution of sphingosine **3** in  $\text{CD}_2\text{Cl}_2$  with increasing amounts of  $\text{TEAHCO}_3$  gave rise to a new  $^1\text{H}$  NMR signal that shifts initially from approximately  $\delta$  4.51 ppm (after addition of 0.75 eq.  $\text{TEAHCO}_3$ ) to  $\delta$  5.38 ppm (after addition of excess  $\text{TEAHCO}_3$ ). This new signal corresponds to the  $-\text{NH}$  of the sphingosine carbamate **27** (Figure 4.22). Additionally, the signals at  $\delta$  2.70 and  $\delta$  3.99 ppm of sphingosine **3** disappear with increasing concentrations of  $\text{TEAHCO}_3$ , with the concurrent appearance of signals at  $\delta$  3.57 and  $\delta$  4.11 ppm. An expanded view of the spectra of 2 mM sphingosine **3** with 3 eq.  $\text{TEAHCO}_3$  can be seen in Figure 4.23, labeled with the diagnostic signals from protons of each species. At these concentrations, sphingosine **3** and the sphingosine carbamate **27** exist in an approximately 1:1 ratio. In this spectrum, a new signal corresponding to the carbamate  $-\text{NH}$  appears at  $\delta$  4.77 ppm. The  $-\text{CH}$  protons in the new sphingosine carbamate **27** headgroup are downfield shifted from the protons in sphingosine **3**. The signal corresponding to the proton alpha to the secondary alcohol shifts downfield approximately 0.1 ppm from  $\delta$  3.95 to  $\delta$  4.05 ppm, while the signal for the

$\alpha$ -CHNH proton shifts from  $\delta$  2.75 to  $\delta$  3.59 ppm. Additionally, doubling of the olefinic protons between  $\delta$  5.40 and  $\delta$  5.80 ppm was observed.

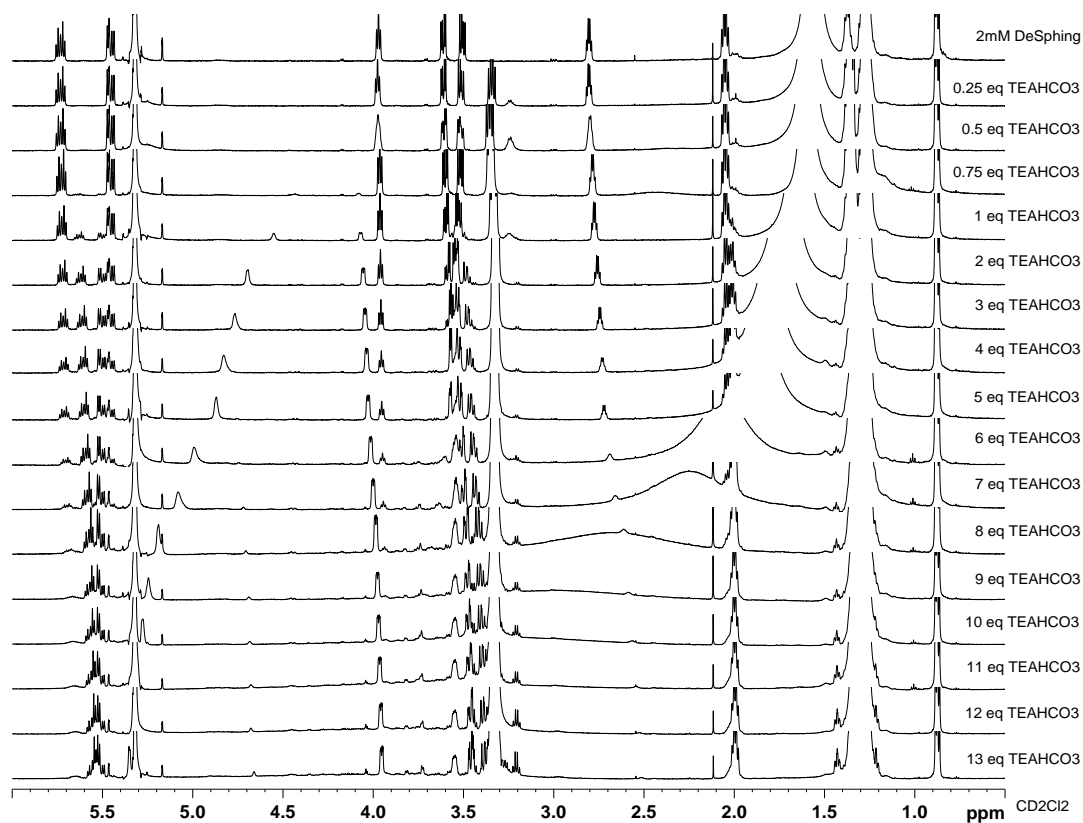


**Figure 4.22.** Titration of sphingosine **3** with TEAHCO<sub>3</sub> in CD<sub>2</sub>Cl<sub>2</sub> shows the formation of sphingosine carbamate **27**.

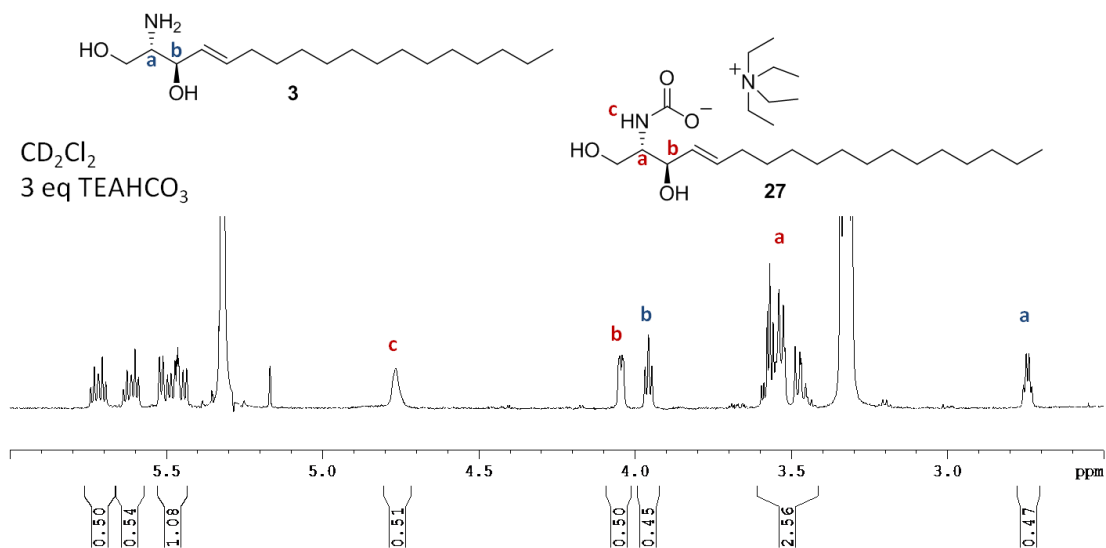


**Figure 4.23.**  $^1\text{H}$  NMR spectrum following the addition of 3 eq. of TEAHCO<sub>3</sub> to a 2 mM solution of sphingosine **3** in CD<sub>2</sub>Cl<sub>2</sub>. This gives approximately a 1:1 mixture of sphingosine **3** and sphingosine carbamate **27**.

In order to gain  $^{13}\text{C}$  NMR evidence for carbamate formation by sphingosine **3**, we needed to use higher concentrations of the sphingolipid. Increasing the concentration of sphingosine **3** to 20 mM in CD<sub>2</sub>Cl<sub>2</sub> allowed for complete conversion (by  $^1\text{H}$  NMR) to sphingosine carbamate **27** following the addition of only 1.5 eq. of TEAHCO<sub>3</sub> (**Figure 4.24**). **Figure 4.25** shows the  $^{13}\text{C}$  NMR spectra of the same samples. Upon the addition of 1.5 eq. TEAHCO<sub>3</sub> to a solution of sphingosine **3** in CD<sub>2</sub>Cl<sub>2</sub>, two signals appeared in the C=O region of the  $^{13}\text{C}$  NMR spectra between  $\delta$  160 and  $\delta$  170 ppm. The signal at  $\delta$  166 ppm corresponds to the carbonyl of the sphingosine carbamate **27**, while the smaller signal at  $\delta$  161 ppm corresponds to the excess TEAHCO<sub>3</sub>. The carbon alpha to the -NH of sphingosine carbamate **27** shifts downfield approximately 2 ppm from  $\delta$  58.1 to  $\delta$  60.2 ppm when compared to sphingosine **3**. Additionally, changes in the olefinic region between  $\delta$  130 and  $\delta$  140 ppm were observed.

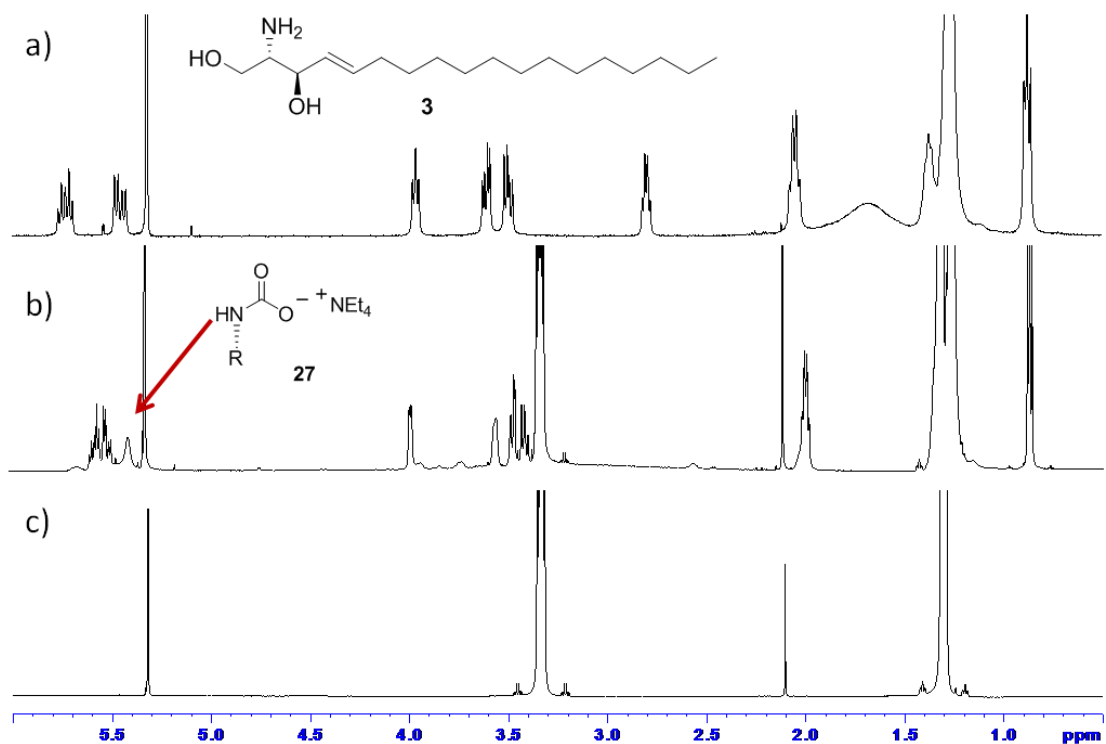


**Figure 4.24.**  $^1\text{H}$  NMR of a) spingosine **3**, b) spingosine carbamate **27**, and c) TEAHCO<sub>3</sub> blank in CD<sub>2</sub>Cl<sub>2</sub>.

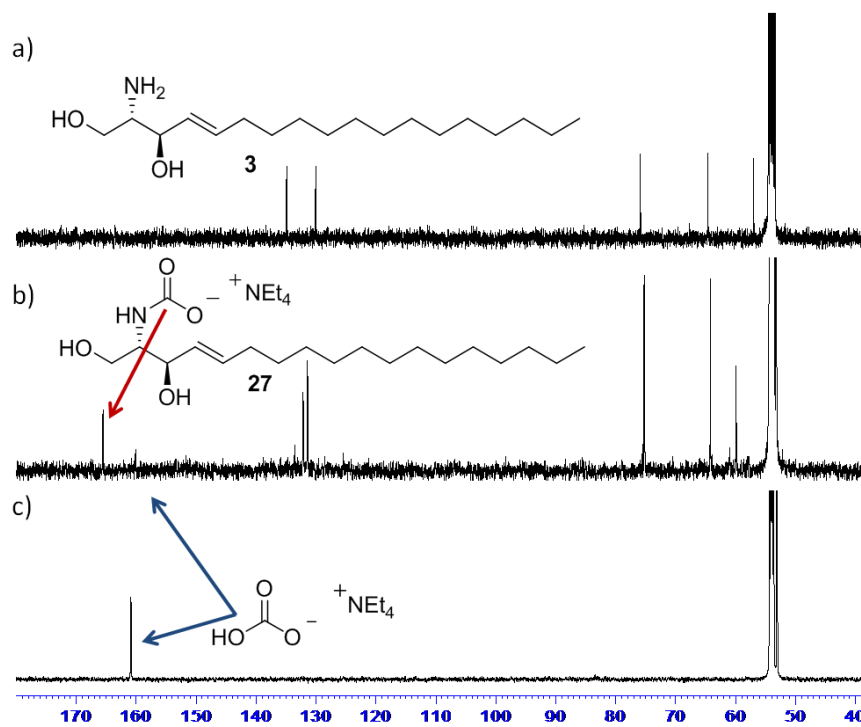


**Figure 4.25.**  $^{13}\text{C}$  NMR of a) spingosine **3**, b) spingosine carbamate **27**, and c) TEAHCO<sub>3</sub> blank in CD<sub>2</sub>Cl<sub>2</sub>.

#### 4.10 Sphingosine Carbamate **27** Formation via CO<sub>2</sub> Bubbling

Following the discovery that sphingosine **3** forms a carbamate in CD<sub>2</sub>Cl<sub>2</sub> in the presence of TEAHCO<sub>3</sub>, we wanted to see if we could form sphingosine carbamate **27** in the presence of CO<sub>2</sub> in a similar manner to that of Dmitry Rudkevich (Section 4.7). The apparatus used to bubble CO<sub>2</sub> through a solution containing sphingosine **3** is shown in Figure 4.10.

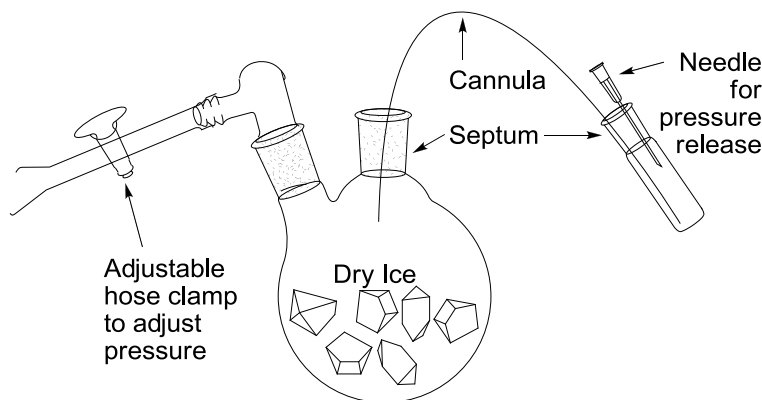


**Figure 4.26.** CO<sub>2</sub> bubbling apparatus.

The CO<sub>2</sub> bubbling apparatus is comprised of a two neck round bottom flask containing dry ice with a pressure release valve attached to one neck. A cannula runs from the flask into a sample vial containing the sample with an additional needle inserted into the vial to allow the CO<sub>2</sub> to escape once bubbled through the solvent. Typically, a 15 mM sample was prepared in 2 mL of solvent and degassed with N<sub>2</sub> for 20 minutes prior to bubbling CO<sub>2</sub> through the solution.

A 15 mM sample of sphingosine **3** was prepared in CD<sub>2</sub>Cl<sub>2</sub>. Following a N<sub>2</sub> purge, CO<sub>2</sub> was bubbled through the sample for 1 hour. Unfortunately, no change in the <sup>1</sup>H NMR spectrum was observed. Additional attempts to form a carbamate from sphingosine **3** and CO<sub>2</sub> in CD<sub>2</sub>Cl<sub>2</sub> in the presence of excess TEA, to ensure that the

primary amine of sphingosine **3** was deprotonated, also failed to show  $^1\text{H}$  NMR evidence for carbamate formation.

With no carbamate formation in non-polar  $\text{CD}_2\text{Cl}_2$ , we decided to switch to a more polar solvent in DMSO. In previously discussed studies, Rudkevich and Ito were able to quantitatively form carbamic acids using the more polar DMSO as a solvent (**Section 4.7**). A 15 mM solution of sphingosine **3** was prepared in  $\text{d}_6$ -DMSO, purged with  $\text{N}_2$ , and then  $\text{CO}_2$  was bubbled through the solution for 1 hour. **Figure 4.27** shows the  $^1\text{H}$  NMR spectrum of the  $\text{d}_6$ -DMSO blank, as well as before and after bubbling with  $\text{CO}_2$ . The appearance of a new signal at  $\delta$  6.12 ppm corresponds to the  $-\text{NH}$  proton of the sphingosine carbamate **27**. The ratio of sphingosine **3** to sphingosine carbamate **27** was roughly 1:1 following one hour of exposure to  $\text{CO}_2$ . A new signal at  $\delta$  4.15 ppm corresponds to the proton alpha to the secondary  $-\text{OH}$  of sphingosine carbamate **27**, and is shifted downfield from the same proton of sphingosine **3** by approximately 0.25 ppm. Additionally, doubling of the  $-\text{OH}$  and olefinic protons was observed between  $\delta$  4.30-5.80 ppm.

The  $^{13}\text{C}$  NMR spectra of the same three samples can be found in **Figure 4.28**. The new signal at  $\delta$  157 ppm corresponds to the carbonyl carbon of the sphingosine carbamate **27** that is formed upon reaction with  $\text{CO}_2$ . Doubling of the carbon signals corresponding to the head group carbons ( $\delta$  57.0-73.0 ppm) and the olefinic carbons ( $\delta$  127-134 ppm) was also observed.

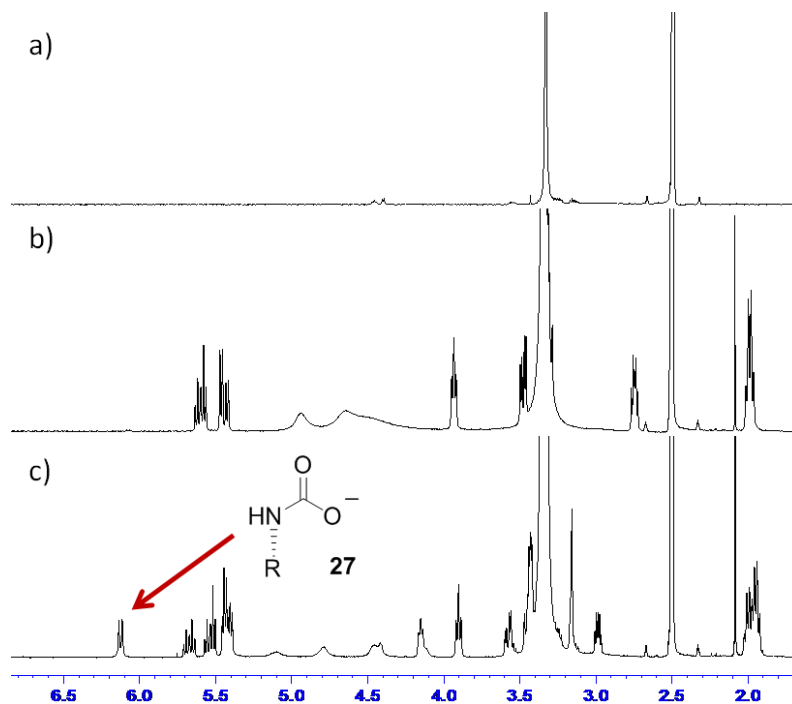


**Figure 4.27.**  $^1\text{H}$  NMR of a)  $\text{CO}_2$  blank, b) sphingosine **3**, and c) sphingosine carbamate **27** following  $\text{CO}_2$  bubbling in  $d_6$ -DMSO.

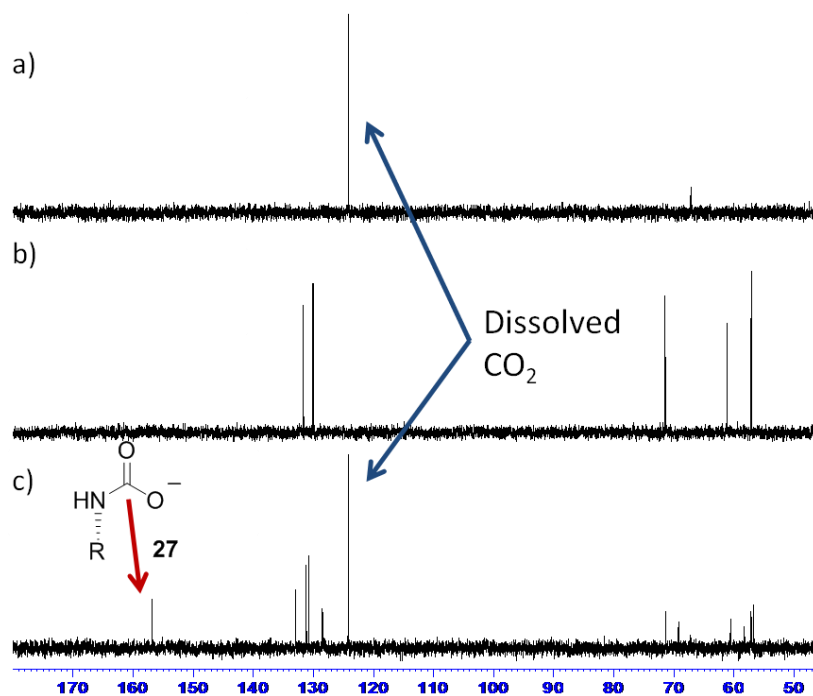


**Figure 4.28.**  $^{13}\text{C}$  NMR of a)  $\text{CO}_2$  blank, b) sphingosine **3**, and c) sphingosine carbamate **27** following  $\text{CO}_2$  bubbling in  $d_6$ -DMSO.

Both the  $^1\text{H}$  and  $^{13}\text{C}$  NMR data obtained from bubbling  $\text{CO}_2$  through solutions of sphingosine **3** in  $\text{d}_6$ -DMSO suggested the formation of a sphingosine ammonium carbamate **45** (**Figure 4.29**). The 1:1 ratio of signals and the chemical shifts of these signals is consistent with results from mechanistic studies of carbamate formation using  $\text{CO}_2$  with simple monoethanolamines,<sup>228</sup> as well as the more complicated supramolecular systems studied by Rudkevich<sup>235,239</sup> and Ito<sup>236</sup> (**Section 4.7**).

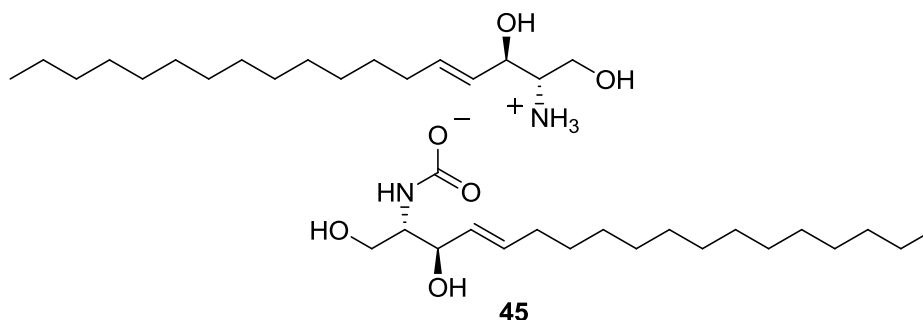


**Figure 4.29.** Sphingosine ammonium carbamate **45** formed upon bubbling  $\text{CO}_2$  through a solution of sphingosine **3** in  $\text{d}_6$ -DMSO.

However, this differs from previously described work in that Rudkevich and Ito were able to get full conversion to carbamic acids in  $\text{d}_6$ -DMSO. In an attempt to push the  $\text{CO}_2$  induced conversion of sphingosine **3** to sphingosine carbamate **27** in  $\text{d}_6$ -DMSO to completion, longer bubbling times were studied. **Figure 4.15** shows  $^1\text{H}$  NMR spectra of 15 mM solution of sphingosine **3** bubbled with  $\text{CO}_2$  for 1 and 4 hours. Interestingly, no change in the chemical shifts or integration was observed when increasing the  $\text{CO}_2$  bubbling time. In each case, a 1:1 ratio of protonated sphingosine **3** to sphingosine carbamate **27** were present in solution.



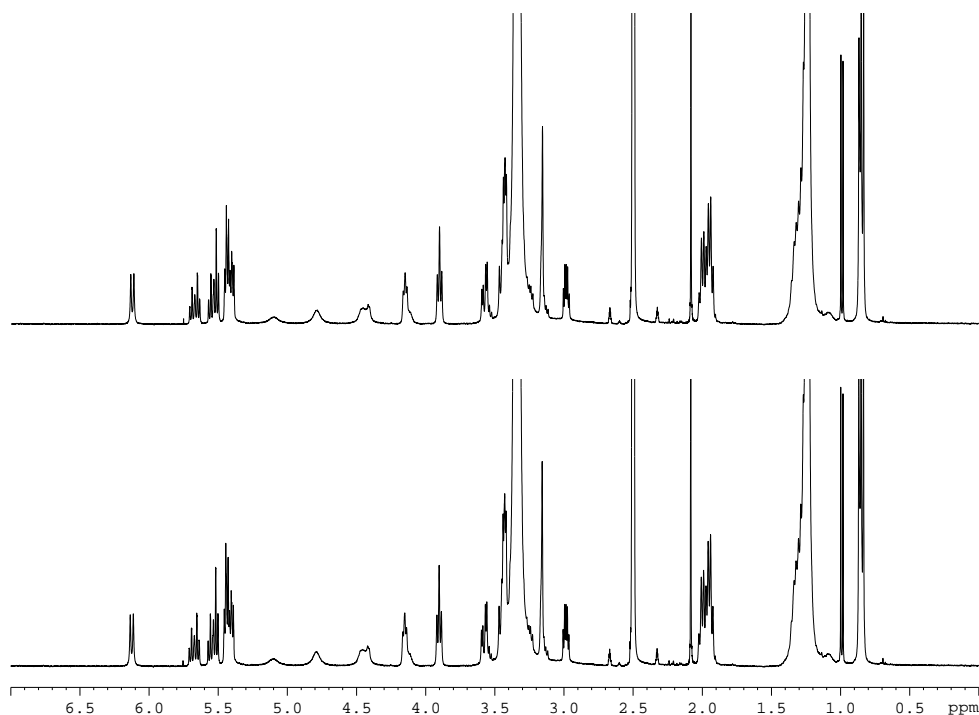


**Figure 4.30.** 1 vs. 4 hours bubbling CO<sub>2</sub> through a 15 mM solution of spingosine **3** in d<sub>6</sub>-DMSO.

In these studies, we found that spingosine **3** forms an ammonium carbamate salt **45** in DMSO upon bubbling with CO<sub>2</sub>, which differs from other studies on carbamate formation. In stark contrast to our findings, Rudkevich and Ito determined that bubbling CO<sub>2</sub> through amine solutions only gave ammonium carbamate salts in non-polar organic solvents such as chloroform. They found that in highly competitive, polar aprotic solvents such as DMF and DMSO, the neutral carbamic acid is favored over the charged ammonium carbamate salts. However, we have found that the spingosine **3** forms the corresponding ammonium carbamate **45** that is stable in DMSO. It is possible that the stability of the spingosine ammonium carbamate **45** in DMSO may be attributed to the 1,3-diol units in the spingosine **3** head group. **Figure 4.31** depicts a model of a possible conformation of the

sphingosine ammonium carbamate **45**, where both intra- and intermolecular hydrogen bonding by the –OH groups provide additional stabilization.

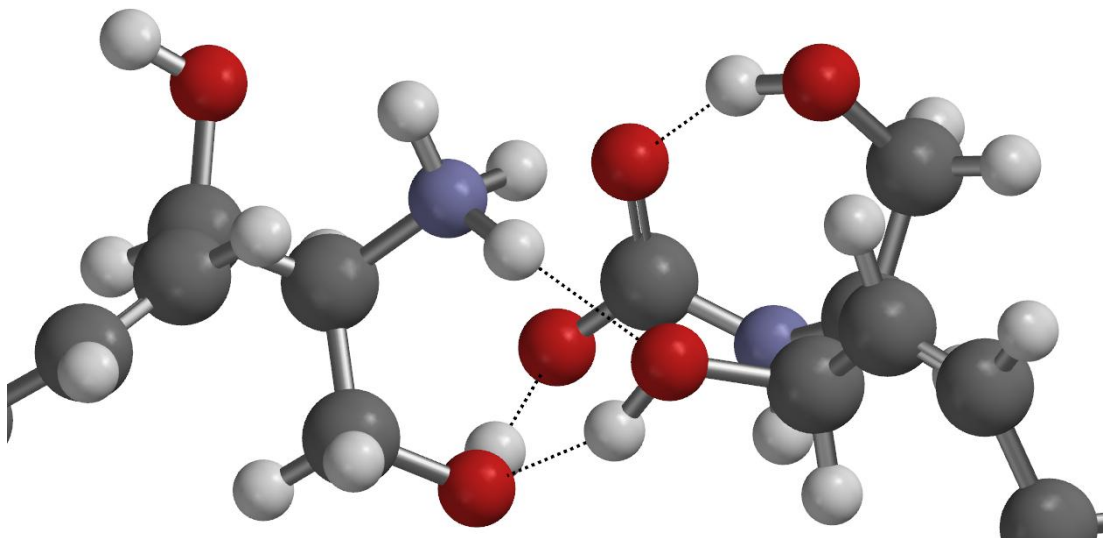


**Figure 4.31.** Model of a possible conformation of the sphingosine ammonium carbamate **45**, showing both intra- and intermolecular hydrogen bond stabilization of the carbamate.

#### 4.11 Conclusions

In this chapter, I described work that led to the discovery of transmembrane transporters for bicarbonate using chloride sensitive electrode, fluorescence, and  $^{13}\text{C}$  NMR assays. In collaboration with the Gale group, we determined that tris thioureas **30** and **31** transport bicarbonate through a  $\text{H}^{13}\text{CO}_3^-/\text{Cl}^-$  anion exchange mechanism. Additionally, we developed simple bicarbonate transporters **33**, **35**, and **37** that take advantage of a thiourea functionality to bind and transport bicarbonate. Another significant finding in this chapter is that the natural product, C2-ceramide **2**, binds and transports bicarbonate. C2-ceramide **2**, along with prodigiosin **21**, are the only two known natural products that can facilitate the transmembrane transport of bicarbonate.

An additional finding described in this chapter is the observation that the natural product sphingosine **3** forms sphingosine carbamate **27** in the presence of bicarbonate in methylene chloride, or in the presence of carbon dioxide in DMSO. In DMSO, sphingosine **3** forms an ammonium carbamate salt **45**, which differs from other studies on carbamate formation. In separate studies, Rudkevich and Ito found that bubbling CO<sub>2</sub> through amine solutions in DMSO yield quantitative conversion to the corresponding carbamic acid. In our case, the sphingosine ammonium carbamate **45** seems to be quite stable in DMSO. This may be due to additional stabilization via hydrogen bonding from adjacent –OH groups in the sphingosine **3** head group. These results also suggest that sphingosine **3** may exist as a carbamate in natural systems where sufficient amounts of HCO<sub>3</sub><sup>-</sup>/CO<sub>2</sub> are present.

## Chapter 5 : Conclusions and Future Directions

Ceramides are known to be involved in a number of cellular processes, including cell differentiation, autophagy, cell senescence, skin water barrier homeostasis, and apoptosis.<sup>1-5</sup> Due to the fact that ceramides are so important for cell metabolism, there is a need to better understand the molecular mechanism that they use to impart function.

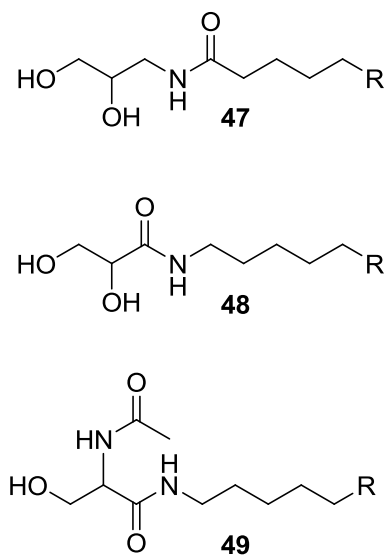
One significant finding in this work is the observation that C2-ceramide **2** can permeabilize phospholipid membranes in various ways. Interesting findings by Colombini suggest that C16-ceramide **1** and C2-ceramide **2** may induce apoptosis by forming large, stable pores in phospholipid membranes.<sup>7</sup> By appending ester functionalities to the –OH groups of C2-ceramide **2**, we have discovered a compound that may be more active in forming pores than the amphiphilic natural product. In fact, C2-diacetate **16** forms pores in phospholipid membranes that are large enough to release the apoptosis-inducing cytochrome c.

However, large pore formation is not the only way that C2-ceramide **2** can permeabilize membranes. At concentrations below that which C2-ceramide **2** forms transmembrane pores, we have discovered that C2-ceramide **2** facilitates the transport of the biologically important chloride and bicarbonate anions through an anion exchange mechanism. It may be that ceramide's ability to transport these physiologically relevant anions across lipid membranes is also important *in vivo*.

With ceramide being important in a variety of biological systems, there is a great need to understand how ceramide is able to impart function. As organic chemists, we are uniquely equipped study biologically-active compounds such as

ceramide through the development of synthetic analogs. Synthetic ceramide analogs, such as the compounds in **Chart 5.1**, may better help us understand structure-function relationships of how ceramide derives its membrane activity.

**Chart 5.1**

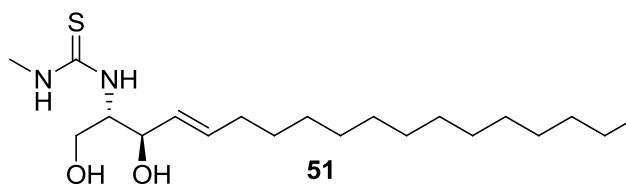
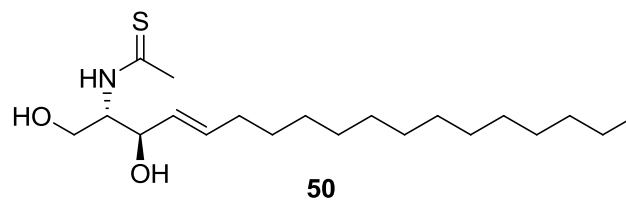


Compounds **47-49** should be easily accessible using commercially available starting materials such as glycerol (**47** and **48**) or serine (**49**). Like C2-ceramide **2**, these compounds each contain three hydrogen-bond donor groups in the hydrophilic head-group, and are connected via an amide linkage to a lipophilic tail. In fact, members of the Davis group are currently studying these compounds and already have some interesting preliminary results in anion transport assays.

Additionally, in **Chapter 4** I described synthetic small molecules **30**, **31**, **33**, **35**, and **37** that are able to facilitate the transmembrane anion transport. In collaboration with the Gale group, we found that only the thiourea versions of these compounds were membrane-active. Based on these results, it is reasonable to believe that introduction of a thioamide (**50**) or thiourea (**51**) moiety into the headgroup of

ceramide may increase its ability to bind and transport anions across phospholipid membranes.

**Chart 5.2**



## Chapter 6 : Experimental Procedures

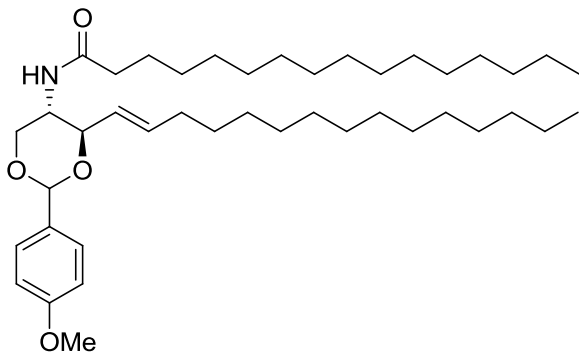
### 6.1 General Experimental

All  $^1\text{H}$  NMR spectra were recorded on a Bruker DRX-400 or a Bruker Advance 400 instrument operating at 400.13 MHz, or a Bruker DRX-500 instrument operating at 500.13 MHz, or a Bruker AVIII-600 instrument operating at 600.13 MHz. All  $^{13}\text{C}$  NMR spectra were recorded on a Bruker DRX-400 instrument operating at 100.52 MHz, a Bruker DRX-500 instrument operating at 125.77 MHz, or a Bruker AVIII-600 instrument operating at 150.92 MHz. Chemical shifts are reported in ppm relative to the residual protonated solvent peak. Electrospray ionization mass spectrometry (ESI-MS) experiments were done with a JEOL AccuTOF spectrometer with an Agilent 1100 HPLC interface. Chromatography was performed using 60-200 mesh silica gel from Baker. Thin layer chromatography was performed on Uniplate<sup>TM</sup> Silica Gel GF silica-coated glass plates and visualized by UV lamp and ceric ammonium molybdate (CAM) stain. The pH of solutions was monitored with a Fisher Scientific AR25 dual channel pH/ion meter. Liposome fluorometric assays were recorded using a Hitachi F-4500 spectrophotometer. Sphingolipids, egg-yolk phosphatidylcholine (EYPC) lipids, Nucleopore polycarbonate membranes, and membrane supports were purchased from Avanti Polar Lipids. High-pressure extrusion was performed using an Avanti mini-extruder. Size-exclusion chromatography was performed using Sephadex G25 (lucigenin), Sephacryl S200 (carboxyfluorescein), or Sephacryl S300HR (FITC-dextran). Deuterated solvents were purchased from Cambridge Isotope Labs. All other chemicals and solvents were purchased from Sigma, Aldrich, Fisher, or Acros and

used without further purification. X-ray crystal structures were obtained on a Bruker Smart1000 diffractometer with CDD area detector by Dr. Peter Y. Zavalij.

## 6.2 Synthetic Procedures

### *p*-Methoxybenzylidene C16-ceramide (C16-pmb 14):

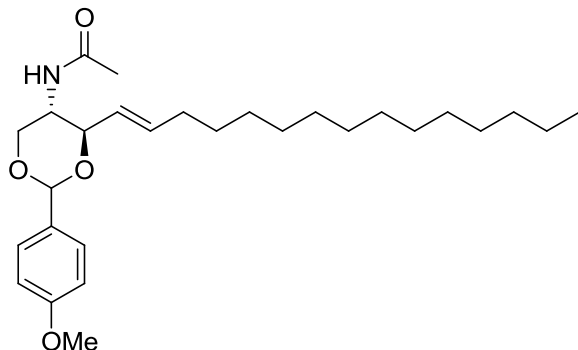


C16-ceramide **1** (Avanti Polar Lipids, 10 mg, 18.6  $\mu\text{mol}$ ) was added to solution of *p*-anisaldehyde (0.56 g, 41.1  $\mu\text{mol}$ ) and  $\text{ZnCl}_2$  (6 mg, 44.0  $\mu\text{mol}$ ) in dry methylene chloride (1.5

mL). The reaction mixture was stirred over molecular sieves at 25 °C under  $\text{N}_2$  overnight. Solid  $\text{NaHCO}_3$  was then added to the reaction mixture and the resulting mixture was stirred for 5 min and filtered. Hexanes was added to the reaction mixture causing a white solid to precipitate out of solution. The white precipitate was filtered off to give pure C16-pmb **14** (9.8 mg, 80 % yield). M.p. 131-133 °C; IR (neat) 3270, 2957, 2917, 2850, 1643  $\text{cm}^{-1}$ ;  $^1\text{H-NMR}$  (600 MHz,  $\text{CDCl}_3$ )  $\delta$  = 7.42 (d, 2H,  $J$  = 8.7 Hz), 6.88 (d, 2H,  $J$  = 8.7 Hz), 5.81 (dt, 1H,  $J$  = 15.4 Hz,  $J$  = 6.7 Hz), 5.52 (dd, 1H,  $J$  = 15.4 Hz,  $J$  = 7.3 Hz), 5.48 (s, 1H), 5.01 (d, 1H,  $J$  = 7.6 Hz), 4.39 (dd, 1H,  $J$  = 4.4 Hz,  $J$  = 10.5 Hz), 4.04 (m, 2H), 3.80 (s, 3H), 3.58 (d, 1H,  $J$  = 10.5 Hz), 2.14 (m, 2H), 2.04 (m, 2H), 1.59 (m, 6H), 1.40-1.20 (m, 42H), 0.89 (t, 6H,  $J$  = 7.0 Hz);  $^{13}\text{C NMR}$  (100 MHz,  $\text{CDCl}_3$ )  $\delta$  = 173.3, 160.5, 137.6, 130.6, 128.0, 126.9, 114.1, 101.7, 82.3, 70.1, 55.7, 47.23, 37.3, 32.8, 32.3, 30.2, 30.1, 30.0, 29.8, 29.7, 29.4, 26.1, 23.1, 14.5; ESI-MS  $[\text{M}+\text{H}]^+$  calculated for  $\text{C}_{42}\text{H}_{74}\text{NO}_4^+$  656.560, found 656.589.



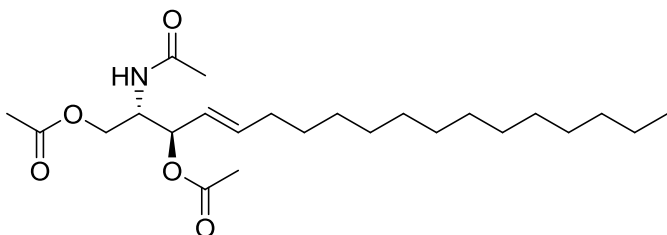
***p*-Methoxybenzylidene C2-ceramide (C2-pmb 15):**



C2-ceramide **2** (Avanti Polar Lipids, 10 mg, 29.3  $\mu\text{mol}$ ) was added to solution of *p*-anisaldehyde (0.56 g, 41.1  $\mu\text{mol}$ ) and  $\text{ZnCl}_2$  (6 mg, 44.0  $\mu\text{mol}$ ) in dry methylene chloride (1.5

mL). The reaction mixture was stirred over molecular sieves at 25 °C under  $\text{N}_2$  overnight. Solid  $\text{NaHCO}_3$  was then added to the reaction mixture and the resulting mixture was stirred for 5 min and filtered. The crude reaction product was then purified by  $\text{SiO}_2$  column chromatography using a solvent system of 2% MeOH in  $\text{CH}_2\text{Cl}_2$  to afford the C2-pmb **15** (9.0 mg, 67 % yield). M.p. 149-150 °C; IR (neat) 3273, 2958, 2919, 2851, 1652  $\text{cm}^{-1}$ ;  $^1\text{H-NMR}$  (400 MHz,  $\text{CDCl}_3$ )  $\delta$  = 7.42 (d, 2H,  $J$  = 8.7 Hz), 6.89 (d, 2H,  $J$  = 8.7 Hz), 5.82 (dt, 1H,  $J$  = 15.4 Hz,  $J$  = 6.8 Hz), 5.53 (dd, 1H,  $J$  = 15.4 Hz,  $J$  = 7.2 Hz), 5.48 (s, 1H), 5.05 (d, 1H,  $J$  = 7.4 Hz), 4.40 (dd, 1H,  $J$  = 4.4 Hz,  $J$  = 10.5 Hz), 4.03 (m, 2H), 3.80 (s, 3H), 3.58 (t, 1H,  $J$  = 10.5 Hz), 2.06 (m, 2H), 1.97 (s, 3H), 1.57 (m, 6H), 1.40-1.20 (m, 16H), 0.89 (t, 3H,  $J$  = 7.1 Hz);  $^{13}\text{C NMR}$  (100 MHz,  $\text{CDCl}_3$ )  $\delta$  = 170.0, 160.3, 137.4, 130.4, 127.8, 126.7, 113.9, 101.5, 82.0, 69.8, 59.7, 55.5, 47.3, 38.4, 32.6, 32.1, 31.5, 29.9, 29.8, 29.7, 29.6, 29.4, 29.2, 23.6, 22.9, 14.4; ESI-MS  $[\text{M}+\text{H}]^+$  calculated for  $\text{C}_{28}\text{H}_{46}\text{NO}_4^+$  460.343, found 460.365. Crystals for x-ray structure determination were grown from DMSO.

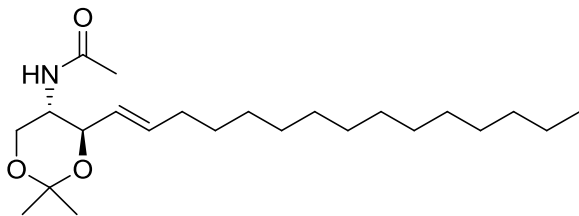
**1,3-diacetyl C2-ceramide (C2-diacetate 16):**



C2-ceramide **2** (Avanti Polar Lipids, 10 mg, 29.3  $\mu\text{mol}$ ) was added to solution of acetyl chloride (6.9 mg, 87.8  $\mu\text{mol}$ )

and triethylamine (8.9 mg, 87.8  $\mu\text{mol}$ ) in dry methylene chloride (1.5 mL). The reaction mixture was stirred at 25  $^{\circ}\text{C}$  under  $\text{N}_2$  overnight. Solid  $\text{NaHCO}_3$  was then added to the reaction mixture and the resulting mixture was stirred for 5 min and filtered. The crude reaction product was then purified by  $\text{SiO}_2$  column chromatography using a solvent system of 2% MeOH in  $\text{CH}_2\text{Cl}_2$  to afford the C2-diacetate **16** (8.7 mg, 70 % yield). M.p. 102-103  $^{\circ}\text{C}$  (lit. 104-105  $^{\circ}\text{C}$ );<sup>240</sup> IR (neat) 3285, 2956, 2920, 2850, 1732, 1655  $\text{cm}^{-1}$ ;  $^1\text{H-NMR}$  (400 MHz,  $\text{CDCl}_3$ )  $\delta$  = 5.80 (dt, 1H,  $J$  = 15.4 Hz,  $J$  = 7.2 Hz), 5.64 (d, 2H,  $J$  = 9.2 Hz), 5.40 (dd, 1H,  $J$  = 15.4 Hz,  $J$  = 7.5 Hz), 5.29 (dd, 1H,  $J$  = 11.7 Hz,  $J$  = 7.5 Hz), 4.44 (m, 1H), 4.31 (dd, 1H,  $J$  = 11.6 Hz,  $J$  = 6.0 Hz), 4.05 (dd, 1H,  $J$  = 11.6 Hz,  $J$  = 3.9 Hz), 2.08 (s, 3H), 2.07 (s, 3H), 2.03 (m, 2H), 1.99 (s, 3H), 1.40-1.20 (m, 22H), 0.89 (t, 3H,  $J$  = 6.8 Hz);  $^{13}\text{C NMR}$  (100 MHz,  $\text{CDCl}_3$ )  $\delta$  = 171.0, 170.1, 169.5, 137.4, 124.3, 73.7, 62.6, 50.9, 32.2, 32.0, 29.8, 29.6, 29.5, 29.4, 29.1, 14.3; ESI-MS  $[\text{M}+\text{H}]^+$  calculated for  $\text{C}_{24}\text{H}_{44}\text{NO}_5^+$  426.327, found 426.341.

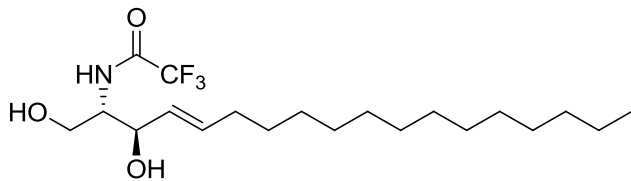
### Isopropylidene C2-ceramide (18):



C2-ceramide **1** (Avanti Polar Lipids, 10.5 mg, 30.7  $\mu\text{mol}$ ) was added to solution of *p*-TsOH $\cdot$ H<sub>2</sub>O (2.3 mg, 12.3

$\mu\text{mol}$ ) in acetone (1 mL) and 2,2'-dimethoxypropane (1 mL). The reaction mixture was stirred at 25 °C under N<sub>2</sub> overnight. Solid NaHCO<sub>3</sub> was then added to the reaction mixture and the resulting mixture was stirred for 5 min, filtered and concentrated *in vacuo*. The crude reaction product was then purified by SiO<sub>2</sub> column chromatography using a solvent system of 2% MeOH in CH<sub>2</sub>Cl<sub>2</sub> to afford the isopropylidene C2-ceramide **18** (11.0 mg, 94 % yield). M.p. 68.0-69.5 °C; IR (neat) 3270, 2957, 2919, 2851, 1638 cm<sup>-1</sup>; <sup>1</sup>H NMR (400 MHz, CDCl<sub>3</sub>)  $\delta$  = 5.75 (td, 1 H,  $J$  = 6.7,  $J$  = 15.2 Hz), 5.43 (dd, 1 H,  $J$  = 7.6,  $J$  = 15.2 Hz), 5.21 (d, 1 H,  $J$  = 8.0 Hz), 4.06 (dd, 1 H,  $J$  = 7.6,  $J$  = 9.2 Hz), 4.01 (dd, 1 H,  $J$  = 5.3,  $J$  = 11.3 Hz), 3.84 (m, 1H), 3.63 (dd, 1 H,  $J$  = 9.3,  $J$  = 11.3 Hz), 2.04 (m, 2 H), 1.94 (s, 3 H), 1.49 (s, 3 H), 1.42 (s, 3 H), 1.25 (m, 22 H), 0.88 (t, 3H,  $J$  = 6.8 Hz); <sup>13</sup>C NMR (100 MHz, CDCl<sub>3</sub>)  $\delta$  = 170.0, 136.8, 127.5, 99.1, 74.4, 63.0, 48.5, 32.6, 32.1, 29.9, 29.9, 29.8, 29.7, 29.6, 29.4, 29.2, 28.7, 23.6, 22.9, 20.2, 14.3; ESI-MS [M+H]<sup>+</sup> calculated for C<sub>23</sub>H<sub>44</sub>NO<sub>3</sub><sup>+</sup> 382.332, found 382.418. Crystals for x-ray structure determination were grown from DMSO.

### Trifluoroacetyl C2-ceramide (**19**):



Trifluoroacetic anhydride (7.0 mg, 33.4  $\mu\text{mol}$ ) was added dropwise to a solution of *D-erythro*-

sphingosine **3** (Avanti Polar Lipids, 10 mg, 33.4  $\mu\text{mol}$ ) and triethylamine (3.4 mg  $\mu\text{mol}$ ) in methylene chloride (2 mL). The reaction mixture was stirred at 25 °C under  $\text{N}_2$  overnight. Solid  $\text{NaHCO}_3$  was then added to the reaction mixture and the resulting mixture was stirred for 5 min, filtered and concentrated *in vacuo*. The crude reaction product was then purified by  $\text{SiO}_2$  column chromatography using a solvent system of 4.5% MeOH in  $\text{CH}_2\text{Cl}_2$  to afford the trifluoroacetyl C2-ceramide **19** (8.6 mg, 59 % yield). M.p. 91.0-92.5 °C (lit. 89.5-90.5);<sup>164</sup> IR (neat) 3455, 3278, 2956, 2917, 2850, 1699  $\text{cm}^{-1}$ ;  $^1\text{H}$  NMR (400 MHz,  $\text{CDCl}_3$ )  $\delta$  = 7.15 (d, 1H,  $J$  = 7.3 Hz), 5.83 (dt, 1H,  $J$  = 15.4 Hz,  $J$  = 7.1 Hz), 5.54 (dd, 1H,  $J$  = 15.4 Hz,  $J$  = 6.5 Hz), 4.39 (t, 1H,  $J$  = 6.5 Hz), 4.11 (dd, 1H,  $J$  = 11.5 Hz,  $J$  = 2.3 Hz), 3.93 (m, 1H), 3.74 (dd, 1H,  $J$  = 11.5, 3.3 Hz), 2.43 (br. s, 1H), 2.37 (br. s, 1H), 2.07 (m, 2H), 1.50-1.20 (m, 22H), 0.88 (t, 3H,  $J$  = 6.8 Hz);  $^{13}\text{C}$  NMR (100 MHz,  $\text{CDCl}_3$ )  $\delta$  = 157.4 (q,  $J_{\text{CF}}$  = 37.2 Hz), 135.6, 128.2, 116.1 (q,  $J_{\text{CF}}$  = 287.5 Hz), 74.4, 61.3, 54.2, 32.4, 32.1, 29.9, 29.8, 29.7, 29.6, 29.4, 29.2, 22.9, 14.3; ESI-MS  $[\text{M}+\text{H}]^+$  calculated for  $\text{C}_{20}\text{H}_{37}\text{F}_3\text{NO}_3^+$  396.271, found 396.298.

## 6.3 Carboxyfluorescein (CF) Liposome Assays

### 6.3.1 Liposome Preparation

A stock solution of EYPC in  $\text{CHCl}_3$  (60 mg in 3 mL) was evaporated under reduced pressure to produce a thin film that was dried *in vacuo* overnight. The lipid film was hydrated with a 1 mL solution containing 10 mM HEPES (pH 7), 38.8 mM NaCl, 1 mM EDTA, 1.5 mM CF, and 6 mM p-xylene-bis-pyridinium bromide (DPX). Freeze/thaw cycles were repeated 9 times, at which time no solids were visible. The frozen solution was warmed to 30-35 °C before each freeze cycle. The mixture was placed on a vortexer every 3 cycles for 30 seconds to facilitate hydration. The cloudy solution was extruded through a 100 nm polycarbonate membrane at least 25 times at room temperature using a high pressure mini-extruder. This solution was passed through a Sephacryl S200 column (11 cm x 1 cm) using a buffer containing 10 mM HEPES (pH 7), 50 mM NaCl, and 1 mM EDTA as the eluant to remove extravesicular CF and DPX. The 6-10 mL of solution isolated from gel filtration was 8-12 mM in lipid, assuming all EYPC was incorporated into the liposomes. Each stock solution of liposomes was used within three days for dye release assays.

### 6.3.2 CF Dye Release Assay<sup>47</sup>

This procedure describes a typical ion transport assay as described **in Chapter 2**. An aliquot (volume varies depending on concentration of stock solution, typically 100-180  $\mu\text{L}$ ) of the stock solution of EYPC liposomes was added to a cuvette and diluted to 2 mL with a solution containing 10 mM HEPES (pH 7), 50 mM NaCl, and 1 mM EDTA give a final concentration of 330  $\mu\text{M}$  phospholipid. The fluorescence of

intravesicular CF was monitored by excitation at 495 nm, and the emission was recorded at 520 nm. At  $t = 30$  s, compounds were injected into the liposomal solution to give a final concentration of compound added of  $50 \mu\text{M}$  (15 mol% of compound relative to EYPC phospholipid). At the end of the experiment, 40 mL of a 10% aqueous Triton-X solution was injected to lyse the liposomes. All data presented is an average of 3 runs.

## **6.4 FITC-Dextran Liposome Assays**

### **6.4.1 Liposome Preparation**

A stock solution of EYPC in  $\text{CHCl}_3$  (60 mg in 3 mL) was evaporated under reduced pressure to produce a thin film that was dried *in vacuo* overnight. The lipid film was hydrated with a 1 mL solution containing 10 mM HEPES (pH 7), 100 mM KCl, 7.5 mM fluorescent isothiocyanate (FITC) dextran FD10. At these concentrations, the fluorescence of FD10 is self-quenched.<sup>81</sup> Freeze/thaw cycles were repeated 9 times, at which time no solids were visible. The frozen solution was warmed to 30-35 °C before each freeze cycle. The mixture was placed on a vortexer every 3 cycles for 30 seconds to facilitate hydration. The cloudy solution was extruded through a 100 nm polycarbonate membrane at least 25 times at room temperature using a high pressure mini-extruder. This solution was passed through a Sephacryl S300HR column (11 cm x 1 cm) using a buffer containing 10 mM HEPES (pH 7), and 100 mM KCl as the eluant to remove extravesicular dye. The 6-10 mL of solution isolated from gel filtration was 8-12 mM in lipid, assuming all EYPC was incorporated into the

liposomes. Each stock solution of liposomes was used within three days for dye release assays.

#### **6.4.2 FITC-Dextran Release Assay**

This procedure describes a typical ion transport assay as described **in Chapter 2**. An aliquot (volume varies depending on concentration of stock solution, typically 10-30  $\mu\text{L}$ ) of the stock solution of EYPC liposomes was added to a cuvette and diluted to 2 mL with a solution containing 10 mM HEPES (pH 7), and 100 mM KCl give a final concentration of 70  $\mu\text{M}$  phospholipid. The fluorescence of intravesicular FD10 was monitored by excitation at 495 nm, and the emission was recorded at 520 nm. At  $t = 30$  s, compounds were injected into the liposomal solution to give a final concentration of compound added of 50  $\mu\text{M}$  (70 mol% of compound relative to EYPC phospholipid). At the end of the experiment, 40 mL of a 10% aqueous Triton-X solution was injected to lyse the liposomes. All data presented is an average of 3 runs.

### **6.5 Lucigenin Liposome Assays**

#### **6.5.1 Liposome Preparation**

A stock solution of EYPC in  $\text{CHCl}_3$  (60 mg in 3 mL) was evaporated under reduced pressure to produce a thin film that was dried *in vacuo* overnight. The lipid film was hydrated with a 1 mL solution containing 20 mM HEPES (pH 7.4), 100 mM NaCl and 2 mM lucigenin. Freeze/thaw cycles were repeated 9 times, at which time no solids were visible. The frozen solution was warmed to 30-35  $^{\circ}\text{C}$  before each freeze

cycle. The mixture was placed on a vortexer every 3 cycles for 30 seconds to facilitate hydration. The cloudy solution was extruded through a 100 nm polycarbonate membrane at least 25 times at room temperature using a high pressure mini-extruder. This solution was passed through a Sephadex G25 column (11 cm x 1 cm) to remove extravesicular lucigenin. The eluant was comprised of 20 mM HEPES and 75 mM Na<sub>2</sub>SO<sub>4</sub> at pH 7.4 in order to replace external Cl<sup>-</sup> with SO<sub>4</sub><sup>-</sup>. The 6-10 mL of solution isolated from gel filtration was 8-12 mM in lipid, assuming all EYPC was incorporated into the liposomes. Each stock solution of liposomes was used within three days for transport assays.

#### **6.5.2 Anion Transport Assay**

This procedure describes a typical ion transport assay as described in **Chapters 3 and 4**. An aliquot (volume varies depending on concentration of stock solution, typically 80-120  $\mu$ L) of the stock solution of EYPC liposomes was added to a cuvette and diluted to 2 mL with a solution of salt NaX and 20 mM HEPES at pH 7.4 to give a final concentration of 200  $\mu$ M phospholipid. The fluorescence of intravesicular lucigenin was monitored by excitation at 372 nm, and the emission was recorded at 503 nm. At  $t = 30$  s, a 2  $\mu$ L aliquot of a 2 mM stock solution of the compound being tested (or a DMSO blank) was injected to give a final concentration of compound added of 2  $\mu$ M (1 mol% of compound relative to EYPC phospholipid). At the end of the experiment, 40 mL of a 10% aqueous Triton-X solution was injected to lyse the liposomes. All data presented is an average of 3 runs.



## 6.6 Direct Monitoring of Bicarbonate Transport via $^{13}\text{C}$ NMR

### 6.6.1 Liposome Preparation

A stock solution of EYPC in  $\text{CHCl}_3$  (280 mg in 14 mL) was evaporated under reduced pressure to produce a thin film that was dried *in vacuo* overnight. The lipid film was hydrated with a 2 mL solution containing 20 mM HEPES (pH 7.4), 100 mM  $\text{NaH}^{13}\text{CO}_3$  in 9:1  $\text{H}_2\text{O}/\text{D}_2\text{O}$ . Freeze/thaw cycles were repeated 9 times, at which time no solids were visible. The frozen solution was warmed to 30-35 °C before each freeze cycle. The mixture was placed on a vortexer every 3 cycles for 30 seconds to facilitate hydration. The cloudy solution was extruded through a 5  $\mu\text{m}$  polycarbonate membrane at least 25 times at room temperature in two separate 1 mL batches. The two batches were then combined and added to dialysis tubing. The dialysis tubing containing the liposome solution was submerged in a 1 L solution containing 20 mM HEPES (pH 7.4) and 75 mM  $\text{Na}_2\text{SO}_4$  in 9:1  $\text{H}_2\text{O}/\text{D}_2\text{O}$ . This solution was stirred for 4 hours to allow  $\text{SO}_4^{2-}$  to replace extraventricular  $\text{H}^{13}\text{CO}_3^-$ . Each stock solution of liposomes was used within three days for transport assays.

### 6.6.2 $^{13}\text{C}$ NMR Bicarbonate Transport Assays

This procedure describes a typical ion transport assay as described in **Chapter 4**.  $^{13}\text{C}$  NMR spectra were recorded on a Bruker AVIII-600 operating at 150.92 MHz, with chemical shifts reported in ppm. The instrument was locked on 9:1  $\text{H}_2\text{O}/\text{D}_2\text{O}$ . Experimental conditions were: temperature, 27 °C; acquisition time, 0.93 s; spectrum width 35,211 Hz; relaxation delay, 0.2 s; number of scans, 196. For each experiment, an initial  $^{13}\text{C}$  NMR spectrum of a 520  $\mu\text{L}$  of the liposome solution was acquired. This

solution consisted of EYPC liposomes containing 100 mM  $\text{NaH}^{13}\text{CO}_3$  buffered to pH 7.4 with 20 mM HEPES, dispersed in 75 mM  $\text{Na}_2\text{SO}_4$  buffered to pH 7.4 with 20 mM HEPES. A NaCl pulse followed, resulting in final extravesicular concentrations of 41 mM lipid and 50 mM NaCl. The  $^{13}\text{C}$  NMR of this liposome mixture was taken, followed by the addition of a solution of compound (in DMSO, 15  $\mu\text{L}$ ) or 15  $\mu\text{L}$  of DMSO. Compounds were added to give a 0.04 molar equiv. to lipid ratio. A  $^{13}\text{C}$  NMR of the ligand containing mixture was acquired before and after the addition 3  $\mu\text{L}$  of a solution of  $\text{MnCl}_2$  (0.5 mM final  $\text{Mn}^{2+}$  concentration).

## **6.7 X-Ray Crystallographic Data**

### **6.7.1 C2-pmb 15**

Crystals were obtained by slow evaporation of a DMSO solution of C2-pmb **15**, and the structure (**Figure 6.1**) was solved by Dr. Peter Y. Zavalij. **Table 6.1** shows crystal data and structure refinement parameters for C2-pmb **15**. Detailed crystallographic data and the structure report for UM1807 (C2-pmb **15**) can be obtained from the Department of Chemistry and Biochemistry, University of Maryland, College Park, MD 20742.

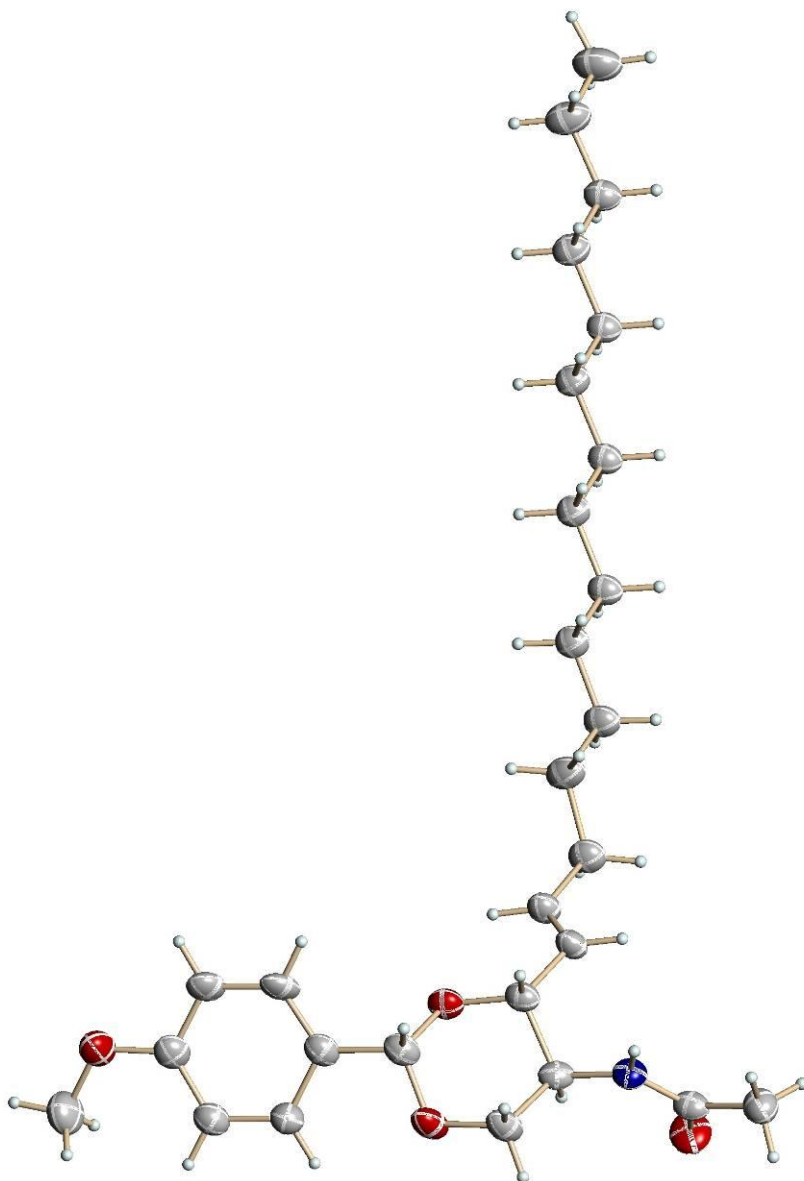


**Figure 6.1.** A view of UM#1807 showing the anisotropic atomic displacement ellipsoids for the non-hydrogen atoms are shown at the 25% probability level. Hydrogen atoms are displayed with an arbitrarily small radius.

**Table 6.1.** Crystal data and structure refinement for UM#1807.

|                                     |   |                  |
|-------------------------------------|---|------------------|
| X-ray lab book No.                  | 1807  |                  |
| Crystal ID                          | Davis/Harrell pMBC2 at 295K =1804 (same xtal)   |                  |
| Empirical formula                   | C <sub>28</sub> H <sub>45</sub> NO <sub>4</sub>   |                  |
| Formula weight                      | 459.65  |                  |
| Temperature                         | 295(2) K  |                  |
| Wavelength                          | 0.71073 Å   |                  |
| Crystal size                        | 0.45 × 0.20 × 0.06 mm <sup>3</sup>  |                  |
| Crystal habit                       | colorless plate   |                  |
| Crystal system                      | Monoclinic  |                  |
| Space group                         | P2 <sub>1</sub>   |                  |
| Unit cell dimensions                | a = 9.4304(5) Å   | α = 90°          |
|                                     | b = 4.9089(3) Å   | β = 91.2750(10)° |
|                                     | c = 30.3484(16) Å   | γ = 90°          |
| Volume                              | 1404.57(14) Å <sup>3</sup>  |                  |
| Z                                   | 2   |                  |
| Density, ρ <sub>calc</sub>          | 1.087 g/cm <sup>3</sup>   |                  |
| Absorption coefficient, μ           | 0.071 mm <sup>-1</sup>  |                  |
| F(000)                              | 504 e <sup>-</sup>  |                  |
| Diffractometer                      | Bruker Smart Apex II CCD area detector  |                  |
| Radiation source                    | fine-focus sealed tube, MoKα  |                  |
| Detector distance                   | 6.000 cm  |                  |
| Detector resolution                 | 8.333 pixels/mm   |                  |
| Total frames                        | 2100  |                  |
| Frame size                          | 512 pixels  |                  |
| Frame width                         | -0.30°  |                  |
| Exposure per frame                  | 60 sec  |                  |
| Total measurement time              | 38.5 hours  |                  |
| Data collection method              | ω and φ scans   |                  |
| θ range for data collection         | 2.01 to 25.00°  |                  |
| Index ranges                        | -11 ≤ h ≤ 11, -5 ≤ k ≤ 5, -36 ≤ l ≤ 35  |                  |
| Reflections collected               | 11341   |                  |
| Independent reflections             | 2789  |                  |
| Observed reflection, I>2σ(I)        | 2125  |                  |
| Coverage of independent reflections | 99.9 %  |                  |
| Variation in check reflections      | 0 %   |                  |
| Absorption correction               | Semi-empirical from equivalents<br>SADABS (Sheldrick, 1996)   |                  |
| Max. and min. transmission          | 0.996 and 0.949   |                  |
| Structure solution technique        | direct  |                  |
| Structure solution program          | SHELXS-97 (Sheldrick, 1990)   |                  |
| Refinement technique                | Full-matrix least-squares on F <sup>2</sup>   |                  |
| Refinement program                  | SHELXL-97 (Sheldrick, 1997)   |                  |
| Function minimized                  | Σw(F <sub>o</sub> <sup>2</sup> - F <sub>c</sub> <sup>2</sup> ) <sup>2</sup>   |                  |
| Data / restraints / parameters      | 2789 / 238 / 366  |                  |
| Goodness-of-fit on F <sup>2</sup>   | 0.995   |                  |
| Δ/σ <sub>max</sub>                  | 0.001   |                  |
| Final R indices:                    | R <sub>1</sub> , I>2σ(I)  | 0.0365           |
|                                     | wR <sub>2</sub> , all data  | 0.0668           |
|                                     | R <sub>int</sub>  | 0.0220           |
|                                     | R <sub>sig</sub>  | 0.0176           |
| Weighting scheme                    | w = 1/[σ <sup>2</sup> (F <sub>o</sub> <sup>2</sup> )+(0.002P) <sup>2</sup> +0.267P], P = [max(F <sub>o</sub> <sup>2</sup> , 0)+2F <sub>o</sub> <sup>2</sup> ]/3 |                  |
| Absolute structure parameter        | not determined  |                  |
| Largest diff. peak and hole         | 0.090 and -0.081 e <sup>-</sup> /Å <sup>3</sup>   |                  |

$$R_1 = \sum ||F_o| - |F_c|| / \sum |F_o|, \quad wR_2 = [\sum w(F_o^2 - F_c^2)^2 / \sum w(F_o^2)^2]^{1/2}$$

### 6.7.2 Isopropylidene C2-Ceramide **18**

Crystals were obtained by slow evaporation of a DMSO solution of isopropylidene C2-ceramide **18**, and the structure (**Figure 6.2**) was solved by Dr. Peter Y. Zavalij. **Table 6.2** shows crystal data and structure refinement parameters for isopropylidene C2-ceramide **18**. Detailed crystallographic data and the structure report for UM1793 (isopropylidene C2-ceramide **18**) can be obtained from the Department of Chemistry and Biochemistry, University of Maryland, College Park, MD 20742.

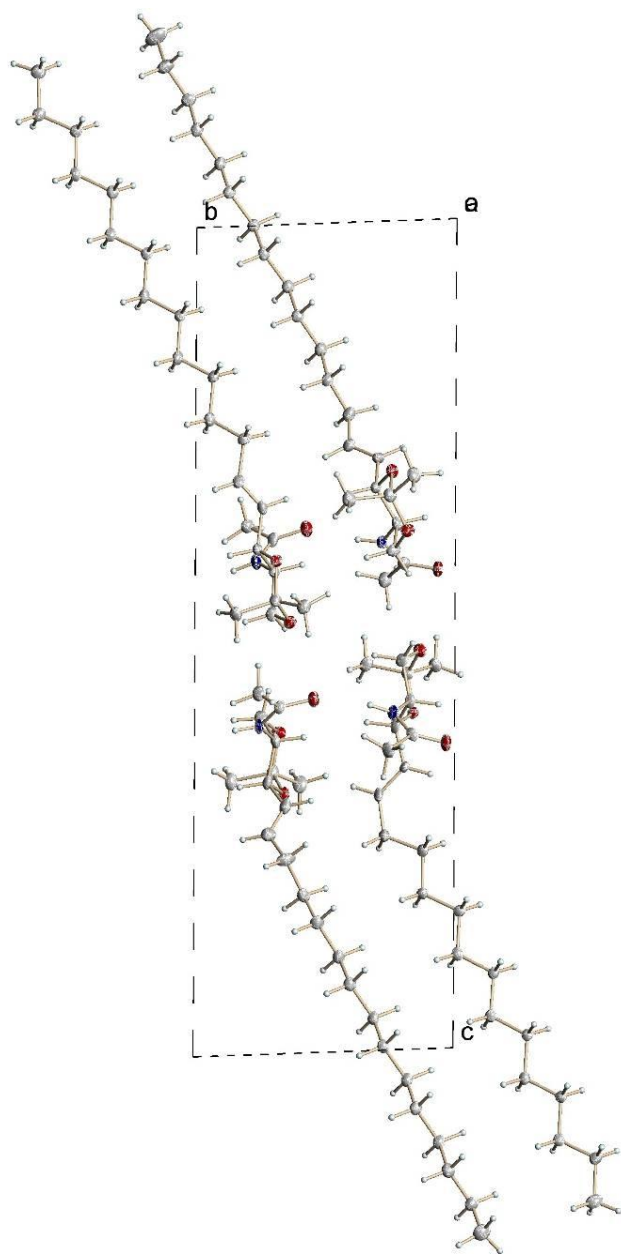


**Figure 6.2.** A view of 4 symmetrically independent molecules in the unit cell of UM#1793. Anisotropic atomic displacement ellipsoids for the non-hydrogen atoms are shown at the 30% probability level. Hydrogen atoms are displayed with an arbitrarily small radius.

**Table 6.2.** Crystal data and structure refinement for UM # 1793

|                                     |  |                |
|-------------------------------------|--|----------------|
| Crystal ID                          | Davis/Harrell C2-ceramide 1,3-isopropylidene <b>2</b> 150K   |                |
| Empirical formula                   | C <sub>23</sub> H <sub>43</sub> NO <sub>3</sub>  |                |
| Formula weight                      | 381.58   |                |
| Temperature                         | 150(2) K   |                |
| Wavelength                          | 0.71073 Å  |                |
| Crystal size                        | 0.51 × 0.12 × 0.06 mm <sup>3</sup>   |                |
| Crystal habit                       | colorless needle   |                |
| Crystal system                      | Triclinic  |                |
| Space group                         | P1   |                |
| Unit cell dimensions                | a = 8.9474(16) Å   | α = 87.563(2)° |
|                                     | b = 9.1515(16) Å   | β = 82.486(2)° |
|                                     | c = 29.391(5) Å  | γ = 88.842(2)° |
| Volume                              | 2383.5(7) Å <sup>3</sup>   |                |
| Z                                   | 4  |                |
| Density, ρ <sub>calc</sub>          | 1.063 g/cm <sup>3</sup>  |                |
| Absorption coefficient, μ           | 0.069 mm <sup>-1</sup>   |                |
| F(000)                              | 848 e <sup>-</sup>   |                |
| Diffractometer                      | Bruker Smart Apex II CCD area detector   |                |
| Radiation source                    | fine-focus sealed tube, MoKα   |                |
| Detector distance                   | 6.000 cm   |                |
| Detector resolution                 | 8.333 pixels/mm  |                |
| Total frames                        | 4230   |                |
| Frame size                          | 512 pixels   |                |
| Frame width                         | -0.30°   |                |
| Exposure per frame                  | 40 sec   |                |
| Total measurement time              | 54.0 hours   |                |
| Data collection method              | ω and φ scans  |                |
| θ range for data collection         | 2.10 to 25.00°   |                |
| Index ranges                        | -10 ≤ h ≤ 10, -10 ≤ k ≤ 10, -34 ≤ l ≤ 34   |                |
| Reflections collected               | 30116  |                |
| Independent reflections             | 8310   |                |
| Observed reflection, I > 2σ(I)      | 6931   |                |
| Coverage of independent reflections | 99.1 %   |                |
| Variation in check reflections      | 0 %  |                |
| Absorption correction               | Semi-empirical from equivalents SADABS (Sheldrick, 1996)   |                |
| Max. and min. transmission          | 0.996 and 0.873  |                |
| Structure solution technique        | direct   |                |
| Structure solution program          | SHELXS-97 (Sheldrick, 1990)  |                |
| Refinement technique                | Full-matrix least-squares on F <sup>2</sup>  |                |
| Refinement program                  | SHELXL-97 (Sheldrick, 1997)  |                |
| Function minimized                  | Σw(F <sub>o</sub> <sup>2</sup> - F <sub>c</sub> <sup>2</sup> ) <sup>2</sup>  |                |
| Data / restraints / parameters      | 8310 / 3 / 989   |                |
| Goodness-of-fit on F <sup>2</sup>   | 1.000  |                |
| Δ/σ <sub>max</sub>                  | 0.000  |                |
| Final R indices:                    | R <sub>1</sub> , I > 2σ(I)   | 0.0586         |
|                                     | wR <sub>2</sub> , all data   | 0.1290         |
|                                     | R <sub>int</sub>   | 0.0454         |
|                                     | R <sub>sig</sub>   | 0.0436         |
| Weighting scheme                    | w = 1/[σ <sup>2</sup> (F <sub>o</sub> <sup>2</sup> ) + (0.02P) <sup>2</sup> + 3.17P], P = [max(F <sub>o</sub> <sup>2</sup> , 0) + 2F <sub>o</sub> <sup>2</sup> ]/3 |                |
| Absolute structure parameter        | unknown  |                |
| Largest diff. peak and hole         | 0.297 and -0.210 e <sup>-</sup> /Å <sup>3</sup>  |                |

$$R_1 = \sum ||F_o| - |F_c|| / \sum |F_o|, \quad wR_2 = [\sum w(F_o^2 - F_c^2)^2 / \sum w(F_o^2)]^{1/2}$$

## Bibliography

1. Radin, N. Killing cancer cells by poly-drug elevation of ceramide - A hypothesis whose time has come? *Eur. J. Biochem.* **2001**, *268*, 193-204.
2. Kolesnick, R. N.; Kronke, M. Regulation of ceramide production and apoptosis. *Annu. Rev. Physiol.* **1998**, *60*, 643-665.
3. Hannun, Y. A. Functions of ceramide in coordinating cellular responses to stress. *Science* **1996**, *274*, 1855-1859.
4. Choi, M. J.; Maibach, H. I. Role of ceramides in barrier function of healthy and diseased skin. *Am. J. Clin. Dermatol.* **2005**, *6*, 215-223.
5. Ariga, T.; Jarvis, W. D.; Yu, R. K. Role of sphingolipid-mediated cell death in neurodegenerative diseases. *J. Lipid Res.* **1998**, *39*, 1-16.
6. Ruiz-Arguello, M.; Basanez, G.; Goni, F.; Alonso, A. Different effects of enzyme-generated ceramides and diacylglycerols in phospholipid membrane fusion and leakage. *J. Biol. Chem.* **1996**, *271*, 26616-26621.
7. Siskind, L. J.; Colombini, M. The lipids C2- and C16-ceramide form large stable channels: implications for apoptosis. *J. Biol. Chem.* **2000**, *275*, 38640-38644.
8. Merrill, A. H., Jr. De novo sphingolipid biosynthesis: a necessary, but dangerous, pathway. *J. Biol. Chem.* **2002**, *277*, 25843-25846.
9. Brodesser, S.; Sawatzki, P.; Kolter, T. Boorganic Chemistry of Ceramide. *Eur. J. Org. Chem.* **2003**, 2021-2034.
10. Nussbaumer, P. Medicinal chemistry aspects of drug targets in sphingolipid metabolism. *ChemMedChem* **2008**, *3*, 543-551.
11. Delgado, A.; Casas, J.; Llebaria, A.; Abad, J. L.; Fabrias, G. Chemical tools to investigate sphingolipid metabolism and functions. *ChemMedChem* **2007**, *2*, 580-606.
12. Goni, F. M.; Alonso, A. Biophysics of sphingolipids I. Membrane properties of sphingosine, ceramides and other simple sphingolipids. *Biochim. Biophys. Acta* **2006**, *1758*, 1902-1921.
13. Meikle, P. J.; Hopwood, J. J.; Clague, A. E.; Carey, W. F. Prevalence of lysosomal storage disorders. *J. Am. Med. Assoc.* **1999**, *281*, 249-254.



14. Futerman, A. H.; van Meer, G. The cell biology of lysosomal storage disorders. *Nat. Rev., Mol. Cell Biol.* **2004**, *5*, 554-565.
15. Kolter, T.; Sandhoff, K. Sphingolipid metabolism diseases. *Biochim. Biophys. Acta* **2006**, *1758*, 2057-2079.
16. Raas-Rothschild, A.; Pankova-Kholmyansky, I.; Kacher, Y.; Futerman, A. H. Glycosphingolipidoses: beyond the enzymatic defect. *Glycoconj. J.* **2004**, *21*, 295-304.
17. Kacher, Y.; Futerman, A. H. Genetic diseases of sphingolipid metabolism: pathological mechanisms and therapeutic options. *FEBS Lett.* **2006**, *580*, 5510-5517.
18. Moser, H. W.; Linke, T.; Fensom, A. H.; Levade, T.; Sandhoff, K. Acid Ceramidase Deficiency: Farber Lipogranulomatosis. In *The Metabolic and Molecular Bases of Inherited Disease*; Scriver, C. R., Beaudet, A. L., Sly, W. S., Valle, D., Eds.; McGraw-Hill: New York, 2001, p 3573-3588.
19. Muramatsu, T.; Sakai, N.; Yanagihara, I.; Yamada, M.; Nishigaki, T.; Kokubu, C.; Tsukamoto, H.; Ito, M.; Inui, K. Mutation analysis of the acid ceramidase gene in Japanese patients with Farber disease. *J. Inherit. Metab. Dis.* **2002**, *25*, 585-592.
20. Tohyama, J.; Oya, Y.; Ezoe, T.; Vanier, M. T.; Nakayasu, H.; Fujita, N.; Suzuki, K. Ceramide accumulation is associated with increased apoptotic cell death in cultured fibroblasts of sphingolipid activator protein-deficient mouse but not in fibroblasts of patients with Farber disease. *J. Inherit. Metab. Dis.* **1999**, *22*, 649-662.
21. Sano, R.; Trindade, V. M.; Tessitore, A.; d'Azzo, A.; Vieira, M. B.; Giugliani, R.; Coelho, J. C. G(M1)-ganglioside degradation and biosynthesis in human and murine G(M1)-gangliosidosis. *Clin. Chim. Acta* **2005**, *354*, 131-139.
22. Suzuki, Y.; Oshima, A.; Nanba, E. beta-Galactosidase deficiency (beta-galactosidosis): GMI gangliosidosis and morquio B disease. In *The Metabolic and Molecular Bases of Inherited Disease*; Scriver, C. R., Beaudet, A. L., Sly, W. S., Valle, D., Eds.; McGraw-Hill: New York, 2001, p 3775-3809.
23. Filho, J. A. F.; Shapiro, B. E. Tay Sachs Disease. *Arch. Neurol.* **2004**, *61*, 466-468.
24. Sandhoff, K.; Harzer, K.; Wassle, W.; Jatzkewitz, H. Enzyme alterations and lipid storage in three variants of Tay-Sachs disease. *J. Neurochem.* **1971**, *18*, 2469-2489.
25. Tsuji, D.; Kuroki, A.; Ishibashi, Y.; Itakura, T.; Itoh, K. Metabolic correction in microglia derived from Sandhoff disease model mice. *J. Neurochem.* **2005**, *94*, 1631-1638.

26. Tsuji, D.; Kuroki, A.; Ishibashi, Y.; Itakura, T.; Kuwahara, J.; Yamanaka, S.; Itoh, K. Specific induction of macrophage inflammatory protein 1-alpha in glial cells of Sandhoff disease model mice associated with accumulation of N-acetylhexosaminyl glycoconjugates. *J. Neurochem.* **2005**, *92*, 1497-1507.
27. Sango, K.; Yamanaka, S.; Hoffmann, A.; Okuda, Y.; Grinberg, A.; Westphal, H.; McDonald, M. P.; Crawley, J. N.; Sandhoff, K.; Suzuki, K.; Proia, R. L. Mouse models of Tay-Sachs and Sandhoff diseases differ in neurologic phenotype and ganglioside metabolism. *Nat. Genet.* **1995**, *11*, 170-176.
28. Kobayashi, T.; Goto, I.; Okada, S.; Orii, T.; Ohno, K.; Nakano, T. Accumulation of lysosphingolipids in tissues from patients with GM1 and GM2 gangliosidoses. *J. Neurochem.* **1992**, *59*, 1452-1458.
29. Schmuth, M.; Man, M. Q.; Weber, F.; Gao, W.; Feingold, K. R.; Fritsch, P.; Elias, P. M.; Holleran, W. M. Permeability barrier disorder in Niemann-Pick disease: sphingomyelin-ceramide processing required for normal barrier homeostasis. *J. Invest. Dermatol.* **2000**, *115*, 459-466.
30. Patterson, M. C. A riddle wrapped in a mystery: understanding Niemann-Pick disease, type C. *Neurolog.* **2003**, *9*, 301-310.
31. Horinouchi, K.; Erlich, S.; Perl, D. P.; Ferlinz, K.; Bisgaier, C. L.; Sandhoff, K.; Desnick, R. J.; Stewart, C. L.; Schuchman, E. H. Acid sphingomyelinase deficient mice: a model of types A and B Niemann-Pick disease. *Nat. Genet.* **1995**, *10*, 288-293.
32. Graber, D.; Salvayre, R.; Levade, T. Accurate differentiation of neuronopathic and nonneuronopathic forms of Niemann-Pick disease by evaluation of the effective residual lysosomal sphingomyelinase activity in intact cells. *J. Neurochem.* **1994**, *63*, 1060-1068.
33. Sidransky, E.; Fartasch, M.; Lee, R. E.; Metlay, L. A.; Abella, S.; Zimran, A.; Gao, W.; Elias, P. M.; Ginns, E. I.; Holleran, W. M. Epidermal abnormalities may distinguish type 2 from type 1 and type 3 of Gaucher disease. *Pediatr. Res.* **1996**, *39*, 134-141.
34. Holleran, W. M.; Ginns, E. I.; Menon, G. K.; Grundmann, J. U.; Fartasch, M.; McKinney, C. E.; Elias, P. M.; Sidransky, E. Consequences of beta-glucocerebrosidase deficiency in epidermis. Ultrastructure and permeability barrier alterations in Gaucher disease. *J. Clin. Invest.* **1994**, *93*, 1756-1764.
35. Zhao, H.; Grabowski, G. A. Gaucher disease: Perspectives on a prototype lysosomal disease. *Cell Mol. Life Sci.* **2002**, *59*, 694-707.

36. Jmoudiak, M.; Futerman, A. H. Gaucher disease: pathological mechanisms and modern management. *Br. J. Haematol.* **2005**, *129*, 178-188.
37. Brady, R. O.; Kanfer, J. N.; Shapiro, D. Metabolism of Glucocerebrosides. II. Evidence of an Enzymatic Deficiency in Gaucher's Disease. *Biochem. Biophys. Res. Commun.* **1965**, *18*, 221-225.
38. Lukacs, Z.; Keil, A.; Kohlschutter, A.; Beck, M.; Mengel, E. The ratio of alpha-galactosidase to beta-glucuronidase activities in dried blood for the identification of female Fabry disease patients. *J. Inherit. Metab. Dis.* **2005**, *28*, 803-805.
39. Ohshima, T.; Murray, G. J.; Swaim, W. D.; Longenecker, G.; Quirk, J. M.; Cardarelli, C. O.; Sugimoto, Y.; Pastan, I.; Gottesman, M. M.; Brady, R. O.; Kulkarni, A. B. alpha-Galactosidase A deficient mice: a model of Fabry disease. *Proc. Natl. Acad. Sci. U.S.A.* **1997**, *94*, 2540-2544.
40. Asano, N.; Ishii, S.; Kizu, H.; Ikeda, K.; Yasuda, K.; Kato, A.; Martin, O. R.; Fan, J. Q. In vitro inhibition and intracellular enhancement of lysosomal alpha-galactosidase A activity in Fabry lymphoblasts by 1-deoxygalactonojirimycin and its derivatives. *Eur. J. Biochem.* **2000**, *267*, 4179-4186.
41. Suzuki, K.; Suzuki, Y. Globoid cell leucodystrophy (Krabbe's disease): deficiency of galactocerebroside beta-galactosidase. *Proc. Natl. Acad. Sci. U.S.A.* **1970**, *66*, 302-309.
42. Escolar, M. L.; Poe, M. D.; Provenzale, J. M.; Richards, K. C.; Allison, J.; Wood, S.; Wenger, D. A.; Pietryga, D.; Wall, D.; Champagne, M.; Morse, R.; Krivit, W.; Kurtzberg, J. Transplantation of umbilical-cord blood in babies with infantile Krabbe's disease. *N. Engl. J. Med.* **2005**, *352*, 2069-2081.
43. Provenzale, J. M.; Peddi, S.; Kurtzberg, J.; Poe, M. D.; Mukundan, S.; Escolar, M. Correlation of neurodevelopmental features and MRI findings in infantile Krabbe's disease. *Am. J. Roentgenol.* **2009**, *192*, 59-65.
44. Witty, J. P.; Bridgham, J. T.; Johnson, A. L. Induction of apoptotic cell death in hen granulosa cells by ceramide. *Endocrinology* **1996**, *137*, 5269-5277.
45. Bose, R.; Verheij, M.; Haimovitz-Friedman, A.; Scotto, K.; Fuks, Z.; Kolesnick, R. Ceramide synthase mediates daunorubicin-induced apoptosis: an alternative mechanism for generating death signals. *Cell* **1995**, *82*, 405-414.
46. Raisova, M.; Bektas, M.; Wieder, T.; Daniel, P.; Eberle, J.; Orfanos, C. E.; Geilen, C. C. Resistance to CD95/Fas-induced and ceramide-mediated apoptosis of human melanoma cells is caused by a defective mitochondrial cytochrome c release. *FEBS Lett.* **2000**, *473*, 27-32.

47. Stiban, J.; Fistere, D.; Colombini, M. Dihydroceramide hinders ceramide channel formation: Implications on apoptosis. *Apoptosis* **2006**, *11*, 773-780.
48. Di Paola, M.; Cocco, T.; Lorusso, M. Ceramide interaction with the respiratory chain of heart mitochondria. *Biochemistry* **2000**, *39*, 6660-6668.
49. Siskind, L. J.; Kolesnick, R. N.; Colombini, M. Ceramide channels increase the permeability of the mitochondrial outer membrane to small proteins. *J. Biol. Chem.* **2002**, *277*, 26796-26803.
50. Delgado, A.; Casas, J.; Llebaria, A.; Abad, J. L.; Fabrias, G. Inhibitors of sphingolipid metabolism enzymes. *Biochim. Biophys. Acta* **2006**, *1758*, 1957-1977.
51. Bittman, R. Synthetic Sphingolipids as Bioactive Molecules. In *Wiley Encyclopedia of Chemical Biology*; Begley, T. P., Ed.; John Wiley & Sons, Inc.: New York, 2008; Vol. 4, p 480-504.
52. Rasmussen, J. M.; Hermetter, A. Chemical synthesis of fluorescent glycerol- and sphingolipids. *Prog. Lipid. Res.* **2008**, *47*, 436-460.
53. Pajewski, R.; Djedovic, N.; Harder, E.; Ferdani, R.; Schlesinger, P. H.; Gokel, G. W. Pore formation in and enlargement of phospholipid liposomes by synthetic models of ceramides and sphingomyelin. *Bioorg. Med. Chem* **2005**, *13*, 29-37.
54. Ferdani, R.; Li, R.; Pajewski, R.; Pajewska, J.; Winter, R. K.; Gokel, G. W. Transport of chloride and carboxyfluorescein through phospholipid vesicle membranes by heptapeptide amphiphiles. *Org. Biomol. Chem.* **2007**, *5*, 2423-2432.
55. Montes, L. R.; Ruiz-Arguello, M. B.; Goni, F. M.; Alonso, A. Membrane restructuring via ceramide results in enhanced solute efflux. *J. Biol. Chem.* **2002**, *277*, 11788-11794.
56. Bieberich, E.; Kawaguchi, T.; Yu, R. K. N-acylated serinol is a novel ceramide mimic inducing apoptosis in neuroblastoma cells. *J. Biol. Chem.* **2000**, *275*, 177-181.
57. Duan, R.-D. Alkaline sphingomyelinase: An old enzyme with novel implications. *Biochim. Biophys. Acta Cell Biol. Lipids* **2006**, *1761*, 281-291.
58. Chanturiya, A.; Yang, J.; Scaria, P.; Stanek, J.; Frei, J.; Mett, H.; Woodle, M. New cationic lipids form channel-like pores in phospholipid bilayers. *Biophys. J.* **2003**, *84*, 1750-1755.
59. Macchia, M.; Barontini, S.; Bertini, S.; Di Bussolo, V.; Fogli, S.; Giovannetti, E.; Grossi, E.; Minutolo, F.; Danesi, R. Design, synthesis, and characterization of the antitumor activity of novel ceramide analogues. *J. Med. Chem.* **2001**, *44*, 3994-4000.

60. McNally, B. A.; O'Neil, E. J.; Nguyen, A.; Smith, B. D. Membrane transporters for anions that use a relay mechanism. *J. Am. Chem. Soc.* **2008**, *130*, 17274-17275.
61. Okazaki, T.; Bell, R.; Hannun, Y. Sphingomyelin turnover induced by Vitamin D3 in HL-60 cells - differentiation. *J. Biol. Chem.* **1989**, *264*, 19076-19080.
62. Obeid, L.; Linardic, C.; Karolak, L.; Hannun, Y. Programmed cell-death induced by ceramide. *Science* **1993**, *259*, 1769-1771.
63. Pascher, I. Molecular arrangements in sphingolipids conformation and hydrogen-bonding of ceramide and their implication on membrane stability and permeability. *Biochim. Biophys. Acta* **1976**, *455*, 433-451.
64. Huang, H.; Goldberg, E.; Zidovetzki, R. Ceramide induces structural defects into phosphatidylcholine bilayers and activates phospholipase A(2). *Biochem. Biophys. Res. Commun.* **1996**, *220*, 834-838.
65. Popov, J.; Vobornik, D.; Coban, O.; Keating, E.; Miller, D.; Francis, J.; Petersen, N. O.; Johnston, L. J. Chemical mapping of ceramide distribution in sphingomyelin-rich domains in monolayers. *Langmuir* **2008**, *24*, 13502-13508.
66. Anishkin, A.; Sukharev, S.; Colombini, M. Searching for the molecular arrangement of transmembrane ceramide channels. *Biophys. J.* **2006**, *90*, 2414-2426.
67. Zhang, X.; Meng, L.; Lu, Q.; Fei, Z.; Dyson, P. J. Targeted delivery and controlled release of doxorubicin to cancer cells using modified single wall carbon nanotubes. *Biomaterials* **2009**, *30*, 6041-6047.
68. Fenske, D. B.; Chonn, A.; Cullis, P. R. Liposomal nanomedicines: an emerging field. *Toxicol. Pathol.* **2008**, *36*, 21-29.
69. Dowling, M. B.; Li, L.; Park, J.; Kumi, G.; Nan, A.; Ghandehari, H.; Fourkas, J. T.; DeShong, P. Multiphoton-absorption-induced-luminescence (MAIL) imaging of tumor-targeted gold nanoparticles. *Bioconjugate Chem.* **2010**, *21*, 1968-1977.
70. Chadha, R.; Kapoor, V. K.; Thakur, D.; Kaur, R.; Arora, P.; Jain, D. V. S. Drug carrier systems for anticancer agents: A review. *J. Sci. Ind. Res.* **2008**, *67*, 185-197.
71. Zhao, H.; Duong, H. H. P.; Yung, L. Y. L. Folate-Conjugated polymer Micelles with pH-Triggered Drug Release Properties. *Macromol. Rapid Commun.* **2010**, *31*, 1163-1169.
72. Abe, A.; Shayman, J. A.; Radin, N. S. A novel enzyme that catalyzes the esterification of N-acetyl sphingosine. Metabolism of C2-ceramides. *J. Biol. Chem.* **1996**, *271*, 14383-14389.

73. O'Connell, A. M.; Pascher, I. The crystal structure of triacetylsphingosine. *Acta Cryst. B* **1969**, *25*, 2553-2561.
74. Matile, S.; Tanaka, H.; Litvinchuk, S. Analyte Sensing Across membranes with Artificial Pores. *Top. Curr. Chem.* **2007**, *277*, 219-250.
75. Rex, S. Pore Formation Induced by the Peptide Melittin in Different Lipid Vesicle Membranes. *Biophys. Chem.* **1996**, *58*, 75-85.
76. Lin, W.-J.; Lu, C.-H. Characterization and permeation of microporous poly(caprolactone) films. *J. Membr. Sci.* **2002**, *198*, 109-118.
77. Toprak, M. S.; McKenna, B. J.; Waite, J. H.; Stucky, G. D. Control of size and permeability of nanocomposite microspheres. *Chem. Mater.* **2007**, *19*, 4263-4269.
78. Schlegel, N.; Meir, M.; Heupel, W. M.; Holthofer, B.; Leube, R. E.; Waschke, J. Desmoglein 2-mediated adhesion is required for intestinal epithelial barrier integrity. *Am. J. Physiol. Gastrointest. Liver. Physiol.* **2010**, *298*, G774-G783.
79. Brooks, A. C.; Menzies-Gow, N.; Bailey, S. R.; Cunningham, F. M.; Elliott, J. Endotoxin-induced HIF-1alpha stabilisation in equine endothelial cells: synergistic action with hypoxia. *Inflamm. Res.* **2010**, *59*, 689-698.
80. Lang, I.; Scholz, M.; Peters, R. Molecular mobility and nucleocytoplasmic flux in hepatoma cells. *J. Cell. Biol.* **1986**, *102*, 1183-1190.
81. Stutzin, A. A fluorescence assay for monitoring and analyzing fusion biological membrane vesicles in vitro. *FEBS Lett.* **1986**, *197*, 274-280.
82. Saito, M.; Korsmeyer, S. J.; Schlesinger, P. H. BAX-dependent transport of cytochrome c reconstituted in pure liposomes. *Nat. Cell. Biol.* **2000**, *2*, 553-555.
83. Sandoval, C. M.; Salzameda, B.; Reyes, K.; Williams, T.; Hohman, V. S.; Plesniak, L. A. Anti-obesity and anti-tumor pro-apoptotic peptides are sufficient to cause release of cytochrome c from vesicles. *FEBS Lett.* **2007**, *581*, 5464-5468.
84. Size information for FITC-dextran can be found on the Sigma-Aldrich webpage. [www.sigmaaldrich.com/etc/medialib/docs/Sigma/Product\\_Information\\_Sheet/1/fd10s.pis.Par.0001.File.tmp/fd10spis.pdf](http://www.sigmaaldrich.com/etc/medialib/docs/Sigma/Product_Information_Sheet/1/fd10s.pis.Par.0001.File.tmp/fd10spis.pdf).
85. Ackers, G. K. Molecular Exclusion and Restricted Diffusion Processes in Molecular-Sieve Chromatography. *Biochemistry* **1964**, *3*, 723-730.
86. Huang, H. C.; Chang, T. M. Ceramide 1 and ceramide 3 act synergistically on skin hydration and the transepidermal water loss of sodium lauryl sulfate-irritated skin. *Int. J. Dermatol.* **2008**, *47*, 812-819.

87. Holleran, W. M.; Feingold, K. R.; Man, M. Q.; Gao, W. N.; Lee, J. M.; Elias, P. M. Regulation of epidermal sphingolipid synthesis by permeability barrier function. *J. Lipid. Res.* **1991**, *32*, 1151-1158.
88. Bouwstra, J. A.; Honeywell-Nguyen, P. L.; Gooris, G. S.; Ponc, M. Structure of the skin barrier and its modulation by vesicular formulations. *Prog. Lipid. Res.* **2003**, *42*, 1-36.
89. Green, T. W.; Wuts, P. G. M. *Protective Groups in Organic Synthesis*; 2 ed.; John Wiley & Sons, Inc.: New York, 1991.
90. Ahmad, M.; Bergstrom, R. G.; Cashen, M. J.; Kresge, A. J.; McClelland, R. A.; Powell, M. F. Ortho ester hydrolysis. The complete reaction mechanism. *J. Am. Chem. Soc.* **1977**, *99*, 4827-4829.
91. Harrell, W. A., Jr.; Bergmeyer, M. L.; Zavalij, P. Y.; Davis, J. T. Ceramide-mediated transport of chloride and bicarbonate across phospholipid membranes. *Chem. Commun.* **2010**, *46*, 3950-3952.
92. Wallace, B. A. Gramicidin channels and pores. *Annu. Rev. Biophys. Biophys. Chem.* **1990**, *19*, 127-157.
93. Pressman, B. C.; Harris, E. J.; Jagger, W. S.; Johnson, J. H. Antibiotic-mediated transport of alkali ions across lipid barriers. *Proc. Natl. Acad. Sci. USA* **1967**, *58*, 1949-1956.
94. Caltagirone, C.; Gale, P. A. Anion receptor chemistry: highlights from 2007. *Chem. Soc. Rev.* **2009**, *38*, 520-563.
95. Gokel, G. W.; Barkey, N. Transport of chloride ion through phospholipid bilayers mediated by synthetic ionophores. *New J. Chem.* **2009**, *33*, 947-963.
96. Davis, A. P.; Sheppard, D. N.; Smith, B. D. Development of synthetic membrane transporters for anions. *Chem. Soc. Rev.* **2007**, *36*, 348-357.
97. Davis, J. T.; Okunola, O.; Quesada, R. Recent advances in the transmembrane transport of anions. *Chem. Soc. Rev.* **2010**, *39*, 3843-6382.
98. Sheth, T. R.; Henderson, R. M.; Hladky, S. B.; Cuthbert, A. W. Ion channel formation by duramycin. *Biochim. Biophys. Acta* **1992**, *1107*, 179-185.
99. Davis, J. T. Anion Binding and Transport by Prodigiosin and its Analogs. In *Topics in Heterocyclic Chemistry*; Gale, P. A., Dehaen, W., Eds.; Springer: New York, NY, 2010; Vol. 24, p 145-176.

100. Asandei, A.; Luchian, T. Ion selectivity, transport properties and dynamics of amphotericin B channels studied over a wide range of acidity changes. *Colloid. Surf., B* **2008**, *67*, 99-106.
101. Jeong, E. J.; Kang, E. J.; Sung, L. T.; Hong, S. K.; Lee, E. Stereoselective synthesis of pamamycin-607. *J. Am. Chem. Soc.* **2002**, *124*, 14655-14662.
102. Shotwell, O. L.; Stodola, F. H.; Michael, W. R.; Lindenfelser, L. A.; Dworschack, R. G.; Pridham, T. G. Antibiotics Against Plant Disease. III. Duramycin, A New Antibiotic from *Streptomyces cinnamomeus* forma *azacoluta*. *J. Am. Chem. Soc.* **1958**, *80*, 3912-3915.
103. Cloutier, M. M.; Guernsey, L.; Mattes, P.; Koeppen, B. Duramycin enhances chloride secretion in airway epithelium. *Am. J. Physiol.* **1990**, *259*, C450-C454.
104. Grasemann, H.; Stehling, F.; Brunar, H.; Widmann, R.; Laliberte, T. W.; Molina, L.; Doring, G.; Ratjen, F. Inhalation of Moli1901 in patients with cystic fibrosis. *Chest* **2007**, *131*, 1461-1466.
105. Sheppard, D. N.; Rich, D. P.; Ostedgaard, L. S.; Gregory, R. J.; Smith, A. E.; Welsh, M. J. Mutations in CFTR associated with mild-disease-form Cl<sup>-</sup> channels with altered pore properties. *Nature* **1993**, *362*, 160-164.
106. Cordat, E.; Casey, J. R. Bicarbonate transport in cell physiology and disease. *Biochem. J.* **2009**, *417*, 423-439.
107. Choi, J. Y.; Muallem, D.; Kiselyov, K.; Lee, M. G.; Thomas, P. J.; Muallem, S. Aberrant CFTR-dependent HCO<sub>3</sub><sup>-</sup> transport in mutations associated with cystic fibrosis. *Nature* **2001**, *410*, 94-97.
108. Lee, M. G.; Choi, J. Y.; Luo, X.; Strickland, E.; Thomas, P. J.; Muallem, S. Cystic fibrosis transmembrane conductance regulator regulates luminal Cl<sup>-</sup>/HCO<sub>3</sub><sup>-</sup> exchange in mouse submandibular and pancreatic ducts. *J. Biol. Chem.* **1999**, *274*, 14670-14677.
109. Wrede, F.; Hettche, O. Prodigiosin, the red coloring matter of *Bacillus prodigiosus*. I *Ber. Deut. Chem. Ges.* **1929**, *62*, 2678-2687.
110. Wasserman, H. H.; McKeon, J. E.; Smith, L.; Forgione, P. Prodigiosin. Structure and partial synthesis. *J. Am. Chem. Soc.* **1960**, *82*, 506-507.
111. Rapoport, H.; Holden, K. G. The synthesis of prodigiosin. *J. Am. Chem. Soc.* **1962**, *84*, 635-642.



112. Williamson, N. R.; Fineran, P. C.; Gristwood, T.; Chawrai, S. R.; Leeper, F. J.; Salmond, G. P. Anticancer and immunosuppressive properties of bacterial prodiginines. *Future Microbiol.* **2007**, *2*, 605-618.
113. Sessler, J. L.; Eller, L. R.; Cho, W. S.; Nicolaou, S.; Aguilar, A.; Lee, J. T.; Lynch, V. M.; Magda, D. J. Synthesis, anion-binding properties, and in vitro anticancer activity of prodigiosin analogues. *Angew. Chem., Int. Ed. Engl.* **2005**, *44*, 5989-5992.
114. Lee, M. H.; Kataoka, T.; Magae, J.; Nagai, K. Prodigiosin 25-C suppression of cytotoxic T cells in vitro and in vivo similar to that of concanamycin B, a specific inhibitor of vacuolar type H(+)-ATPase. *Biosci. Biotechnol. Biochem.* **1995**, *59*, 1417-1421.
115. Kataoka, T.; Muroi, M.; Ohkuma, S.; Waritani, T.; Magae, J.; Takatsuki, A.; Kondo, S.; Yamasaki, M.; Nagai, K. Prodigiosin 25-C uncouples vacuolar type H(+)-ATPase, inhibits vacuolar acidification and affects glycoprotein processing. *FEBS Lett.* **1995**, *359*, 53-59.
116. Sato, T.; Konno, H.; Tanaka, Y.; Kataoka, T.; Nagai, K.; Wasserman, H. H.; Ohkuma, S. Prodigiosins as a new group of H<sup>+</sup>/Cl<sup>-</sup> symporters that uncouple proton translocators. *J. Biol. Chem.* **1998**, *273*, 21455-21462.
117. Konno, H.; Matsuya, H.; Okamoto, M.; Sato, T.; Tanaka, Y.; Yokoyama, K.; Kataoka, T.; Nagai, K.; Wasserman, H. H.; Ohkuma, S. Prodigiosins uncouple mitochondrial and bacterial F-ATPases: evidence for their H<sup>+</sup>/Cl<sup>-</sup> symport activity. *J. Biochem.* **1998**, *124*, 547-556.
118. Ohkuma, S.; Sato, T.; Okamoto, M.; Matsuya, H.; Arai, K.; Kataoka, T.; Nagai, K.; Wasserman, H. H. Prodigiosins uncouple lysosomal vacuolar-type ATPase through promotion of H<sup>+</sup>/Cl<sup>-</sup> symport. *Biochem. J.* **1998**, *334*, 731-741.
119. Seganish, J. L.; Davis, J. T. Prodigiosin is a chloride carrier that can function as an anion exchanger. *Chem. Commun.* **2005**, 5781-5783.
120. Hartsel, S.; Bolard, J. Amphotericin B: new life for an old drug. *Trends Pharmacol. Sci.* **1996**, *17*, 445-449.
121. Bolard, J. How do the polyene macrolide antibiotics affect the cellular membrane properties? *Biochim. Biophys. Acta* **1986**, *864*, 257-304.
122. Bonilla-Marin, M.; Moreno-Bello, M.; Ortega-Blake, I. A microscopic electrostatic model for the amphotericin B channel. *Biochim. Biophys. Acta* **1991**, *1061*, 65-77.

123. Gruszecki, W. I.; Gagos, M.; Herec, M.; Kernen, P. Organization of antibiotic amphotericin B in model lipid membranes. A mini review. *Cell Mol. Biol. Lett.* **2003**, *8*, 161-170.
124. Baginski, M.; Resat, H.; McCammon, J. A. Molecular properties of amphotericin B membrane channel: a molecular dynamics simulation. *Mol. Pharmacol.* **1997**, *52*, 560-570.
125. Khutorsky, V. Ion coordination in the amphotericin B channel. *Biophys. J.* **1996**, *71*, 2984-2995.
126. Resat, H.; Baginski, M. Ion passage pathways and thermodynamics of the amphotericin B membrane channel. *Eur. Biophys. J.* **2002**, *31*, 294-305.
127. Kondo, S.; Yasui, K.; Katayama, M.; Marumo, S.; Kondo, T.; Hattori, H. Structure of pamamycin-607, an aerial mycelium-inducing substance of *Streptomyces alboniger*. *Tetrahedron Lett.* **1987**, *28*, 5861-5864.
128. Pogell, B. M. The pamamycins: developmental autoregulators and antibiotics from *Streptomyces alboniger*. A review and update. *Cell. Mol. Biol.* **1988**, *44*, 461-463.
129. Kondo, S.; Yasui, K.; Natsume, M.; Katayama, M.; Marumo, S. Isolation, physico-chemical properties and biological activity of pamamycin-607, an aerial mycelium-inducing substance from *Streptomyces alboniger*. *J. Antibiot.* **1988**, *41*, 1196-1204.
130. Uhlmann, E.; Hornung, L.; Will, D. W.; Grafe, U. Synthesis of novel oligodeoxynucleotide conjugates containing the anionophoric moiety of panamycin. *Nucleos. Nucleot.* **1988**, *17*, 309-316.
131. Pedersen, C. J. Cyclic polyethers and their complexes with metal salts. *J. Am. Chem. Soc.* **1967**, *89*, 2495-2496.
132. Pedersen, C. J. Cyclic polyethers and their complexes with metal salts. *J. Am. Chem. Soc.* **1967**, *89*.
133. Stengel, C.; Reinhardt, G.; Grafe, U. A simple screening procedure for microbial phase-transfer mediators conveying anions. *J. Basic Microbiol.* **1992**, *32*, 339-345.
134. Sessler, J. L.; Gale, P. A.; Cho, W. S. *Anion Receptor Chemistry*; RSC: Cambridge, U.K., 2006.
135. Kubik, S. Amino acid containing anion receptors. *Chem. Soc. Rev.* **2009**, *38*, 585-605.

136. Albert, J. S.; Hamilton, A. D. Synthetic Analogs of the Ristocetin Binding-Site - Neutral, Multidentate Receptors for Carboxylate Recognition. *Tetrahedron Lett.* **1993**, *34*, 7363-7366.
137. Davis, A. P.; Gilmer, J. F.; Perry, J. J. A steroid-based cryptand for halide anions. *Angew. Chem., Int. Ed.* **1996**, *35*, 1312-1315.
138. Coteron, J. M.; Hacket, F.; Schneider, H. J. Interactions of hydroxy compounds and sugars with anions. *J. Org. Chem.* **1996**, *61*, 1429-1435.
139. Smith, D. K. Rapid NMR screening of chloride receptors: uncovering catechol as a useful anion binding motif. *Org. Biomol. Chem.* **2003**, *1*, 3874-3877.
140. Kondo, S.; Okada, N.; Tanaka, R.; Yamamura, M.; Unno, M. Anion recognition by 1,3-disiloxane-1,1,3,3-tetraols in organic solvents. *Tetrahedron Lett.* **2009**, *50*, 2754-2757.
141. Luecke, H.; Quioco, F. A. High Specificity of a Phosphate-Transport Protein Determined by Hydrogen-Bonds. *Nature* **1990**, *347*, 402-406.
142. He, J. J.; Quioco, F. A. A Nonconservative Serine to Cysteine Mutation in the Sulfate-Binding Protein, a Transport Receptor. *Science* **1991**, *251*, 1479-1481.
143. Dutzler, R.; Campbell, E. B.; Cadene, M.; Chait, B. T.; MacKinnon, R. X-ray structure of a CIC chloride channel at 3.0 angstrom reveals the molecular basis of anion selectivity. *Nature* **2002**, *415*, 287-294.
144. Pflugrath, J. W.; Quioco, F. A. The 2 Å resolution structure of the sulfate-binding protein involved in active transport in *Salmonella typhimurium*. *J. Mol. Biol.* **1988**, *200*, 163-180.
145. Weiss, L. A.; Sakai, N.; Ghebremariam, B.; Ni, C. Y.; Matile, S. Rigid rod-shaped polyols: Functional nonpeptide models for transmembrane proton channels. *J. Am. Chem. Soc.* **1997**, *119*, 12142-12149.
146. Sakai, N.; Ni, C.; Bezrukov, S.; Matile, S. Voltage-dependent ion channel formation by rigid rod-shaped polyols in planar lipid bilayers. *Bioorg. Med. Chem. Lett.* **1998**, *8*, 2743-2746.
147. Winstanley, K. J.; Sayer, A. M.; Smith, D. K. Anion binding by catechols--an NMR, optical and electrochemical study. *Org. Biomol. Chem.* **2006**, *4*, 1760-1767.
148. Winstanley, K. J.; Smith, D. K. Ortho-substituted catechol derivatives: the effect of intramolecular hydrogen-bonding pathways on chloride anion recognition. *J. Org. Chem.* **2007**, *72*, 2803-2815.

149. Miyaji, H.; Sessler, J. L. Off-the-Shelf Colorimetric Anion Sensors *Angew. Chem., Int. Ed.* **2001**, *40*, 154-157.
150. Berezin, S. K.; Davis, J. T. Catechols as Membrane Anion Transporters. *J. Am. Chem. Soc.* **2009**, *131*, 2458-2459.
151. Thomas, R. L.; Matsko, C. M.; Lotze, M. T.; Amoscato, A. A. Mass spectrometric identification of increased C16 ceramide levels during apoptosis. *J. Biol. Chem.* **1999**, *274*, 30580-30588.
152. Hsu, F. F.; Turk, J. Characterization of ceramides by low energy collisional-activated dissociation tandem mass spectrometry with negative-ion electrospray ionization. *J. Am. Soc. Mass. Spectrom.* **2002**, *13*, 558-570.
153. Li, L.; Tang, X. P.; Taylor, K. G.; Dupre, D. B.; Yappert, M. C. Conformational characterization of ceramides by nuclear magnetic resonance spectroscopy. *Biophys. J.* **2002**, *82*, 2067-2080.
154. Hynes, M. J. Eqnmr - a Computer-Program for the Calculation of Stability-Constants from Nuclear-Magnetic-Resonance Chemical-Shift Data. *J. Chem. Soc., Dalton Trans.* **1993**, 311-312.
155. Lopez-Montero, I.; Rodriguez, N.; Cribier, S.; Pohl, A.; Velez, M.; Devaux, P. F. Rapid transbilayer movement of ceramides in phospholipid vesicles and in human erythrocytes. *J. Biol. Chem.* **2005**, *280*, 25811-25819.
156. Pohl, A.; Lopez-Montero, I.; Rouviere, F.; Giusti, F.; Devaux, P. F. Rapid transmembrane diffusion of ceramide and dihydroceramide spin-labelled analogues in the liquid ordered phase. *Mol. Membr. Biol.* **2009**, *26*, 194-204.
157. McNally, B. A.; O'Neil, E. J.; Nguyen, A.; Smith, B. D. Membrane Transporters for Anions That Use a Relay Mechanism. *J. Am. Chem. Soc.* **2008**, *130*, 17274-17275.
158. Siskind, L. J.; Colombini, M. The lipids C-2- and C-16-ceramide form large stable channels - Implications for apoptosis. *J. Biol. Chem.* **2000**, *275*, 38640-38644.
159. Matile, S.; Tanaka, H.; Litvinchuk, S. Analyte sensing across membranes with artificial pores. *Top. Curr. Chem.* **2007**, *277*, 219-250.
160. Ferdani, R.; Li, R. Q.; Pajewski, R.; Pajewska, J.; Winter, R. K.; Gokel, G. W. Transport of chloride and carboxyfluorescein through phospholipid vesicle membranes by heptapeptide amphiphiles. *Org. Biomol. Chem.* **2007**, *5*, 2423-2432.

161. McNally, B. A.; Koulov, A. V.; Smith, B. D.; Joos, J. B.; Davis, A. P. A fluorescent assay for chloride transport; identification of a synthetic anionophore with improved activity. *Chem. Commun.* **2005**, 1087-1089.
162. Marcus, Y. Thermodynamics of Solvation of Ions .5. Gibbs Free-Energy of Hydration at 298.15-K. *J. Chem. Soc., Faraday Trans.* **1991**, 87, 2995-2999.
163. Bordwell, F. G. Equilibrium acidities in Dimethyl Sulfoxide Solution. *Acc. Chem. Res.* **1988**, 21, 456-463.
164. Mori, K.; Nishio, H. Synthesis of (2S,3R,4E)-1-O-(beta-D-Glucopyranosyl)-N-[24-(linoleoyloxy)tetracosanoyl]-4-sphinganine. The Structure Proposed for the Esterified Cerebroside in the Epidermis of Guinea Pigs. *Leibigs Ann. Chem.* **1991**, 3, 253-257.
165. Davis, F. A.; Reddy, G. V. Aziridine-2-Carboxylic Acid Mediated Asymmetric Synthesis of D-erythro- and L-threo-Sphingosine from a Common Precursor. *Tetrahedron Lett.* **1996**, 37, 4349-4352.
166. Siskind, L. J.; Kolesnick, R. N.; Colombini, M. Ceramide forms channels in mitochondrial outer membranes at physiologically relevant concentrations. *Mitochondrion* **2006**, 6, 118-125.
167. Harrell, W. A., Jr.; Bergmeyer, M. L.; Zavalij, P. Y.; Davis, J. T. Ceramide-mediated transport of chloride and bicarbonate across phospholipid membranes. *Chem. Commun.* **2010**, 46, 3950-3952.
168. Busschaert, N.; Gale, P. A.; Haynes, C. J.; Light, M. E.; Moore, S. J.; Tong, C. C.; Davis, J. T.; Harrell, W. A., Jr. Tripodal transmembrane transporters for bicarbonate. *Chem. Commun.* **2010**, 46, 6252-6254.
169. Andrews, N. J.; Haynes, C. J. E.; Light, M. E.; Moore, S. J.; Tong, C. C.; Davis, J. T.; Harrell, W. A., Jr.; Gale, P. A. Structurally simple lipid bilayer transport agents for chloride and bicarbonate. *Chem. Sci.* **2011**, 2, 256-260.
170. Nakayama, F. S. Sodium bicarbonate and carbonate ion pairs and their relation to the estimation of the first and second dissociation constants of carbonic acid. *J. Phys. Chem.* **1970**, 74, 2726-2728.
171. Geers, C.; Gros, G. Carbon dioxide transport and carbonic anhydrase in blood and muscle. *Physiol. Rev.* **2000**, 80, 681-715.
172. Hempling, H. G. In *Intracellular water and the regulation of cell volume and pH*; Bittar, E. E., Bittar, N., Eds.; JAI Press: Greenwich, CT, 1995, p 217-246.
173. Casey, J. R. Why bicarbonate? *Biochem. Cell Biol.* **2006**, 84, 930-939.

174. Alvarez, B. V.; Kieller, D. M.; Quon, A. L.; Markovich, D.; Casey, J. R. Slc26a6: a cardiac chloride-hydroxyl exchanger and predominant chloride-bicarbonate exchanger of the mouse heart. *J. Physiol.* **2004**, *561*, 721-734.
175. Cleland, W. W.; Andrews, T. J.; Gutteridge, S.; Hartman, F. C.; Lorimer, G. H. Mechanism of Rubisco: The Carbamate as General Base. *Chem. Rev.* **1998**, *98*, 549-562.
176. McNamara, J.; Worthley, L. I. Acid-base balance: part I. Physiology. *Crit. Care. Resusc.* **2001**, *3*, 181-187.
177. Chegwiddden, W. R.; Dodgson, S. J.; Spencer, I. M. The roles of carbonic anhydrase in metabolism, cell growth and cancer in animals. *EXS* **2000**, 343-363.
178. Chou, C. Y.; Yu, L. P.; Tong, L. Crystal structure of biotin carboxylase in complex with substrates and implications for its catalytic mechanism. *J. Biol. Chem.* **2009**, *284*, 11690-11697.
179. Burns, B. P.; Hazell, S. L.; Mendz, G. L. Acetyl-CoA carboxylase activity in *Helicobacter pylori* and the requirement of increased CO<sub>2</sub> for growth. *Microbiology* **1995**, *141*, 3113-3118.
180. Strater, N.; Sun, L.; Kantrowitz, E. R.; Lipscomb, W. N. A bicarbonate ion as a general base in the mechanism of peptide hydrolysis by dizinc leucine aminopeptidase. *Proc. Natl. Acad. Sci. U.S.A.* **1999**, *96*, 11151-11155.
181. Thrower, J. S.; Blalock, R., 3rd; Klinman, J. P. Steady-state kinetics of substrate binding and iron release in tomato ACC oxidase. *Biochemistry* **2001**, *40*, 9717-9724.
182. Xu, W. M.; Shi, Q. X.; Chen, W. Y.; Zhou, C. X.; Ni, Y.; Rowlands, D. K.; Yi Liu, G.; Zhu, H.; Ma, Z. G.; Wang, X. F.; Chen, Z. H.; Zhou, S. C.; Dong, H. S.; Zhang, X. H.; Chung, Y. W.; Yuan, Y. Y.; Yang, W. X.; Chan, H. C. Cystic fibrosis transmembrane conductance regulator is vital to sperm fertilizing capacity and male fertility. *Proc. Natl. Acad. Sci. U.S.A.* **2007**, *104*, 9816-9821.
183. Demarco, I. A.; Espinosa, F.; Edwards, J.; Sosnik, J.; De La Vega-Beltran, J. L.; Hockensmith, J. W.; Kopf, G. S.; Darszon, A.; Visconti, P. E. Involvement of a Na<sup>+</sup>/HCO<sub>3</sub><sup>-</sup> cotransporter in mouse sperm capacitation. *J. Biol. Chem.* **2003**, *278*, 7001-7009.
184. Fujinaga, J.; Loisel, F. B.; Casey, J. R. Transport activity of chimaeric AE2-AE3 chloride/bicarbonate anion exchange proteins. *Biochem. J.* **2003**, *371*, 687-696.

185. Steward, M. C.; Ishiguro, H.; Case, R. M. Mechanisms of bicarbonate secretion in the pancreatic duct. *Annu. Rev. Physiol.* **2005**, *67*, 377-409.
186. Ishiguro, H.; Steward, M. C.; Naruse, S.; Ko, S. B.; Goto, H.; Case, R. M.; Kondo, T.; Yamamoto, A. CFTR functions as a bicarbonate channel in pancreatic duct cells. *J. Gen. Physiol.* **2009**, *133*, 315-326.
187. Sindic, A.; Chang, M. H.; Mount, D. B.; Romero, M. F. Renal physiology of SLC26 anion exchangers. *Curr. Opin. Nephrol. Hypertens.* **2007**, *16*, 484-490.
188. Todd, R. C.; Lovejoy, K. S.; Lippard, S. J. Understanding the effect of carbonate ion on cisplatin binding to DNA. *J. Am. Chem. Soc.* **2007**, *129*, 6370-6371.
189. Supuran, C. T.; Scozzafava, A. In *Carbonic anhydrase activators as potential anti-Alzheimer's disease agents, Protein misfolding in Neurodegenerative Diseases* 2008, p 265-288.
190. Wynn, E.; Krieg, M. A.; Aeschlimann, J. M.; Burckhardt, P. Alkaline mineral water lowers bone resorption even in calcium sufficiency: alkaline mineral water and bone metabolism. *Bone* **2009**, *44*, 120-124.
191. Supuran, C. T. Carbonic anhydrases--an overview. *Curr. Pharm. Des.* **2008**, *14*, 603-614.
192. Sterling, D.; Reithmeier, R. A.; Casey, J. R. A transport metabolon. Functional interaction of carbonic anhydrase II and chloride/bicarbonate exchangers. *J. Biol. Chem.* **2001**, *276*, 47886-47894.
193. Kopito, R. R.; Lodish, H. F. Primary structure and transmembrane orientation of the murine anion exchange protein. *Nature* **1985**, *316*, 234-238.
194. Sterling, D.; Casey, J. R. Bicarbonate transport proteins. *Biochem. Cell. Biol.* **2002**, *80*, 483-497.
195. Sterling, D.; Casey, J. R. Transport activity of AE3 chloride/bicarbonate anion-exchange proteins and their regulation by intracellular pH. *Biochem. J.* **1999**, *344 Pt 1*, 221-229.
196. Dawson, P. A.; Markovich, D. Pathogenetics of the human SLC26 transporters. *Curr. Med. Chem.* **2005**, *12*, 385-396.
197. Dorwart, M. R.; Shcheynikov, N.; Yang, D.; Muallem, S. The solute carrier 26 family of proteins in epithelial ion transport. *Physiology* **2008**, *23*, 104-114.

198. Markovich, D.; Bissig, M.; Sorribas, V.; Hagenbuch, B.; Meier, P. J.; Murer, H. Expression of rat renal sulfate transport systems in *Xenopus laevis* oocytes. Functional characterization and molecular identification. *J. Biol. Chem.* **1994**, *269*, 3022-3026.
199. Markovich, D. Physiological roles and regulation of mammalian sulfate transporters. *Physiol. Rev.* **2001**, *81*, 1499-1533.
200. Mount, D. B.; Romero, M. F. The SLC26 gene family of multifunctional anion exchangers. *Pflugers. Arch.* **2004**, *447*, 710-721.
201. Simpson, J. E.; Schweinfest, C. W.; Shull, G. E.; Gawenis, L. R.; Walker, N. M.; Boyle, K. T.; Soleimani, M.; Clarke, L. L. PAT-1 (Slc26a6) is the predominant apical membrane Cl<sup>-</sup>/HCO<sub>3</sub><sup>-</sup> exchanger in the upper villous epithelium of the murine duodenum. *Am. J. Physiol. Gastrointest. Liver Physiol.* **2007**, *292*, G1079-1088.
202. Singh, A. K.; Sjoblom, M.; Zheng, W.; Krabbenhoft, A.; Riederer, B.; Rausch, B.; Manns, M. P.; Soleimani, M.; Seidler, U. CFTR and its key role in in vivo resting and luminal acid-induced duodenal HCO<sub>3</sub><sup>-</sup> secretion. *Acta Physiol.* **2008**, *193*, 357-365.
203. Koulov, A. V.; Lambert, T. N.; Shukla, R.; Jain, M.; Boon, J. M.; Smith, B. D.; Li, H.; Sheppard, D. N.; Joos, J. B.; Clare, J. P.; Davis, A. P. Chloride transport across vesicle and cell membranes by steroid-based receptors. *Angew. Chem., Int. Ed.* **2003**, *42*, 4931-4933.
204. Sato, T.; Konno, H.; Tanaka, Y.; Kataoka, T.; Nagai, K.; Wasserman, H. H.; Ohkuma, S. Prodigiosins as a new group of H<sup>+</sup>/Cl<sup>-</sup> symporters that uncouple proton translocators. *J. Biol. Chem.* **1998**, *273*, 21455-21462.
205. Seganish, J. L.; Davis, J. T. Prodigiosin is a chloride carrier that can function as an anion exchanger. *Chem Commun (Camb)* **2005**, 5781-3.
206. Davis, J. T.; Gale, P. A.; Okunola, O. A.; Prados, P.; Iglesias-Sánchez, J. C.; Torroba, T.; Quesada, R. Using "Small" Molecules to Facilitate Exchange of Bicarbonate and Chloride Anions Across Liposomal Membranes *Nat. Chem.* **2009**, 138-144.
207. Gale, P. A.; Tong, C. C.; Haynes, C. J.; Adeosun, O.; Gross, D. E.; Karnas, E.; Sedenberg, E. M.; Quesada, R.; Sessler, J. L. Octafluorocalix[4]pyrrole: a chloride/bicarbonate antiport agent. *J. Am. Chem. Soc.* **2010**, *132*, 3240-3241.
208. McNally, B. A.; Koulov, A. V.; Smith, B. D.; Joos, J. B.; Davis, A. P. A fluorescent assay for chloride transport; identification of a synthetic anionophore with improved activity. *Chem. Commun.* **2005**, 1087-1089.



209. Hamai, H.; Keyserman, F.; Quittell, L. M.; Worgall, T. S. Defective CFTR increases synthesis and mass of sphingolipids that modulate membrane composition and lipid signaling. *J. Lipid. Res.* **2009**, *50*, 1101-1108.
210. Winstanley, K. J.; Allen, S. J.; Smith, D. K. Encapsulated binding sites--synthetically simple receptors for the binding and transport of HCl. *Chem. Commun.* **2009**, 4299-4301.
211. Boon, J. M.; Smith, B. D. Facilitated phospholipid translocation across vesicle membranes using low-molecular-weight synthetic flippases. *J. Am. Chem. Soc.* **1999**, *121*, 11924-11925.
212. Seganish, J. L.; Santacroce, P. V.; Salimian, K. J.; Fettingner, J. C.; Zavalij, P.; Davis, J. T. Regulating supramolecular function in membranes: calixarenes that enable or inhibit transmembrane Cl<sup>-</sup> transport. *Angew. Chem., Int. Ed.* **2006**, *45*, 3334-3338.
213. Santacroce, P. V.; Davis, J. T.; Light, M. E.; Gale, P. A.; Iglesias-Sanchez, J. C.; Prados, P.; Quesada, R. Conformational control of transmembrane Cl<sup>-</sup> transport. *J. Am. Chem. Soc.* **2007**, *129*, 1886-1887.
214. McNally, B. A.; Koulov, A. V.; Lambert, T. N.; Smith, B. D.; Joos, J. B.; Sisson, A. L.; Clare, J. P.; Sgarlata, V.; Judd, L. W.; Magro, G.; Davis, A. P. Structure-activity relationships in cholapod anion carriers: enhanced transmembrane chloride transport through substituent tuning. *Chem.-Eur. J.* **2008**, *14*, 9599-9606.
215. Shirono, K.; Morimatsu, T.; Takemura, F. Gas solubilities (CO<sub>2</sub>, O<sub>2</sub>, Ar, N<sub>2</sub>, H<sub>2</sub>, and He) in liquid chlorinated methanes. *J. Chem. Eng. Data* **2008**, *53*, 1867-1871.
216. Hua, L.; Wanren, C. Solubility of dilute SO<sub>2</sub> and CO<sub>2</sub> in dimethyl sulfoxide. *Phys. Chem. Liq.* **2005**, *43*, 289-298.
217. Kruus, P.; Hayes, C. A. Solubility of carbon dioxide in water-*t*-butanol solutions. *Can. J. Chem* **1985**, *63*, 3403-3410.
218. Wilhelm, E.; Battino, R.; Wilcock, R. J. Low-pressure solubility of gases in liquid water. *Chem. Rev.* **1977**, *77*, 219-262.
219. Yang, B.; Fukuda, N.; van Hoek, A.; Matthay, M. A.; Ma, T.; Verkman, A. S. Carbon dioxide permeability of aquaporin-1 measured in erythrocytes and lung of aquaporin-1 null mice and in reconstituted proteoliposomes. *J. Biol. Chem.* **2000**, *275*, 2686-2692.

220. Endeward, V.; Musa-Aziz, R.; Cooper, G. J.; Chen, L. M.; Pelletier, M. F.; Virkki, L. V.; Supuran, C. T.; King, L. S.; Boron, W. F.; Gros, G. Evidence that aquaporin 1 is a major pathway for CO<sub>2</sub> transport across the human erythrocyte membrane. *FASEB J.* **2006**, *20*, 1974-1981.
221. Endeward, V.; Cartron, J. P.; Ripoche, P.; Gros, G. RhAG protein of the Rhesus complex is a CO<sub>2</sub> channel in the human red cell membrane. *FASEB J.* **2008**, *22*, 64-73.
222. Schimel, D. S.; House, J. I.; Hibbard, K. A.; Bousquet, P.; Ciais, P.; Peylin, P.; Braswell, B. H.; Apps, M. J.; Baker, D.; Bondeau, A.; Canadell, J.; Churkina, G.; Cramer, W.; Denning, A. S.; Field, C. B.; Friedlingstein, P.; Goodale, C.; Heimann, M.; Houghton, R. A.; Melillo, J. M.; Moore, B., 3rd; Murdiyarso, D.; Noble, I.; Pacala, S. W.; Prentice, I. C.; Raupach, M. R.; Rayner, P. J.; Scholes, R. J.; Steffen, W. L.; Wirth, C. Recent patterns and mechanisms of carbon exchange by terrestrial ecosystems. *Nature* **2001**, *414*, 169-172.
223. Metz, B.; Davidson, O.; de Coninck, H.; Loos, M.; Meyer, L. *IPPC Special Report on Carbon Dioxide Capture and Storage*; Cambridge University Press: New York, 2005.
224. Kovvali, A. S.; Sirkar, K. K. Dendrimer Liquid Membranes: CO<sub>2</sub> Separation from Gas Mixtures. *Ind. Eng. Chem. Res.* **2001**, *40*, 2502-2511.
225. Sada, E.; Kumazawa, H.; Han, Z. Q. Kinetics of reaction between carbon dioxide and ethylenediamine in nonaqueous solvents. *Chem. Eng. J.* **1985**, *31*, 109-115.
226. Yamaguchi, T.; Boetje, L. M.; Koval, C. A.; Noble, R. D.; Bowman, C. N. Transport Properties of Carbon Dioxide through Amine Functionalized Carrier Membranes. *Ind. Eng. Chem. Res.* **1995**, *34*, 4071-4077.
227. Yamaguchi, T.; Koval, C. A.; Nobel, R. D.; Bowman, C. Transport mechanism of carbon dioxide through perfluorosulfonate ionomer membranes containing an amine carrier. *Chem. Eng. Sci.* **1996**, *51*, 4781-4789.
228. McCann, N.; Phan, D.; Wang, X.; Conway, W.; Burns, R.; Attalla, M.; Puxty, G.; Maeder, M. Kinetics and mechanism of carbamate formation from CO<sub>2</sub>(aq), carbonate species, and monoethanolamine in aqueous solution. *J. Phys. Chem. A* **2009**, *113*, 5022-5029.
229. Leontiev, A. V.; Rudkevich, D. M. Encapsulation of gases in the solid state. *Chem. Commun.* **2004**, 1468-1469.
230. Sgarlata, V.; Organo, V. G.; Rudkevich, D. M. A procedure for filling calixarene nanotubes. *Chem. Commun.* **2005**, 5630-5632.

231. Organo, V. G.; Sgarlata, V.; Firouzbakht, F.; Rudkevich, D. M. Long synthetic nanotubes from calix[4]arenes. *Chem. Eur. J.* **2007**, *13*, 4014-4023.
232. Organo, V. G.; Leontiev, A. V.; Sgarlata, V.; Dias, H. V.; Rudkevich, D. M. Supramolecular features of calixarene-based synthetic nanotubes. *Angew. Chem., Int. Ed.* **2005**, *44*, 3043-3047.
233. Leontiev, A. V.; Dias, H. V.; Rudkevich, D. M. Sulfamides and sulfamide polymers directly from sulfur dioxide. *Chem. Commun.* **2006**, 2887-2889.
234. Morrow, J. S.; Keim, P.; Gurd, F. R. CO<sub>2</sub> adducts of certain amino acids, peptides, and sperm whale myoglobin studied by carbon 13 and proton nuclear magnetic resonance. *J. Biol. Chem.* **1974**, *249*, 7484-7494.
235. Stastny, V.; Anderson, A.; Rudkevich, D. M. Supramolecular structures from lysine peptides and carbon dioxide. *J. Org. Chem.* **2006**, *71*, 8696-8705.
236. Masuda, K.; Ito, Y.; Horiguchi, M.; Fujita, H. Studies on the solvent dependence of the carbamic acid formation from w-(1-naphthyl)alkylamines and carbon dioxide. *Tetrahedron* **2005**, *61*, 213-229.
237. Zhang, H.; Rudkevich, D. M. Using carbon dioxide and calix[4]arenes to separate sodium. *Chem. Commun.* **2007**, 4893-4894.
238. Xu, H.; Rudkevich, D. M. Reversible chemistry of CO<sub>2</sub> in the preparation of fluorescent supramolecular polymers. *J. Org. Chem.* **2004**, *69*, 8609-8617.
239. Xu, H.; Rudkevich, D. M. CO<sub>2</sub> in supramolecular chemistry: preparation of switchable supramolecular polymers. *Chemistry* **2004**, *10*, 5432-42.
240. Kistic, A.; Tsuda, M.; Kulmacz, R. J.; Wilson, W. K.; Schroepfer, G. J., Jr. Sphingolipid bases. A revisitation of the O-methyl derivatives of sphingosine. Isolation and characterization of diacetate derivatives, with revised <sup>13</sup>C nuclear magnetic resonance assignments for D-erythro-sphingosine. *J. Lipid. Res.* **1995**, *36*, 787-803.